

The Use of Acoustic Emission in Improving hardwood timber seasoning productivity

by

James Derek Booker
B.E. (hons.)

Submitted in fulfilment of the requirements for the
Degree of Doctor of Philosophy

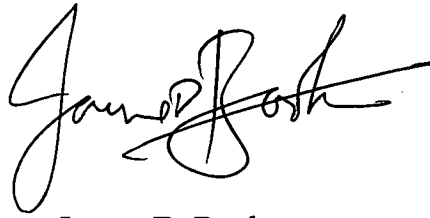
in the Faculty of Engineering
UNIVERSITY OF TASMANIA

Australia

October 1994

graduated 1996

I hereby declare that, except as stated herein, this thesis contains no material which has been accepted for the award of any other degree or diploma in any university and that, to the best of my knowledge and belief, this thesis contains no copy or paraphrase of material previously published or written by any other person, except where due reference is made in the text of the thesis.

A handwritten signature in black ink, appearing to read "James D. Booker". The signature is fluid and cursive, with the first name "James" and last name "Booker" clearly distinguishable.

James D. Booker

Contents

Preface	iv
Abstract	vi
Additional Publications	x
Acknowledgements	xi
Chapter 1. Seasoning	1
Chapter 2. Literature review	14
Chapter 3. Material properties and AE related to timber structure	27
Chapter 4. AE data acquisition and experimental kiln	35
Chapter 5. One-dimensional drying model for Tasmanian eucalypt and related bulk material property tests	49
Chapter 6. Determining the AE checking threshold	68
Chapter 7. Relationship between surface instantaneous strain, AE and drying conditions	90
Chapter 8. AE and strain energy	106
Chapter 9. SMARTKILN	121
Chapter 10. Clever Kiln Controller®	133
References	147
Appendix A. Typical AE Responses in Tasmanian Eucalypt	153
Appendix B. Relevant computer program listings	156
Appendix C. Clever Kiln Controller user screen	159
Appendix D. Nomenclature	161

Preface

This thesis describes the implementation of a kiln control system for drying hardwoods based on real-time measurements of acoustic emission (AE) in drying boards. As a brief introduction, acoustic emission are stress waves generated at localised sources in solid materials under stress. These waves are typically very low-energy and are detectable only with extremely sensitive transducers. The most common engineering application for acoustic emission is its ability to provide a nondestructive measure of the structural integrity of components in situ. Prior to this study, it was thought that the acoustic emission detected in drying timber might be used as a feedback mechanism to prevent surface checking. Surface checks are large cracks in drying boards that result from the formation of excessive surface stress.

The work of this author builds on the work of previous postgraduate students and staff at the University of Tasmania over the past 15 years. Therefore, this thesis is prefaced with a brief description of these previous worker's contributions to the overall research strategy and the state of the research at the commencement of this author's study.

Schaffner (1981) combined the theories of heat and mass transfer and stress analysis to develop a model of timber drying based upon Fickian diffusion and incorporating linearly elastic material behaviour. The one-dimensional model was used to accurately calculate the required moisture transfer characteristics of a semi-permeable coating adhered to board surfaces to limit the development of steep moisture gradients and resulting surface checking. The coating process was commercialised and used successfully by one large sawmill in particular.

Oliver (1984, 1991) refined Schaffner's initial work and developed a one-dimensional, nonlinear model of the stress-strain behaviour of timber during drying. Oliver wrote the computer program, KILNSCHED, which was used extensively in this author's work. KILNSCHED is described in detail in this thesis but as a brief introduction, the program models the development of the boundary layer in the air at the surface of a drying board to calculate the surface drying behaviour. KILNSCHED uses this calculated surface moisture loss to calculate internal moisture distributions. These are

used to calculate the distribution of shrinkage through the board and finally stress and strain distributions. KILNSCHED simulates drying schedules comprising arbitrary drying conditions at arbitrary times, allowing the user to rapidly test drying regimes for timber with a wide range of material properties.

Wu (1989) performed a detailed investigation of the air flow through a timber stack, primarily to study the structure and development of the boundary layer. He incorporated measurements of surface shear stress and friction factor into KILNSCHED. Drying behaviour calculated with KILNSCHED was compared directly with measured moisture distributions in drying tests lasting up to 700 hours and close agreement was obtained. Wu also investigated the mechano-sorptive effect in Tasmanian 'peppermint' eucalypt specimens subject to bending and found that a significant behavioural change occurred when specimens attained FSP. These measurements were also incorporated into KILNSCHED.

Parsons (1989) performed an Honours thesis aimed primarily at developing suitable hardware to process the acoustic emission recorded in Tasmanian eucalypt specimens subject to external load and in specimens allowed to dry in a research kiln. Parsons recorded remarkably periodic acoustic emission behaviour in drying timber specimens subject to collapse shrinkage. The hardware developed by Parsons was employed in the initial period of this study until an improved understanding of the acoustic emission phenomenon led to the need for refinements in the data acquisition hardware.

Thus at the commencement of this author's study, a quite accurate description of timber drying had evolved. The author aimed to combine the simulation tool provided by KILNSCHED with the nondestructive stress measurement technique provided by acoustic emission to further advance our understanding of the timber drying process. The ultimate aim of the study was to develop a reactive, predictive kiln control system to optimise the hardwood drying process.

Abstract

The Tasmanian sawmilling industry typically does not season eucalypt material specifically for furniture applications because of its highly refractory seasoning characteristics. Boards cut with wide faces parallel to the growth rings ('backsawn' or 'flatsawn' boards), in particular, shrink significantly with drying and often experience surface checking (seasoning 'degrade'). It is standard practice to season timber batches under schedules designed to produce relatively high-grade structural material and sell the small proportion of boards that do not suffer seasoning degrade as furniture grade material. The aim of this study was to investigate optimum seasoning of backsawn material specifically for furniture applications to take advantage of the premium prices paid by furniture manufacturers for degrade-free material.

Acoustic emission is a well known non-destructive testing tool. Acoustic emission results from stress waves generated by irreversible stress release activity such as the growth of small cracks in a solid material under load. Acoustic emission is typically used in homogeneous materials such as plastics and metals to determine the structural integrity of components in situ.

Acoustic emission was first measured in timber subject to external load over thirty years ago and has subsequently been measured in drying timber specimens where differential drying rates between the surface and centre of a sample may cause appreciable drying stresses. Acoustic emission appeared to be related to the severity of the drying conditions and the development of surface checking (Becker 1982, Noguchi et al. 1987). Under harsh drying regimes, surface checking occurred and a significantly higher AE rate was measured than in the same species subject to mild drying conditions. The 'AE rate' is a measure of the occurrence of high-energy bursts of acoustic waves during a particular time-period - the higher the AE rate, the more energetic bursts are measured. On this basis, it appeared feasible to measure acoustic emission in sample boards in a kiln during drying and adjust the drying conditions as the AE rate approached levels previously determined to correspond to surface checking. Various AE-based kiln control systems were reported in the literature (Honeycutt et al. 1985, Noguchi et al. 1987) but it appears acoustic emission was not satisfactorily related to surface check

development. These control systems controlled the drying conditions based on arbitrary AE rates that were nominally selected as 'safe' without optimising the drying process. The heterogeneous structure of timber posed significant obstacles to forming a clear picture of the stress release processes occurring in timber.

Acoustic emission measured in drying Tasmanian eucalypt boards was employed in this project as an online measure of the magnitude of the stresses during drying. Numerous batches of eucalypt boards were obtained from a sawmill during the project and dried under harsh conditions to induce surface checking. It was determined that the AE rate generated at the onset of surface checking in backsawn and quartersawn boards was effectively constant (within the variability of the material). This 'AE checking threshold' was independent of basic density and clearly independent of bulk stiffness (since the bulk tangential stiffness is effectively half the radial stiffness in the species studied). It appeared that the acoustic emission phenomenon was independent of the timber bulk material properties.

It is proposed that acoustic emission waves propagate from irreversible slips or dislocations in the crystalline cellulose regions of cell walls under high stress. These slips are sudden, energetic stress release events which propagate stress waves from the local site. The amorphous regions of the cell structure behave in a rather plastic manner with local stress expected to be consumed by ductile flow processes that do not generate elastic waves. Dinwoodie (1968) reported the existence of such crystalline slips in spruce timber under external compression. Siau (1984) reported that the proportion by mass of cellulose in normal wood (as opposed to tension and compression wood) was remarkably constant and apparently independent of species. Further, the proportion of crystalline cellulose is also relatively constant (Siau 1984). This appears to be directly related to the remarkably constant AE rate measured at the onset of surface checking in this study.

This finding led to the measurement of acoustic emission in other species. It was hoped that the same AE rate would be measured at the onset of checking in different woods. Acoustic emission was measured in backsawn radiata pine (*Pinus radiata*) and myrtle (*Nothofagus cunninghamii*). The acoustic emission measured in radiata pine was significantly different from the acoustic emission measured in the eucalypt material, with relatively

'massive' AE rates detected in boards free of seasoning degrade. This behaviour was attributed to brittle failure in the resin canals, structural elements not present in the eucalypt genus. The characteristic AE responses measured in drying myrtle boards resembled the behaviour measured in the eucalypt boards, apparently due to the more similar structure. Surface checking was detected at approximately the same AE rate as that measured in the eucalypt boards.

Much of the improved understanding of the acoustic emission phenomenon developed in this study was facilitated by the existence of a one-dimensional nonlinear drying model developed by Oliver (1991). Oliver wrote KILNSCHED (KILN SCHEDULING PROGRAM), a computer program based on this model, which simulates the drying behaviour of a single board, with arbitrary bulk material properties, subject to arbitrary drying conditions. KILNSCHED is particularly suited to low temperature drying of eucalypt materials. Kiln drying trials quickly revealed that 'green' Tasmanian eucalypt boards invariably suffered surface checking within 24 hours when subject to drying temperatures as low as 23°C dry bulb temperature and 21°C wet bulb temperature (at 0.5 m/s airspeed). Such temperatures are significantly lower than those often employed in drying material direct off-saw in the timber industry but none-the-less are considered 'harsh' in this study.

At the commencement of this study, KILNSCHED was used in a purely predictive mode to assess drying schedules prior to drying. The author of this thesis modified KILNSCHED to simulate drying using the real-time drying temperatures measured in the experimental kiln. This allowed measured acoustic emission during drying to be compared with the drying behaviour calculated with KILNSCHED. This modification revealed that Tasmanian eucalypt timber is far more sensitive to small temperature *fluctuations* than was previously expected. The reader must keep this material sensitivity to temperature and temperature change in mind at all times when reading this thesis.

The AE rate measured during drying was successfully related to the instantaneous strain at a board surface calculated with KILNSCHED using the measured drying conditions. Instantaneous strain is the strain component employed as the failure criterion in the drying model. This

enabled the author to place considerable confidence in behaviour calculated with KILNSCHED and the 'optimum drying' program SMARTKILN discussed below.

This author modified KILNSCHED to incorporate an optimisation algorithm that determined the optimum drying conditions required to dry the timber in the minimum time at a preset arbitrary maximum surface instantaneous strain. The resulting program, SMARTKILN, develops drying schedules to maintain the calculated surface instantaneous strain at a preset 'Control Strain' below the ultimate surface instantaneous strain. Together, SMARTKILN and acoustic emission measurement form the basis of Clever Kiln Controller®, a kiln control system to dry Tasmanian eucalypt timber in the minimum time with minimum degrade.

In Clever Kiln Controller, SMARTKILN uses datalogged real time drying conditions to simulate the drying behaviour of a sample board in the kiln. Calculated drying behaviour is continuously compared with measured drying behaviour (measured AE rate and moisture profiles measured by regularly slicing sample boards). Provided the calculated and measured drying behaviour are satisfactorily matched, the optimum drying schedule developed by SMARTKILN is applied to the kiln. When the AE rate approaches the AE checking threshold, the drying conditions are automatically ameliorated to prevent surface checking. Subsequently, SMARTKILN develops a refined optimum schedule to incorporate the new datalogged drying conditions.

This study has developed the understanding of acoustic emission from the existing (often misleading) information recorded in the literature to a level that could be incorporated with current knowledge of the behaviour of drying timber. The thesis describes how this was achieved. Various aspects of the understanding have been reported in papers published, in press or under review.

The final result is the development of a commercial kiln controller which is described and already implemented in some selected experimental kilns at present restricted to eucalypt materials.

Additional Publications

The following papers were published or were in press at the time of submitting this thesis :

1. Booker J.D. 1994. Acoustic emission related to instantaneous strain in Tasmanian eucalypt timber during seasoning. Wood Sci. Tech. 28(4):249-259.
2. Booker J.D. 1994. Acoustic emission and surface checking in *Eucalyptus regnans* boards during drying. Holz Roh Werkstoff. (accepted for publication)
3. Doe, P.E.* , Oliver, A.R** . and Booker, J.D. (1994) 'A non-linear strain and moisture content model of variable hardwood drying schedules'. Paper presented at 4th International IUFRO wood drying conference, Rotorua, NZ, August 9-13 1994
4. Booker J.D. 1995. Optimum drying schedules for Tasmanian eucalypt material calculated with a one-dimensional nonlinear drying model. Wood. Sci. Tech. (accepted for publication)
5. Booker J.D., Doe P.E. 1995. Acoustic emission related to strain energy during drying of *Eucalyptus regnans* boards. Wood. Sci. Tech. (submitted for publication)
6. Booker J.D. 1995. Optimal drying of Tasmanian eucalypts using acoustic emission and an online drying simulation program. Wood. Sci. Tech. (submitted for publication)

* Associate Professor of Mechanical Engineering, University of Tasmania

** Emeritus Professor of Civil and Mechanical Engineering, University of Tasmania

Acknowledgements

The author gratefully acknowledges the support of the following companies and individuals throughout the project :

Associate Professor Peter Doe, supervisor, for his excellent advice and enthusiasm throughout the study.

Emeritus Professor Arch Oliver, associate supervisor, for his wonderful guidance and support.

Trevor Innes, post-graduate coworker, for his advice and enthusiasm.

Australian Furniture Research and Development Institute, for financial assistance during the project.

McKay's Sawmill, for generously donating timber and their overall support of the project.

My family and friends, and Sue in particular, for their patience and understanding. Special thanks to Dad for your support.

This project was undertaken with the assistance of an Australian Postgraduate Research Award (Industry).

Chapter 1

Seasoning

The process of removing moisture from saturated or 'green' timber is known as 'seasoning'. The typically high shrinkage and low mass diffusivity of Tasmanian eucalypts make the material extremely difficult to season without degrade, especially backsawn boards. This refractory seasoning behaviour means the majority of Tasmanian eucalypt is seasoned as structural grade timber rather than high quality furniture grade material (market demand also controls the industry seasoning practices). Moderate (and thus slower) drying schedules must be employed to season furniture material and this strategy has typically been considered to be uneconomic in the past. However, the value adding potential of the furniture material means this philosophy is rapidly changing. This chapter commences with a basic introduction to timber seasoning. The chapter introduces the concept of 'optimum' drying to reduce drying times and improve seasoning productivity and concludes with a discussion of the basic requirements of an automatic 'optimal' kiln control system.

1.1. Moisture and shrinkage

The eucalypt material dried in this project typically had initial moisture contents (on a dry-mass basis) in the vicinity of 80% and higher. Softwood trees such as radiata pine typically contain a high proportion of sapwood with significantly different initial moisture content and permeability to the heartwood. This leads to significantly different drying behaviour within an individual board and consequently often causes seasoning degrade. Tasmanian eucalypt logs, by comparison, are predominantly heartwood with a very narrow sapwood band which is effectively removed during the sawing process.

Saturated or 'green' wood contains bound water and free water, as described by Tiemann (1906). The bound water is mechanically adsorbed to the solid components of the cell walls, usually by hydrogen bonding, whereas the free water resides within the cell lumen and is not so bound. During seasoning, free water evaporates before the bound water because more energy is

required to remove the latter from a cell. When all the free water has been removed, leaving only bound water, the wood is said to have attained Fibre Saturation Point (FSP). No such clearly defined point exists during the drying process but FSP is a useful starting point in discussing the behaviour of wood during seasoning. Seasoning is performed until the moisture in the timber is in equilibrium with the surrounding atmosphere, a moisture content known as Equilibrium Moisture Content (EMC).

Above FSP, the free moisture is removed from the cell lumens without affecting the cell dimensions and no bulk shrinkage occurs. Below FSP, the bound moisture diffuses from the amorphous regions of the cellulose microfibrils comprising cell walls (the detailed structure of cell walls is discussed in 3.3) and the cell walls contract at nearly constant lumen volume (Chafe et al. 1992). The bulk specimen shrinks with a volumetric shrinkage roughly equal to the volumetric strain caused by the removal of the bound water (Oliver 1991). Shrinkage typically increases nearly linearly with moisture loss between FSP and EMC. The majority of microfibrils in a typical cell wall lie nearly longitudinally, meaning the bulk longitudinal shrinkage is generally negligible but the transverse shrinkages are significant.

This description of moisture loss and shrinkage is based on the idealised case discussed by Tiemann (1906) where no shrinkage occurs above FSP. Such shrinkage is termed 'normal shrinkage'. An abnormal form of shrinkage known as 'collapse shrinkage' does occur above FSP in various species, particularly the low to medium density Tasmanian eucalypts. Hydrostatic tension is induced in the moisture within cell lumens as the timber dries and regions of cells, depending on the wall stiffness and lumen size, may suddenly collapse when the compressive stress in the fibre walls exceeds the buckling strength. Collapse shrinkage induces surface and internal checking and is discussed in more detail in 1.3.2.

1.2. Processing logs into sawn boards

The significant cross-sectional variation in wood structure leads to different moisture flow rates and bulk material properties in the three principal directions i.e. the radial, tangential and longitudinal directions with respect to the tree. The radial and tangential directions are of particular interest

during seasoning since longitudinal shrinkage and moisture loss are generally negligible.

There are two basic cutting patterns by which sawn boards are obtained from a log :

- quartersawing, in its simplest form, involves 'quartering' the log and then cutting boards from the resulting flitches with wide faces parallel to the faces of the quarters. The wide board faces predominantly lie in the radial direction with respect to a tree cross-section.
- backsawing involves cutting the log to produce boards with the wide faces lying tangential to the growth rings.

In practice, a sawmiller often combines these strategies to best utilise the timber in a particular log.

Processing backsawn boards is desirable because :

- the conversion of a given log is between 8 and 12% more efficient on a volume basis when it is processed into backsawn boards than when it is processed into quartersawn boards. This increased yield becomes increasingly significant with decreasing log diameter.
- the faces of backsawn boards cut from trees that have not grown perfectly straight may be heavily 'figured' whereas the quartersawn boards will possess faces with straight grain patterns. This aesthetic characteristic is particularly desirable when the material is used in furniture applications.
- the maximum width of quartersawn board that can be cut from a log is less than half the log diameter, because of the unusable heartwood.
- backsawn boards dry faster than quartersawn boards because rapid moisture loss occurs through the radially orientated medullary rays (rays are described in 3.4).

However these economic advantages are often outweighed by the more refractory seasoning characteristics of backsawn boards. Bulk tangential

stiffness is nominally half the radial stiffness in the Tasmanian eucalypts i.e. the timber is stiffer when loaded radially rather than tangentially. Bulk stiffness defines the stress~strain behaviour of a material under load and ultimate strength is nearly linearly related to stiffness, as discussed in 3.5. Bulk tangential shrinkage is typically twice the radial shrinkage. The combination of reduced tangential strength and greater tangential shrinkage means backsawn boards are particularly prone to seasoning degrade during drying. Campbell and Hartley (1978) reported that 'it has been traditional practice in Victoria and Tasmania to quarter-saw Ash eucalypt timber for use as flooring, mouldings and joinery'.

1.3. Seasoning degrade

Tasmanian eucalypt boards experience relatively high transverse shrinkage with moisture loss. Tasmanian eucalypts also possess very low diffusivities at the temperatures employed in kiln drying 'green' material, meaning moisture diffuses from the saturated centre regions to the relatively dry surface regions very slowly. This induces high *differential* shrinkage between the rapidly dried surface fibres and the saturated interior fibres. Differential shrinkage describes the *differential* in shrinkage at various sections of the board thickness. Differential shrinkage causes a tensile surface stress since the surface fibres are restrained by the still-saturated board centre. This surface tensile stress eventually surface checks when the surface stress exceeds the ultimate material strength. Schaffner (1981) defined checks as 'cracks or fissures in wood fibre running in the longitudinal direction but not extending through the piece from one surface to another'. The initially small checks extend with drying due to the stress concentrations at the sharp check tips. These checks dramatically reduce the value and strength of the seasoned boards. Internal checks may also occur during the seasoning process. While these are invisible at the surface, they significantly reduce material strength and cause machining problems when the material is used in furniture applications. Surface checks and internal checks are known as seasoning degrade.

Surface and internal checking are related primarily to excessive *differential* shrinkage within a drying board. Even if relatively high, uniform shrinkage occurred through an entire board, no differential shrinkage would exist and surface checks would not occur. As discussed below, the processes of surface

and internal check formation appear to be rather more similar than was previously thought.

1.3.1. Surface checking

The moisture gradient at a board surface (the slope of the moisture content profile at a board surface) directly controls the development of surface stress and instantaneous strain. Campbell (1959) and Christensen and Neylon (1979) reported that the development of stress due to differential shrinkage is a direct effect of the moisture gradients in the timber. The differential shrinkage between the surface fibres and the internal regions increases as the surface moisture gradient steepens and thus the likelihood of surface checking increases markedly when steep moisture gradients are induced during drying.

In conventional drying processes, the surface of a board dries far quicker than the internal regions and a moisture gradient forms between the surface and the core. The surface fibres commence to shrink once the surface moisture content attains FSP (provided collapse shrinkage has not occurred). However, the centre is still effectively saturated and has not started to shrink. The surface shrinkage is restrained by the bulk of the board and a relatively large tensile stress forms across the board surface, with balancing compressive stresses within the board. In other words the drying stresses are due to the difference between the 'free' or unconfined shrinkage and actual shrinkage in the surface fibres. The stress distribution through the board in the early stages of drying may be visualised as a very narrow zone of tensile stress at the surface, with the crossover point to compression (a plane of zero stress) just below the surface and a deep compressive stress field ranging into the centre of the board. The surface tensile stress causes a tensile instantaneous strain to act at the surface. Instantaneous strain is equivalent to the strain measured in a timber specimen, at constant moisture content, in a short term loading test. A detailed description of instantaneous strain is presented in detail in 5.3.2.

With drying, the surface attempts to shrink further as the surface moisture content approaches EMC. The increasing differential shrinkage between surface and core causes the surface stress and instantaneous strain to increase. When the drying conditions are sufficiently severe, the surface

stress exceeds the material strength and a surface check forms to relieve the applied stresses. The generation of new surfaces at the check site consumes material strain energy as surface energy, and this decrease in the local strain energy constitutes a decrease in the local tensile stress field. The check immediately runs into the board until it attains a depth at which the stress is sufficiently low that the material can withstand the combined tensile stress and the stress concentrations at the tip of the check without further stress release (possibly where the material is behaving in an elastic manner). Check propagation is then temporarily arrested.

With further drying, internal regions that were initially under very low tensile stress or even compressive stress attain FSP and commence to shrink. The surface tensile stress increases, causing new surface checks to form, and existing checks propagate deeper into the board.

Apart from the 'shrinkage strain' and 'instantaneous strain' discussed so far, two time-dependent strain components act during drying. The 'creep' and 'mechano-sorptive effect' are related to dimensional changes in wood under load alone and in wood subject to simultaneous changes in load and moisture content respectively. These components and their relative effects on the overall net shrinkage during drying are discussed in detail in 5.3. The surface creep and mechano-sorptive effect result from the surface tensile stress and thus initially act in the same direction as the instantaneous strain. Hence, at the commencement of drying the instantaneous strain, creep and mechano-sorptive effect all act in the opposite direction to the shrinkage. The prolonged effect of a high tensile surface stress means the time-dependent strain components eventually reduce the instantaneous strain in the surface fibres. Furthermore, board centres eventually attain FSP and commence to shrink. This induces a decrease in the compressive stress in the interior of a board, resulting in a decrease in the tensile stress at the surface. The combined effect of the increasing creep and mechano-sorptive effect and decreasing centre stress result in unloading of the surface fibres. This eventually produces a complete stress reversal through the board. The surface fibres enter compression and the interior fibres enter tension to maintain the condition of static equilibrium that there be no net force on any section. Surface checks are forced closed by this stress reversal. However, staining processes applied during furniture manufacturing reveal the compressed surface checks as unacceptable dark lines on board faces.

Surface checking is also induced by underlying collapse shrinkage and this phenomenon is discussed in detail in 6.5. Briefly, localised collapse shrinkage increases the local differential shrinkage between the surface fibres directly above the collapse and the surrounding fibres and surface checks result.

1.3.2. Internal checking

Internal checking induced by collapse is particularly common in Tasmanian eucalypts, especially at elevated temperatures. Tiemann (1915) was the first to distinguish normal shrinkage from collapse shrinkage. The phenomenon has subsequently been extensively researched in the last fifty years, especially in Australia (Kauman 1964, Chafe et al. 1992). Whilst it is conceivable that internal checking is due to internal tensile stresses exceeding the material ultimate strength after stress reversal, hydrostatic tension is generally accepted as the primary contributory factor. Numerous KILNSCHED simulations revealed that the maximum internal tensile stress never exceeded the ultimate strength.

Consider a fibre lumen completely filled with free moisture with no air bubbles. The water can escape through the small interstitial pores in the cell wall connecting overlapping fibres or by diffusion through the cell walls (wood cell structure is discussed in detail in Chapter 3). When a meniscus forms at the air-water interface in a pore, a hydrostatic tension force is induced in the water (Tiemann 1915). This tension induces a compressive stress in the fibre wall. If, in the water, there exists a nucleus about which a vapour bubble can form, and there are sufficient gas molecules in the local vicinity, a bubble will form and relieve the tensile stresses. However, when the fibre is sufficiently small that a bubble cannot form the compressive stresses in the wall increase.

It is likely that the compressive stresses initially cause the cell walls to contract without catastrophic deformation. However, the compressive stresses eventually exceed the wall buckling strength and the fibre suddenly collapses to a new configuration in which the internal tension can be resisted by the fibre wall. The stress field redistribution resulting from the collapse of

this fibre probably causes neighbouring fibres near the critical collapse condition to collapse in sympathy.

During drying, collapse can not occur in surface fibres because these are damaged by the saw and thus lose all free moisture rapidly. However fibres just below the surface are intact and these are the first to lose sufficient moisture for hydrostatic tension forces to grow. Differential shrinkage exists between a region of collapsed fibres and the intact surrounding fibres. When the local stress exceeds the local material strength, internal checks form as stress release mechanisms. Internal checks propagate radially through a board because the radial-longitudinal plane is the weakest plane in the timber structure. Check initiation and propagation are discussed in detail in 6.1 and 6.7. Collapse induces seasoning degrade and must be avoided when drying material for furniture applications.

1.4. Seasoning

Most practical wood applications require the wood to be dried to EMC. Seasoning ensures that the wood is as dimensionally stable as possible in its working environment. Seasoning significantly increases mechanical properties such as compressive strength, bending strength and the modulus of elasticity of most species. Seasoning produces a less dense product and board surfaces that are far more receptive to coating and painting. Seasoning is also required before various preservative treatments can be applied.

The following discussion is relevant to eucalypt seasoning strategies employed in Tasmania.

Air dried timber is typically stacked in the open air without roofed cover and the combined drying effect of the sun and wind remove the moisture. Air drying is relatively slow because the drying temperature is restricted to the atmospheric temperature and moisture is re-absorbed during rainy periods. Air dried Tasmanian eucalypt species typically require 12 months per 25mm of board thickness before moisture gradients are within acceptable limits. Air drying involves minimal capital investment and low operating costs. However slow drying practices introduce the high opportunity cost of a full yard of timber (the potential value of the timber dried to a very high quality, not the price paid by the sawmill for the logs).

In general, surface checking is most likely to occur during the early stages of drying when the centre sections are at a high moisture content and thus particularly steep moisture gradients exist at board surfaces. Curing sheds are becoming a popular predrying technique for higher quality material. The sheds protect the green timber from direct sunlight and rain and excessive wind and retard the formation of excessive moisture gradients. The evaporation occurring within the sheds maintains the air temperature below the ambient temperature, promoting slow surface drying and thus less steep moisture gradients. The initially saturated off-saw boards lose moisture readily without external heat input (except that provided by the atmosphere). Generally board centres commence to lose moisture after six to eight weeks and moisture gradients decrease, diminishing the likelihood of surface checking. After several months in the sheds, the partly dried boards are relocated in the open air or kiln dried.

Moisture in timber becomes progressively harder to remove with decreasing moisture content, so kilns are employed for high-temperature 'final drying'. Ideally, high temperature final drying (drying at temperatures in excess of 60°C) should not be performed until the *core* moisture content approaches FSP because at that point all the free moisture has been removed and collapse shrinkage is prevented. In practice, the core loses moisture very slowly at low temperatures and financial constraints cause final drying to be introduced when the *average* moisture approaches FSP. When incorporated with air or shed predrying, kiln drying produces vastly reduced drying times (say 2-3 months per 25mm thickness from green).

Tasmanian eucalypts are generally not kiln dried from green because surface checking is so prevalent in the early stages of drying that very mild drying conditions are required. Furthermore, this study revealed that collapse is induced in green Tasmanian eucalypt material at temperatures not much greater than 22°C. It is generally deemed uneconomic to run kilns at such low temperatures when natural drying is so effective, at least in the first weeks after sawing. However, kiln drying theoretically provides far more accurate control of the drying conditions and thus naturally allows higher quality of the dried end product.

Air drying is commonly considered to be cheaper than kiln drying because large capital investments in equipment and kiln operating costs are avoided. However, this philosophy ignores the opportunity cost of degrade (the cost of not producing the highest quality material seasoned in kilns with accurate temperature control) and the opportunity cost of large quantities of air-dried timber sitting in the sawmill. The primary purpose of seasoning research is to 'optimise' the drying process and thus reduce the overall cost. Optimal drying is defined as seasoning timber boards to a specific moisture content in the minimum time with minimum degrade at the minimum cost.

In practice, optimum seasoning criteria depend on the intended end use of the dried material. The market value of structural material is relatively low so economic constraints determine that such material be dried at the minimum cost with little emphasis placed on preventing degrade, within acceptable limits. Furniture grade material on the other hand must be seasoned without degrade. This project concentrates on optimising the seasoning of furniture grade material to take advantage of the value adding potential and premium prices of such material.

1.5. Optimum drying

Significant research efforts have been directed towards improving the seasoning productivity of Tasmanian eucalypt species, especially by the Commonwealth Scientific and Industrial Research Organisation, Division of Building Research (CSIRO). Schaffner (1981) reported that the CSIRO evaluated experimentally the effects of numerous treatments to improve the drying process. These methods included more accurate control of drying conditions, physical treatments intended to modify the behaviour of the timber during drying (such as pre-steaming), chemical treatments designed to penetrate the wood and adjust the drying behaviour (such as moisture gradient control) and surface treatment (to reinforce surface fibres or provide vapour barriers). Schaffner (1981) reported that some of the treatments showed promise during initial testing, but none could be extended to commercial viability.

Schaffner (1981) developed and refined a 'pre-surfacing' treatment to maintain the surface fibres in drying boards above FSP for a sufficiently long period to prevent the formation of steep moisture gradients and thus limit

differential shrinkage. Schaffner used a semi-permeable membrane (PVC) glued to the surface of a board fresh off-saw. The moisture transfer characteristics required of this membrane coating were accurately determined. The process was commercialised and used successfully by one large sawmill in Western Australia in particular. This 'plastic wrap' process successfully reduced seasoning degrade but did not optimise the drying process because the drying rate was significantly reduced by the permeable coating. An optimal seasoning strategy dries the timber as fast as possible without allowing seasoning degrade.

An inherent disadvantage of treatments such as the 'plastic wrap' process is that it is applied to all material, regardless of the relative 'seasonability' of that material. In other words, a relatively expensive treatment will frequently be applied to batches of material that subsequently turn out to be particularly easy to season. Similarly, empirical schedules developed for generic thickness and grade material are inherently conservative. Ideally, a drying regime will be specific to the particular material in the kiln; online feedback measurements would indicate the refractory nature or otherwise of the material and the kiln control system would implement an appropriate schedule. Such a control system requires a real-time feedback measure of the drying behaviour and a simulation model to calculate an optimum drying schedule.

Vermaas et al. (1993) developed an online drying model of moisture movement to monitor the development of the moisture gradient in a sample drying board. A critical gradient was selected prior to drying and the drying conditions were continuously adjusted to maintain the gradient below this critical gradient. This strategy successfully reduced drying time but did not optimise the drying process because the critical moisture gradient constraint employed was "only tentative and not necessarily optimal".

Clearly, seasoning degrade and drying time are intimately related to the moisture gradient at a board surface. However, optimum drying control should be implemented in terms of stress feedback directly rather than moisture gradient feedback as surface check development is the constraining factor in the seasoning process, in Tasmanian eucalypts at least. Vermaas (1992) reported that "actual wood characteristics or processes occurring during drying are not taken into account", primarily because "current

measurement techniques do not allow continuous and non-destructive monitoring of the stress condition".

Acoustic emission has been measured in timber subject to external load and drying stresses in a wide range of studies performed in the last 30 years (Miller 1963, Porter et al. 1972, Ansell 1982, Noguchi et al. 1987, Quarles 1992). Acoustic emission results from transient elastic stress waves generated by intermittent, localised sudden redistribution events in a solid material under load. Acoustic emission is measured with sensitive accelerometers or transducers clamped hard to a board surface. Provided the acoustic emission represents stress redistribution events that precede material failure (surface checking) and allows subsequent preventative action to avoid checking, it might satisfy the requirements of an optimum kiln control system. Various researchers have measured acoustic emission during drying to assess the affect of varying climatic conditions. Becker (1982) and Noguchi et al. (1987) reported that the acoustic emission generated in sample boards during drying was suppressed by an increase in relative humidity and activated by a decrease in relative humidity. Provided some relationship exists between measured acoustic emission and the development of surface checks during drying (and thus the magnitude of the surface stress), a basic control system might prevent surface checking by adjusting the drying conditions when the acoustic emission approaches a preset level below the critical level corresponding to surface check development. However, the condition change applied would be arbitrary and might significantly reduce the drying rate when a more moderate change may have sufficed. Thus surface check control with acoustic emission alone would not optimise the process.

An accurate online drying model is required to optimise the temperature and humidity changes applied during seasoning. The model would use measured material properties and the measured kiln temperatures to simulate the historical drying behaviour of the particular material in the kiln. Provided the calculated behaviour accurately matched measured drying behaviour, the model would subsequently simulate purely theoretical drying conditions to determine the optimum schedule based on suitable 'optimisation' criteria. Oliver (1984, 1991) developed a nonlinear moisture and stress model of low temperature timber drying suitable for the Tasmanian eucalypt material. A computer program based on this model was

employed by Wu (1989) to accurately predict the time of surface checking in trials performed over periods of weeks. Hence this program was incorporated into this project.

At present, no *economic* means of seasoning backsawn Tasmanian eucalypt material is commercially available; such boards are either seasoned under such mild conditions that drying times are uneconomic or unacceptable degrade occurs under schedules aimed primarily at producing structural grade material. The economic incentives detailed in 1.2 and the ever increasing proportion of small-diameter regrowth logs being felled means it is critical that seasoning strategies be refined to improve the seasoning productivity of backsawn Tasmanian eucalypt boards.

The aim of this study was to develop an automatic kiln control system to dry backsawn furniture grade Tasmanian eucalypt timber in the minimum time with minimum drying degrade. The resulting system, known as Clever Kiln Controller® (CKC) incorporates acoustic emission as the feedback measure of surface stress and an online drying simulation program to determine the optimum schedule for the particular batch of timber in the kiln. By developing the system for difficult to season backsawn furniture grade material, we ensure the system is applicable to quartersawn boards and material of lower quality with some allowance for degrade as defined by the relevant grading rules.

Chapter 2

Literature Review

The pioneering acoustic emission research with timber was performed on seasoned boards under external load. Wood material was presumed to contain a large number of inherent microscopic flaws such as fibre ends or ray crossings. These microfailures or microfractures were considered to initiate during tree growth or processing. Material fracture under load was considered to consist of two phases, slow or stable extension of the microfractures and eventually catastrophic failure when a critical stress condition and microfailure size occurred. The acoustic emission measured during loading was considered to be due to the extension of these microfailures. This originally led to this author's misconception that the acoustic emission measured during seasoning was due to the extension of microflaws but subsequent detailed analysis resulted in the hypothesis that acoustic emission was generated by intermittent crystalline slips within fibre walls. Differences in data acquisition hardware and data analysis techniques used by researchers mean caution must be applied in comparing results in different studies, particularly in light of the very high amplifications used in acoustic emission data processing. This literature review is interspersed with comments from this author where it is considered useful in the development of the hypothesis that crystalline slips cause the acoustic emission.

'AE rate', 'ringdown counts' and 'AE count rate' are analogous terms referred to throughout the literature. AE rate is used in this study and is defined in detail in 4.1 but a brief introduction is presented here as a prelude to the data acquisition and terminology employed in the studies described below. The amplified acoustic emission transducer output is compared with a preset, constant threshold voltage and a 'count' is recorded each time the threshold is exceeded during a discrete time-period (a particularly energetic AE burst might cause several counts to be recorded). The number of threshold crossings during the period is referred to as the AE rate. AE rate therefore is not representative of the magnitude of the peak acoustic emission burst but rather indicative of the amount of high-energy acoustic emission activity recorded during the time-period.

Considerable work has been performed with acoustic emission generated in various man-made materials (Harris et al. 1972, Ravenhall 1977, Rotem et al. 1979). However, the following literature review is restricted to acoustic emission measured in timber.

2.1. AE in specimens under external load

Miller (1963) recorded sounds generated in clear 1 x 1 x 16 inch maple specimens tested to failure in static bending. Acoustic emission was measured with a contact microphone attached to the specimens and the sounds were recorded on a tape recorder. It was suspected the pitch and/or tone of the sounds generated under load might change as the specimen approached failure, providing a potential warning of failure. However, the fundamental frequency of the sounds remained essentially constant with increasing load to destruction. In 53% of the specimens, the first detectable sound coincided with ultimate failure. Of those that produced early sounds, 81% emitted sound only above 95% of the ultimate load. It was concluded that no change in the sound pitch or tone occurred during loading and no distinct warning of imminent failure was generated.

Debaise et al. (1966) employed a piezoelectric crystal, an amplifier, a band-pass filter and electronic counter to detect acoustic emission bursts when flaws enlarged in Western White pine specimens under various types of external load. This hardware was considerably more sensitive than that used by Miller (1963). Acoustic emission was generated by loading at a constant rate of deformation under compressive, tensile and flexural conditions. Creep, relaxation and cleavage testing were also investigated. One count was accumulated for each acoustic emission burst with an amplitude greater than about twice the background noise.

Flaw growth was detected at stresses between 5 and 25% of the ultimate stress in the parallel and perpendicular to grain tension tests. Fewer acoustic emission were detected during compression loading. This was considered to be due to the compression loads closing intrinsic flaws. Flexural creep tests revealed the acoustic emission increased in a stepwise manner, due to irregular flaw growth. Local stresses attained above-average values and flaws propagated beyond the high stress region where they were arrested. A period of relatively low acoustic emission activity followed before

microcompression failures caused tensile stresses to exceed the local strength in another region and further flaw extension occurred.

When specimens in the constant rate of deformation tests were loaded to 50% ultimate stress and then unloaded, acoustic emission activity ceased during the unloading. Negligible acoustic emission were recorded during reloading until the previous maximum stress was attained. The irreversible nature of acoustic emission in various materials was reported by Kaiser (1950).

Wood failure was described as a fracture process consisting of the initial growth of intrinsic flaws that developed during the seasoning process. These flaws are initiated at low stress and extend short distances in a stable manner until they enter a neighbouring zone of lower stress or greater fracture resistance where they are retarded. With further loading, the available strain energy was sufficient to sustain rapid or unstable fracture, reflected by a sudden drop in the applied load. This fracture mechanics approach lead to an analysis of the strain energy release rate in the opening cleavage mode of fracture.

Initiation of unstable crack extension was not consistently associated with anatomical features. Microscopic investigation of crack surfaces revealed that cracks initiated most often at a minor discontinuity in the orientation of the tracheids, especially at ray crossings and tracheid ends.

Adams (1969) used acoustic emission to investigate crack growth in Douglas-fir, western Hemlock and western red cedar beams stressed in three-point bending. The acoustic emission sensor was not clamped directly to the specimen surfaces but rather to a steel block embedded in the surface. Specimens tested were clear or contained knots and seasoning checks to investigate their effect on the generated acoustic emission. Acoustic emission was assumed to emanate as a by product of flaw growth and thus the acoustic emission pattern reflected the microfailure development. Observation of the proportional limit at approximately the same time as a marked increment in AE rate provided evidence that the proportional limit was at least in part associated with microfailure development. Further, the entire load-deflection curve was surmised to be linked to microfailure development. During preliminary testing, when a stressed specimen was unloaded before failure, then reloaded, fewer acoustic emission were

detected until the load approached the previous maximum. Material failure was generally heralded with an increase in AE rate but this feature was inconsistent and frequently too late to be useful in failure prediction.

Porter et al. (1972) used acoustic emission to estimate the ultimate bending strength of Douglas-fir finger joints to within $\pm 10\%$ by loading just past the proportional limit. Acoustic emission was considered to be due to the stable growth of inherent flaws. Failure in wood was reported to occur in two distinct phases, the phases separated by the proportional limit. Initially, flaws redistributed the increasing load as regions of high stress concentration formed in localised regions. At a load slightly below the proportional limit, the number of microfailures increased due to the inability of the material to sufficiently accommodate the rising stress concentrations. In beams tested in flexure, the micro-failure rate increased near the proportional limit. Catastrophic failure occurred when a microfailure reached a critical size for the imposed stress condition and a crack propagated through the specimen.

Ansell (1982) related the acoustic emission-strain characteristics of Parana pine, Douglas Fir and Scots pine specimens tested in tension to mechanisms of deformation observed by scanning electron microscopy. Acoustic emission-strain curves comprised sharp vertical increases interspersed with more gradual accumulations of counts. Slow AE count were attributed to 'the gradual opening of microflaws as the helically wound cellulose wall reinforcement extends elastically within the matrix of hemicellulose and lignin'. Rapid increases were assigned to either interlaminar shear in planes of weakness or to brittle failure of tracheids. The cumulative count at failure was very nearly constant within each species, but failure strains within species showed some scatter. Species with greater latewood/earlywood variations (lumen size, wall thickness and so on) generated higher cumulative acoustic emission.

Ansell reported that 'wood has a close to linear stress~strain curve right up to failure'. This author proposes that the stress concentrations at a minor flaw in tension tests such as these may lead to catastrophic failure when the material has not progressed significantly beyond the proportional limit. Oliver (1991) proposes that in the seasoning situation, a minor flaw redistributes the local stress field without much affecting the overall stress fields, as discussed in 3.6. As a result, board surfaces progress well into the

nonlinear range of the stress~strain curve before catastrophic failure (surface checking) occurs. The author of this thesis concludes that acoustic emission and acoustic emission-strain characteristics measured in tension tests are not directly applicable to the seasoning situation since material fails in tension tests before extending significantly along the non-linear section of the stress~strain curve.

Sato et al. (1984) used the acoustic emission measured during parallel to grain tensile testing to estimate the tensile strength. The AE cumulative count was proportional to the square of the stress and up to a limiting stress, the AE cumulative count at failure had a negative correlation with the strength of the wood. Two types of acoustic emission were detected, 'slow AE' reported to be generated by the opening of microflaws and 'fast AE' considered to correspond to a property like ductility in the fracture process of wood.

Quarles (1988) measured burst type emissions generated by pencil lead breaks in solid wood samples to determine attenuation effects. In samples with growth ring curvature, acoustic emission signals propagated into the convex face were significantly greater than those generating into the concave face. Otherwise, acoustic emission propagation was relatively insensitive to changes in transverse grain directions. Propagation in the transverse grain direction was relatively insensitive to changes in moisture content, except at the saturation moisture condition, where significantly lower acoustic emission was recorded.

Rice and Skaar (1990) monitored the acoustic emission generated at the lower surfaces of small tangential red oak wafers experiencing failure perpendicular to the grain under third point loading. This loading technique was used because the surface failures were similar in form to surface checks produced during drying.

Green wafers at 90% moisture content generated no acoustic emission until the material entered the nonlinear region of the load-deflection curve. Partially dried wafers produced acoustic emission from the commencement of loading. Rice suggested this behaviour supported the proposition that a major cause of acoustic emission during drying is shrinkage at the cellular level, with moisture loss within the cell wall leading to delamination or

microchecking between the cell wall layers and consequent acoustic emission. The green material load-deflection curve contained a well defined linear section whereas the curves measured in the partially dried wafers were nonlinear from the commencement of loading. The nonlinear behaviour was related to the presence of the microchecks.

This author contends that it is possible the predried material was simply prestressed beyond the proportional limit during the drying process. Subsequent loading caused the material to continue to load along the nonlinear portion of the stress~strain curve.

Molinski et al. (1991) reported that the acoustic emission measured in small *Pinus silvestris* L. samples during soaking was discrete or intermittent. The number of acoustic pulses was reduced by 30 to 85% when the wood swelling was totally mechanically restrained in the radial and tangential directions respectively. The primary acoustic emission source was determined to be radial cracks in the wood tissue unpenetrated by water.

The threshold voltage or discrimination voltage was set to prevent liberated air bubbles from being recorded. Acoustic emission became clearly pronounced only after a certain amount of swelling, corresponding to the lag time required to cause high tensile stresses in specimen interiors.

2.2 Acoustic Emission in drying specimens

Noguchi et al. (1980) measured acoustic emission in drying oak and birch samples. The rate of acoustic emission generation was determined to be related to species; under the same drying conditions, wood more prone to checking produced a higher AE rate than less refractory species. Drying stresses were determined to play a greater role in acoustic emission generation than thermal stresses because the AE rate was not increased by an increase in temperature but was increased by a decrease in humidity and suppressed with an increase in humidity.

A critical finding of the investigation reported here is that there is no direct relationship between AE rate during drying and *relative humidity*. AE rate is in fact related to the absolute humidity of the air or more precisely the differential between the moisture concentration at board surfaces and the

concentration of the moisture in the air (in effect the absolute humidity) outside the boundary layer. The greater this differential, the greater the surface drying rate and the larger the differential shrinkage between board surface and core. This differential shrinkage creates large tensile surface stresses (as described in 1.3.1) and high rates of acoustic emission activity. A detailed description of the interaction of air temperature, air absolute humidity and AE rate is presented in 7.2.5. The literature concentrating on relative humidity is quite misleading in this regard. This misconception probably stems from the fact that at constant temperature an increase in relative humidity also constitutes an increase in absolute humidity, and many studies reported in the literature are based on single temperature drying conditions.

Becker (1982) investigated the relationship between drying conditions and acoustic emission measured in small end-grained and straight-grained specimens of Scots pine. During drying, the AE rate generally increased rapidly to a maximum rate and then decreased more slowly towards zero as drying equilibrium was attained. A positive relationship between the severity of the drying conditions and the rate of acoustic emission during drying was reported. The aim of Becker's study was to develop a technique in which the drying was controlled by the acoustic emission generated in a sample board.

Noguchi et al. (1983) detected acoustic emission during drying of oak, beech and birch and determined that oak, being more prone to checking, generated a much higher AE rate. The AE rate was determined to be suppressed by an apparent increase in atmospheric humidity and was much more sensitive to changes in atmospheric humidity than changes in internal moisture content. The AE rate was hardly 'activated' or increased by an apparent increase in temperature.

Quarles (1990) measured the acoustic emission generated in rough sawn Californian black oak (*Quercus kelloggii*). Transducers were clamped to a small machined region on the rough surfaces to ensure adequate contact between the transducer and board sample. Acoustic emission data was segregated into four amplitude groups. The 10 minute data period employed was determined to be convenient for extended drying trials but too large for a control algorithm. Ringdown counts (AE rate) were found to

represent essentially the same information as AE event rate (a measure of the occurrence of *individual* bursts of acoustic emission rather than the total number of threshold crossings). A measure of acoustic emission signal energy was also calculated but this parameter was found to behave in virtually the same manner as the AE rate. A repeatable initial peak in the acoustic emission curves before subsequent larger peaks was conjectured to be caused by cavitation of water in the cell lumens, a process documented by Tyree and Dixon (1983).

Surface check initiation and propagation was not associated with a consistent and repeatable pattern of acoustic emission. The transducers were unable to detect acoustic emission activity associated with internal checking. Quarles reported that the need to select sample boards to control the drying of entire kiln batches was a potential disadvantage of an acoustic emission-based drying control system.

Parsons (1989) recorded acoustic emission generated in Tasmanian eucalypt boards. A transducer was mounted to wood specimens (at constant moisture content and temperature) in a tensile loading machine to gain an understanding of the acoustic emission phenomena. Acoustic emission was not detected until the tensile load exceeded approximately one-third of the ultimate stress, proving acoustic emission was an indicator of irreversible structural deformation.

Parsons measured remarkably periodic peaks in the AE rate behaviour during drying tests. He reported that surface checks on boards free of natural defects are often distributed in a quite uniform arrangement. He surmised that the first check forms near the centre of the board as the tensile stress are maximum there. This first check effectively divides the board face into two half-boards with the subsequent stress pattern comprising a maximum tensile stress at the midpoints of these intact halves, since no stress can act on the sides of the check. Further surface checks occur when the stresses exceed the material strength at the midpoints of the half-boards and the process repeats itself. It was plausible that such a pattern of stress growth and stress redistributions might repeat with constant time intervals and hence the periodic nature of the acoustic emission peaks.

Quarles (1992) monitored time-domain acoustic emission parameters during the drying of 25- and 50-mm thick Californian Black Oak (*Quercus kelloggii*) under conditions designed to produce surface and internal checking. A video camera monitored the development of surface checking during the first 12 hours of drying. The videotapes were played back in an image analysis system and the length of each check was measured as a function of drying time.

2.3 Kiln control by Acoustic Emission

Skaar et al. (1980) discussed the feasibility of devising a system of automatic control in a kiln, based on acoustic emission, to permit the most rapid drying of oak lumber, while minimising the development of excessive surface checking.

Honeycutt et al. (1985) developed a prototype drying control system based on acoustic emission. A microcomputer controlled the humidity in a small laboratory drying chamber by controlling the dry bulb temperature and maintaining a constant dew-point temperature. The microcomputer maintained the acoustic emission in a drying red oak specimen essentially constant by increasing the humidity when the AE rate exceeded this preset level and decreasing the humidity when the AE rate was below this threshold. The acoustic emission was controlled in this manner until the specimen moisture content dropped below 25%. The AE rate then decreased and further decreases in humidity had no apparent effect on the acoustic emission. Unacceptable end checking occurred because the optimum AE rate that minimised drying checks but maximised drying rate was not known.

This author describes the acoustic emission behaviour below 25% in the following manner. Once the average specimen moisture content attains the nominal FSP (typically near 30%), the acoustic emission is expected to decrease because the surface has attained EMC and negligible additional surface shrinkage will occur once the centre of the specimen has commenced to shrink. Acoustic emission is due to stress release events arising from the stresses generated by differential shrinkage between board surfaces and board centres. When the board centre is shrinking, this differential shrinkage decreases and the surface tensile stress decreases (with a corresponding decrease in acoustic emission). Eventually a stress reversal occurs and the

surface is under compression. The relationship between acoustic emission and surface stress (more precisely acoustic emission and surface instantaneous strain) is described in detail in 7.2.

Kitayama et al. (1985a) reported that the peak AE rate and increasing rate of AE rate were higher and steeper, respectively, in checked specimens. Drying checks always occurred before the peak AE rate was attained.

This author contends that surface checks relieve the local stress field near the check tip but redistribute the tensile stress on the intact surface regions. These initial checks will grow with further drying and new surface checks will form. Clearly, acoustic emission will increase after the first surface check(s) form.

Kitayama et al. (1985b) developed an automatic control system that used acoustic emission parameters as feedback variables to dry zerkova disks without surface checks. The AE event rate and the average rate of increase of this parameter were determined to be critical in the development of surface checks. Arbitrary control values were selected and the disks were successfully dried free of degrade by decreasing the wet bulb depression when either of these threshold acoustic emission parameters were exceeded. Surface checking was prevented using these techniques but again the actual control parameters were arbitrary.

Noguchi et al. (1985) examined the AE cumulative count, AE event rate, amplitude distribution of acoustic emission signals and the waveform and spectrum of acoustic emission signals measured in drying mizunara and keyaki (hardwoods) and suzi (softwood). The hardwoods generated far more acoustic emission during drying than the softwood. The amplitudes of the acoustic emission signals were distributed in an almost constant pattern, irrespective of species and their mean values were nearly equal. The acoustic emission decreased (and increased) rapidly when the relative humidity was increased (and decreased) respectively in trials performed at constant temperature.

Noguchi et al. (1987) investigated controlled drying of *Zelkova serrata* disks by acoustic emission. These tests were specifically related to end checking. The resistance of a ring of conductive material painted on the disks was

continuously monitored. Surface checking was detected when the electric circuit was broken by an underlying fracture. Noguchi determined that acoustic emission was a sensitive index of the onset of specimen shrinkage and its rate of change; no acoustic emission was detected until the surface moisture content attained FSP, that moisture content above which ideally no shrinkage occurs, and the acoustic emission ceased when the shrinkage was complete. In the specimens with surface checks, the acoustic emission increased rapidly to a maximum and then decreased rapidly, whilst in those cases where no checks occurred, the acoustic emission increased slowly and then decreased. Surface checks always occurred before the peak AE rate.

Specimen diameter and thickness, dry bulb temperature and air speed had little effect on surface checks (end checks when the specimen geometry is considered) but relative humidity had a significant effect. No specimens dried at 50% relative humidity developed surface checks while 5 of the 6 specimens dried at 30% humidity developed checks. As a result, it was concluded that the development of surface checks could be satisfactorily prevented with changes in relative humidity only.

Noguchi determined that the average increasing rate of AE event rate (peak AE rate divided by the time since acoustic emission generation commenced) and peak AE rate were determined to be the critical acoustic emission parameters associated with surface degrade during drying. The AE cumulative count bore little relation with the development of checks. Preparatory trials revealed nominal 'safe' values of average rate of increase of acoustic emission and peak AE rate, values below which surface checking never occurred. These values were used in a controller that increased the humidity when the average rate of increase of acoustic emission increased faster than this threshold and decreased the humidity when the AE rate was lower than the setpoint value. Surface checks did not form during drying but the process was not optimised because the control parameters were not directly related to surface checking. A critical value of peak differential (that is, rate of increase of AE event rate) could not be used as the control variable because the AE peak rates did not occur at the same time. Noguchi reported that the control variable used in a drying controller must be independent of the drying conditions and the pattern of acoustic emission generation.

Bernatowicz and Militzer (1992) reported that micro- and macro-cracks as well as plastic deformations caused acoustic emission. The three sources were successfully separated by amplitude distribution. Specimens free of cracks generated acoustic emission with only one-tenth the maximum energy of the acoustic emission generated in cracked specimens. Surface mounted transducers were unable to detect acoustic emission associated with any internal checking that occurred in test samples.

Cumulative count was determined not to be indicative of the propensity of surface check development and thus was not applicable as a feedback parameter in a computer-controlled kiln. Provided specimens were properly end-coated to prevent end drying, acoustic emission activity was not a function of specimen size. This is explained in detail in 7.2.1 but briefly, only the surface fibres and a thin region of the board beneath the surface appear to exceed the proportional limit and produce acoustic emission, independent of the board thickness.

2.4 Summary (with Author's comments)

Acoustic emission research can be neatly divided into studies investigating acoustic emission generated in timber under external load, such as tension tests, and studies investigating acoustic emission generated as a result of drying stresses. The ultimate aim of the latter stream of research is the development of a 'clever' kiln control system that moderates the drying conditions depending on the acoustic emission measured in sample boards.

Much of the external load-based research was performed parallel to the grain and the results are thus not applicable to the seasoning situation where the significant stresses act across the grain. The acoustic emission recorded in external loading is not applicable because the applied stress field results in local, minor fractures causing catastrophic specimen failure due to the high stress concentration factor at the fracture tip, whereas in the seasoning situation, the local fracture simply redistributes the local stress without significantly affecting the overall stress pattern. Therefore, the acoustic emission generated during external loading provides useful information on the nature of timber fracture and the behaviour of macroscopic cracks but any relationships determined between acoustic emission and stress or strain are not directly relevant during seasoning.

Acoustic emission detected during seasoning has not been related to either stress or strain because the stress can not be measured and the strain measured with a strain gauge is the resultant of four separate strain components introduced in 1.3.1. Unlike the external load tests, where the material fails soon after the proportional limit is attained, timber surfaces during seasoning progress well into the nonlinear range of behaviour. KILNSCHED, a drying model developed by Oliver (1991) and discussed in detail in Chapter 5 was used in this study to determine a relationship between stress and strain.

Apart from Quarles (1992), previous researchers have not reported the size of incipient surface checks observed in drying specimens. In general, it appears incipient checks have not been detected until they were relatively large. Chapter 6 in this thesis reveals that incipient surface checks in Tasmanian eucalypt boards were as small as 1mm long and only a fraction of a millimetre across and were not visible with the naked eye. It is plausible previous researchers may have attained more useful results had they monitored specimen surfaces for smaller checks.

Chapter 3

Material properties and AE related to timber structure

This chapter presents a description of the chemical and structural composition of fibre cell walls in timber. The bulk material properties are then related to the microscopic structure and behaviour of the fibre walls. The chapter concludes with the hypothesis that the acoustic emission in drying timber is generated by intermittent slips within the crystalline cellulose regions of cell walls under high stress.

The detailed descriptions of cellular structure and composition below are obtained from excellent texts such as Panshin and de Zeeuw (1980), Siau (1984) and Kollmann and Cote (1984).

3.1. Development of the fibre cell

Wood is cellular in structure with cell walls composed of polymers of cellulose, hemicelluloses and lignin organised as a reinforced matrix. Cells differ considerably in shape and size and each cell is adapted to one or more specialised functions. When first formed, the cell comprises thin-walled tubes of cellulose. This original cell wall is called the primary wall and is capable of rapid changes in size and shape to accommodate the increasing cell volume. The primary walls of individual cells are separated by the middle lamella, a plastic substance that allows slippage of the expanding cells. When the primary wall attains its final size, additional material is laid down inside the primary wall without increasing the overall cell dimensions. These subsequent layers constitute the secondary wall. Finally, the walls are thickened and strengthened again by the deposition of lignin.

Pits are areas of the primary wall that remain unthickened during the formation of the secondary wall and these theoretically aid moisture transfer between cells. However, a flexible membrane with very small pores or holes may cover the pits. These pores may become 'occluded' or blocked, increasing the resistance to moisture transport from this cell.

3.2. The chemical composition of wood

Wood consists of three main components : cellulose, hemicellulose and lignin. The cellulose and hemicellulose are polysaccharides or polymers of simple sugars while the lignins are three-dimensional polymers of phenylpropane units.

Cellulose is the single most important component in the woody cell wall in terms of its volume and its effect on the characteristics of wood (Panshin and de Zeeuw 1980). Cellulose occurs in both a crystalline and non-crystalline state. Siau (1984) reported that the cellulose content of normal wood of both hardwoods and softwoods was remarkably constant at $42\pm 2\%$. The cellulose content of tension wood is higher than in normal wood due to the presence of an unlignified innermost layer, consisting only of cellulose while in compression wood the cellulose content is lower due to an increased presence of lignin (Siau 1984). It is likely that the wide range in cellulose content (40-50%) frequently reported in the literature covers the tension wood and compression wood variations. Crystalline cellulose is impermeable to water and it is only in the amorphous regions that the water molecules become strongly bonded to the hydroxyl groups of the cellulose.

Hemicelluloses are polysaccharides associated with cellulose and lignin in the cell wall and account for 20-35% of the dry weight of the cell wall substance (Siau 1984).

Lignin is an amorphous three-dimensional polymer. Siau (1984) reported that most normal softwoods contain $30\pm 4\%$ lignin and hardwoods of the temperate zone $25\pm 3\%$.

3.3. The structure of the cell wall

Panshin and de Zeeuw (1980) reported that the polysaccharides in woody plant cells are physically aggregated into very long strands known as microfibrils. The microfibrils essentially comprise a core of crystalline cellulose encased in a sheath of hemicellulose. During wall formation, these microfibrils are surrounded by lignin. Panshin and de Zeeuw (1980) described the organisation of the wall components in terms of the *reinforced*

matrix theory, in which the strands of microfibrils, with high tensile strength parallel to their length are embedded in a plastic, amorphous matrix.

The cell wall can be conveniently subdivided into a number of different layers dependent upon the arrangement of the microfibrils. The following measurements were obtained from Siau (1984). The primary wall is only 0.1 to 0.2 μm thick and the microfibrils are essentially oriented in a random manner. The secondary wall is subdivided into the S1, S2 and S3 layers. The outermost, S1, layer is 0.2 to 0.5 μm wide in earlywood but can reach a width of 1.0 μm in latewood. The microfibrils are oriented at an average angle of 60 to 80° to the fibre axis. The middle, S2, layer thickness varies from 1.0 to 2.0 μm in earlywood and from 3.0 to 8.0 μm in latewood. In the former wood the microfibril angle is about 10° while reaching 30° in the latter. The S3 layer is only 0.1 to 0.2 μm thick in both earlywood and latewood and its microfibrils are almost transverse to the fibre axis. The S2 layer has the most pronounced influence on shrinkage because it constitutes such a high proportion of the secondary wall. The S1 and S3 layers act as constricting elements. The behaviour of wood has been shown to be closely related to the microfibrillar angle of the S2 layer (Siau 1984).

3.4. Tasmanian Eucalypts

The outstanding feature of Tasmanian eucalypts is the presence of large, tubular vessels running longitudinally in the tree, distributed through a matrix of smaller fibre cells. Vessels are composite tubelike structures, initially composed of a large number of closed cells lying end to end. The end walls of these cells ultimately break down, leaving long, thin-walled 'tubes' running longitudinally through the tree. Vessels also diverge radially ('medullary rays') and to a lesser extent tangentially, forming a 3-dimensional conduction system through the wood. The vessels perform the major water carrying functions in the living tree.

Fibres are long, narrow cells with closed ends containing a cavity or lumen. Boards dried in this study were typically 120 x 30 x 500mm while the nominal fibre dimensions were 600 μm long by 15 μm external diameter (Hasan 1994). Fibres overlap longitudinally and the lumens of adjacent fibres are often connected by pits. The fibres are 'cemented' together by the middle lamella.

3.5. Bulk material properties related to structure

Eucalypt material is less stiff when loaded in the tangential direction (that is parallel to the growth rings) than in the radial direction, despite the greater stiffness of the relatively dense fibres in the latewood bands. It appears the large diameter, thin-walled medullary rays incident on the tangential surface of a board significantly reduce the bulk stiffness provided by the fibres. It is useful to consider the material less stiff in the tangential direction rather than more stiff in the radial direction. The nearly linear relationship between stiffness and ultimate strength results in the tangential ultimate strength being lower than the radial ultimate strength.

Tangential unconfined shrinkage is typically twice the radial shrinkage in the Tasmanian eucalypt species. Various theories explaining this anisotropic behaviour have been advanced and these are summarised in Panshin and de Zeeuw (1980). One theory involves the reduced transverse shrinkage measured in earlywood compared with latewood, due to dissimilarities in cell-wall thickness and cell-wall layer orientation. In the tangential direction, the latewood shrinkage is said to be sufficient to force the earlywood to comply with it, whereas in the radial direction, the overall shrinkage is the summation of the weighted contributions of the earlywood and latewood bands, this being less than the total tangential shrinkage because of the presence of the low shrinkage earlywood bands. In addition, the rays have been shown to experience relatively little radial shrinkage so these restrain the relatively weak earlywood, reducing the radial dimensional change. Another explanation involves a possibly higher lignin content in radial cell walls, shrinkage decreasing with lignification. Another concept bases the differential shrinkage on a smaller angular microfibril orientation in the radial walls.

The greater tangential shrinkage and lower tangential ultimate stress explain the proliferation of surface checking on the wide surfaces of backsawn boards and the edges of quartersawn boards.

3.6. AE related to crystalline slips within cell walls

The studies described in the literature review in Chapter 2 typically ascribe the acoustic emission generated in timber to the stable extension of microfractures (Debaise et al. 1966, Adams 1969, Ansell 1982). These tiny cracks were thought to initiate in localised regions of high stress and extend a short distance before striking a region of higher fracture resistance and halting. The elastic stress waves generated by the sudden release of strain energy during crack extension cause the AE sensor to ring.

The 'AE checking threshold' is the measured AE rate corresponding to surface check formation during drying. The trials described in Chapter 6 reveal remarkably repeatable acoustic emission behaviour between backsawn boards with different basic densities and even between backsawn and quartersawn boards with inherently different bulk stiffnesses. This suggests acoustic emission is independent of the bulk properties.

Microfractures in a specimen under external tensile load reduce the material strength, due to the stress concentrations at the tips of the cracks. In such tests, the applied stress does not increase significantly beyond that stress which caused the first stress release event (ideally the stress at the proportional limit) before ultimate material failure. During seasoning, the surface stress increases significantly beyond the proportional limit before surface checking occurs. A board surface appears to undergo significant 'strain hardening' before surface checks form and thus behaves rather like a ductile metal under tensile load; elastic straining up to the proportional limit followed by plastic straining. Taylor (1934) hypothesised that this increase in strength beyond the proportional limit in metals was due to dislocations within the crystal structure of the material.

During plastic flow in crystal structures such as metals, planes of atoms pass across each other and broken bonds reform with new adjoining atoms (Gordon 1968). These dislocations exist as displacements along preferred planes within the crystals but the crystal structure is preserved. Far from reducing material strength, the dislocation mechanism involves an increase in potential energy in individual molecules and is thought to be the mechanism by which materials withstand increasing stresses beyond the proportional limit before ultimate failure (strain hardening).

Referring to a typical stress~strain diagram for a standard sized specimen of a ductile material such as mild steel in tension, we see a smooth curve comprising elastic straining up to the proportional limit followed by nonlinear behaviour, Figure 3.1a. The onset of plastic flow is due to dislocation motion but the dislocations are so small they are not discerned on the curve (Gordon 1968). However, when a very thin specimen, such as a large whisker, of the same material is tested in a Marsh tensile testing machine, sensitive to displacements as little as 4 or 5 Angstroms, the stress~strain diagram resembles that shown in Figure 3.1b. Elastic extension is interrupted by the sudden operation of dislocation sources. These sources operate erratically or intermittently and produce virtually instantaneous slip.

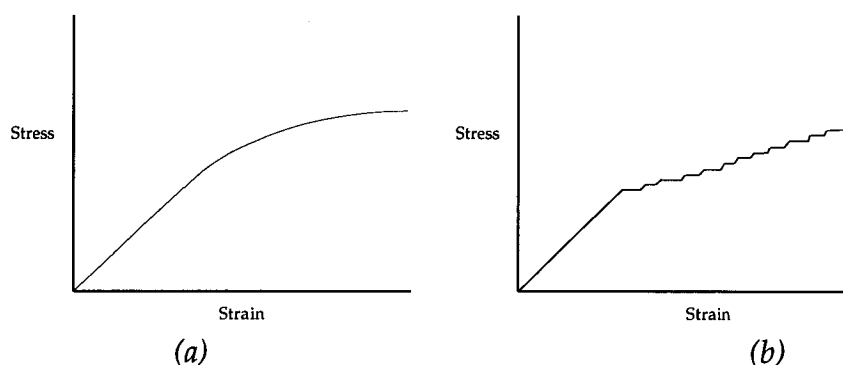


Figure 3.1. Macroscopic and microscopic stress~strain curves for a ductile material

Returning to timber, a typical AE response detected in eucalypt material during seasoning is seen in Figure 6.1 and Appendix A. Each response comprises intermittent bursts of energy release interspersed between periods of relatively low energy release. The 'burst' nature of the acoustic emission detected during drying suggests the acoustic emission events are sudden, intermittent rearrangements of the stress and strain at localised sites throughout the material, similar to the concept of intermittent crystalline slips in ductile metals.

Dinwoodie (1968) detected the sequential development of different types of dislocations with increasing stress in sections of spruce wood compressed to different percentages of longitudinal failing load. The slip planes were generally regarded as "...a dislocation or crinkling of the fibrils comprising the cell wall and, as such, are quite distinct from the slip planes in the crystallographic sense". Dinwoodie (1966) reported that slip planes had also

been recorded to a limited extent during tension and shear failure of timber. Bucur (1991) reported that "...modification of the orientation of crystallites in microfibrils" were a source of acoustic emission in wood materials. This author hypothesises that slip planes also exist when timber is stressed in tension across the grain.

Siau (1984) reported that the cellulose microfibrils comprising cell walls are between 50 and 60% crystalline. It is plausible acoustic emission in timber is generated by intermittent dislocations or slips in the crystalline cellulose components within cell walls. Cell walls also comprise hemicelluloses and lignin but these components are expected to undergo ductile flows rather than sudden slips since the hemicellulose is only partially crystalline and the lignin is noncrystalline. The bonding material between cells, the middle lamella, is also noncrystalline. The AE transducer oscillates at its natural frequency when high energy stress waves impinge on the transducer face, and a particular AE rate is measured. Ductile flows are not expected to generate high amplitude waves of sufficient energy to cause the transducer to ring.

It is proposed that the acoustic emission in Tasmanian eucalypts is primarily generated in the walls of fibres rather than the vessels and rays, despite the large volumetric composition of the vessels, because the cumulative wall thickness of the fibres far exceeds the corresponding cumulative wall thickness of the vessels and rays.

The analogy between crystalline slips within wood cell walls and the crystal dislocations occurring during plastic flow in metals must not be carried too far because changes in temperature and moisture content during drying directly also affect the structural nature of the cell wall.

Another potential source of acoustic emission during drying is shrinkage at the cellular level in the wood. Rice and Skaar (1990) detected differences in the acoustic emission behaviour and load-deformation curves in green and drying wafers under transverse bending. They reported that these differences supported the proposition that a major cause of acoustic emission in drying wood is shrinkage at the cellular level, with intracellular and intercellular microchecks resulting. Noguchi et al. (1987) reported that more acoustic emission was generated in *Zelkova serrata* disks when the surface

moisture content reached FSP. Further, acoustic emission was reported to be a sensitive index of the origin of shrinkage and its rate of change. Mudakai and Yata (1986) proposed that the mechanism of viscoelastic behaviour under moisture change was attributable to the 'looseness' of the interface between the S1 and S2 layers in a cell wall.

It is very difficult to prove or disprove any of the preceding hypotheses. For example, it is insufficient to measure acoustic emission in a specimen under load, observe microfractures of some form at the completion of loading with a high-power microscope and conclude that these were solely responsible for the acoustic emission. All that can be said is that the crystalline cellulose argument is certainly plausible and agrees with the results described in this study. It appears that microfractures also occur during seasoning but it is envisaged that so many more crystalline slips are 'active' that they dominate the measured AE signal.

Chapter 4

AE data acquisition and experimental kiln

This chapter presents specific details of the acoustic emission measurement and processing employed in this project. The AE transducer output signal is amplified and then compared with a preset DC threshold. A digital counter is incremented each time the output exceeds the threshold within a fifteen second period. The total threshold crossings or counts within this fifteen second data period is referred to as the AE rate. During the course of the project, new transducers were purchased so a calibration process is described. The chapter concludes with a detailed description of the experimental kiln and the generic Proportional Integral Derivative (PID) controller employed to accurately control kiln temperatures.

4.1. AE data processing

Acoustic emission was detected with a Physical Acoustics Corporation R6I AE transducer, a sensor with a resonant frequency of 60kHz and peak sensitivity of -67dB, for a reference of 1V/ μ bar. The pre-amp gain of the sensor is 40dB. The sensing element (probably lead zirconate, PZT) is a crystal mounted on a ceramic wear plate. No specific backing or damping material is present inside the case and thus the transducer acts as a resonator giving an output that is typically a decaying sinusoid.

AE rate has been the most popular time-domain acoustic emission parameter in timber research. AE rate refers to the number of times the amplified transducer voltage exceeds a preset DC threshold voltage during a data period. This threshold voltage is selected sufficiently high to exclude signals generated by extraneous noise sources such as the vent motors and water spray solenoids in the kiln, but not so great as to exclude the detection of low magnitude acoustic waves.

Time-domain parameters used by other researchers in previous acoustic emission studies include the AE event rate (the rate at which particularly energetic 'AE events' occur), the cumulative count (the cumulative ringdown counts over the duration of an entire test) and characteristics of the event

envelope such as peak amplitude, rise time, event duration and a measure of energy (Quarles 1988). AE rate was used in this study because Kline (1983) reported that AE rate was probably more closely likened to the energy of an acoustic emission event than any other physical parameter and Quarles (1988) reported that ringdown counts represented essentially the same information as a calculated measure of energy in drying California black oak samples. This author intended to relate the measured acoustic emission to the strain energy absorbed by the timber during drying and thus ringdown counts appeared to be the most practical acoustic emission parameter to use. The relationship between acoustic energy and surface strain energy is discussed in detail in 8.4.

The acoustic emission data acquisition hardware and processing strategy were refined regularly during the project as the author's understanding of the acoustic emission phenomenon improved. The initial processing strategy was based primarily on the concept that individual, relatively energetic, AE events caused the transducer to ring (represented by the idealised situation in Figure 4.1). Increasing AE rates with drying were considered to be due to an increasing (discrete) number of events of increasing energy, each causing the transducer output to ring above the DC threshold for a longer period and cause more counts. With experience, it became apparent that the acoustic emission 'driving' the transducers was probably due to the cumulative effect of a 'massive' number of tiny events, such as crystalline slips, rather than the extension of individual, localised microfractures. The modifications to the acoustic emission hardware (described in 4.3) and the resulting acoustic emission behavioural changes appear to support this proposition.

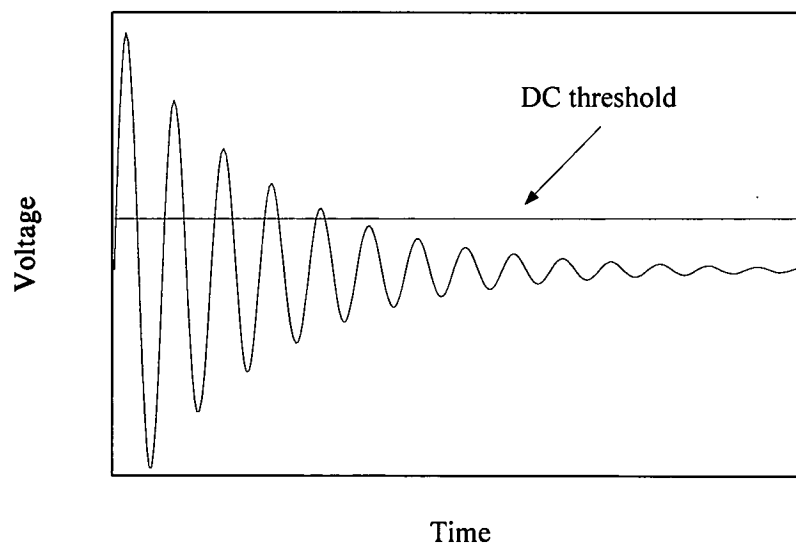


Figure 4.1 Idealised transducer response to an 'AE event'.

It is important to note that it is impossible to determine the exact nature and characteristics of the acoustic emission signals 'driving' the transducers because monitoring the transducer output signal with a Cathode Ray Oscilloscope (CRO) is representative of the ringing characteristics of the transducer and not the impinging stress waves. The waves themselves are of insufficient magnitude to monitor directly.

The measured acoustic emission was initially processed in the following manner. An additional 60dB amplification was applied to the transducer output after the 40dB pre-amplification to ensure the high amplitude peaks caused the amplifier to saturate, facilitating detection of the very small acoustic emission signals. The amplified transducer output voltage was then compared with a DC threshold voltage using a comparator. Each time the threshold was exceeded during the 15 second data period, the comparator triggered a monostable which generated a pulse to increment a digital counter. Five counts would be accumulated by the digital counter in Figure 4.1.

The pulse driving the counter has a finite width defined by resistance and capacitance timing components in the acoustic emission data acquisition hardware so an inherent 'dead-time' exists between the registering of one threshold crossing (count) and the next; once the threshold is exceeded, the counter is not incremented again until the monostable output goes 'low'. In this study, the dead-time was 1ms so a very energetic AE event would cause the counter to record more than one count during that event; when an event was of sufficient amplitude, the amplified signal was still above the DC threshold voltage after the dead-time and further counts were recorded as shown in Figure 4.1.

At the end of each 15 second data period, the counter output is latched into a Digital to Analog Converter (DAC) and recorded on disk. The counter is then reset. Twelve bit DACs, Analog to Digital Converters (ADCs) and digital counters were used in the data-acquisition equipment, providing the facility of measuring $2^{12} = 4096$ counts per 15 second period before saturation occurred in the digital counter. Preliminary trials revealed surface checking was present on board surfaces well below this AE rate.

Scrubby (1987) and Adams (1969) reported that the transducer output wave shape was considerably modified by factors such as the imperfect nature of the transducer and the fact that it is not a point detector. The AE rate measured in this project was dependent only on the frequency of the acoustic waves of sufficient amplitude to exceed the threshold and was independent of their shape. Indeed, saturation was deliberately induced in the transducer output to facilitate detection of the acoustic emission signal.

4.2. AE measurement

In Section 3.6, the source of acoustic emission in drying timber was hypothesised to be most likely due to intermittent crystalline slips. It is important not to conceptualise acoustic emission measurement in terms of a transducer being triggered by a single, relatively close propagating flaw such as a surface check. It is expected that the transducer is caused to ring by the cumulative affect of a 'massive' number of tiny events occurring within the immediate vicinity of the transducer. On this basis, the acoustic emission measured in a clear board should be independent of the position of the transducer along the length of the board (however the transducer should be placed in the midpoint of the board surface as discussed below).

We are not interested in locating the exact position of the AE events. As discussed in 2.2, Parsons (1989) reported that a rough approximation to the stress pattern in a clear board during seasoning has the maximum stress at the board midpoint. Incipient surface checks were usually detected near the board midpoint in this study. Surface checks were to be avoided, independent of their position on the board so only one transducer was attached to each board.

Private communication with an experienced sawmiller revealed the bottom faces of air-seasoned boards generally exhibited less surface checking than the top faces. Low air speeds are present within timber stacks in the open air because the majority of the air-flow passes around and over the stack. At these low speeds, buoyancy effects produce a moisture gradient in the airflow between the boards. The less dense moist air rises whilst the dry air sinks, leading to relatively harsh drying conditions at the top surface of each board. This contributes to greater drying stresses on the top surfaces of drying boards. This study involved kiln drying green material and therefore

the temperatures and airspeeds employed were similar to those expected in open-air drying (the kiln was utilised primarily to maintain accurate control of temperature and airspeed). For this reason, the transducers were attached to the centre of the top surface of each AE Board.

The transducer wear plate diameter is 30mm. The transducer is clamped firmly to the centre of the wide face of a sample board (AE Board) with a constant force spring and aluminium clamp to limit attenuation of the acoustic signal. A petroleum-based grease is placed on the transducer face as a transmission couplant to further limit signal attenuation.

For the first experiments, a small region in the centre of the AE Board was machined to maximise contact area between the transducer wear plate and the board surface. The transducer was subsequently applied directly to the rough surface when it was realised the machined surface was not representative of the stresses in the rough face.

Figure 4.2. AE transducers and a spring-loaded clamp.

Figure 4.2 shows a transducer clamped to the board and grease marks on the surface where two other transducers were attached during transducer calibration trials (discussed below).

4.3. Calibrating AE transducers

The AE checking threshold trials described in Chapter 6 incorporated one AE transducer only clamped to a single AE Board. The associated data acquisition hardware described above in 4.2 processed this signal. It was predicted that an acoustic emission-based kiln control system suitable for industrial kilns would require the acoustic emission measured in at least three boards (nominally located at stack inlet, centre and outlet). Two additional R6I transducers were purchased and new hardware comprising three printed circuit boards, each capable of processing the acoustic emission recorded by a single transducer, was constructed. The monostables driving each digital counter in the new hardware were retriggerable whilst the original monostable was not retriggerable.

The initial calibration trials incorporated the two new transducers connected to two channels of the new hardware and the existing transducer connected to the existing hardware. The original AE transducer is referred to as the 'reference transducer' and the AE rate measured with the original hardware is the 'reference AE rate'. The AE rate processed by each channel was adjusted with a potentiometer that attenuated the amplified transducer output signal before it was compared with the DC threshold voltage.

A common means of artificially generating acoustic emission has been the 'pencil lead break' (Quarles 1988), whereby a pencil lead is pushed against a specimen surface until the lead suddenly breaks. The site acts as a point source of acoustic emission. Acoustic emission in the initial calibration process reported here was generated by lightly striking a dry board surface with a metal implement. The force of the impact was varied to generate a wide range of AE rates measured by transducers clamped to the board. A dry board was used to ensure no extraneous acoustic emission due to natural drying was recorded. The transducers were placed within 30mm of each other to minimise the possibility that a single transducer recorded acoustic emission not recorded by the other transducers. The potentiometer settings of the new channels were adjusted by trial and error to force the processed AE rates to match the reference AE rate.

The three transducers were then clamped to a green backsawn board allowed to dry naturally in the laboratory environment. Again the transducers were placed as near as practicable to each other to ensure attenuation effects did not cause acoustic emission events to be recorded by only one transducer. Soon after the commencement of drying, a low reference AE rate was recorded. No acoustic emission activity was recorded on the new channels. After several hours, small surface checks were detected and a relatively high reference AE rate was recorded. Very low AE rates were measured on the two new channels, despite the close agreement between the new signals and the reference AE rate during the 'single impulse' calibration.

The original hardware incorporated a non-retriggerable monostable. A 'count' was only registered on a positive-going monostable output. Therefore when the monostable output was 'high' and sufficiently energetic acoustic emission was recorded to cause the comparator to drive the monostable high again, the monostable went 'low' after the 1ms period before going high. This ensured numerous counts were registered. The IC's on the new hardware incorporated a retriggerable monostable. When relatively energetic AE waves were continuously impinging on a board surface, the comparator was continuously retriggered and the monostable remained high for extended periods. This caused the low AE rates since the positive going monostable output occurred infrequently. Further calibration trials revealed that the AE rate in the new channels increased with the reference AE rate up to a certain count rate before decreasing, presumably when the monostable was triggered too frequently.

This behaviour was strong evidence that the transducer is caused to ring by the cumulative effect of numerous, coincident AE events of relatively low energy and not by individual events of high energy. This was confirmed by using a CRO to monitor the amplified transducer output signal (as described above, the AE waves themselves cannot be monitored) with a transducer clamped to a drying timber specimen. With drying, the AE rate increased as the transducer was caused to ring by ever more frequent 'bursts' of AE rather than by increasing amplitude, individual bursts. This finding is critical in developing the arguments involving the acoustic emission phenomenon in the following Chapters of this thesis.

Clearly, the single impact noise source is not an adequate means of causing the AE transducer to ring and is thus not a valid calibration technique. The pencil lead break technique commonly employed in AE investigations does not satisfactorily emulate the AE events in drying timber.

This discovery led to subsequent calibration trials being performed on drying green boards. The AE generated during drying was used to calibrate the transducer outputs. Again the transducers were placed as close as practicable to each other to minimise attenuation effects due to the separation of the sensors. This led to 'decent' calibration between the sensors but was inevitably hampered by the intermittent nature of the AE events.

This was overcome by developing a noise source incorporating a small plate caused to oscillate with varying magnitude pulses. A crystal clock was used to trigger a 4-bit DAC, the output of which was fed to a 50dB amplifier. The amplifier drove the plate at 16 cycles per second, each cycle comprising $2^4 = 16$ amplitude spikes, allowing a maximum possible AE rate of $16 \times 16 \times 15 = 3840$ counts per 15 seconds. The potentiometer setting of each channel is adjusted to produce the desired AE rate. This allowed the author to force all transducer outputs to the same AE rate. This immediately led to close agreement between the AE rates produced by all transducers.

4.4. The experimental kiln

Drying trials were performed in the fully instrumented batch kiln (Figure 4.3 over page) constructed by the Timber Research Group of the Tasmanian Timber Promotion Board, in conjunction with the Department of Civil and Mechanical Engineering, University of Tasmania and is the same as that used by Wu (1989).

The kiln is situated outside under roofed cover. Temperature control was performed with a computer inside the laboratory. Being relatively small and exposed to the atmosphere, the kiln was particularly susceptible to changes in ambient condition and wind speed during drying trials, especially rapid changes associated with rain showers and so on.

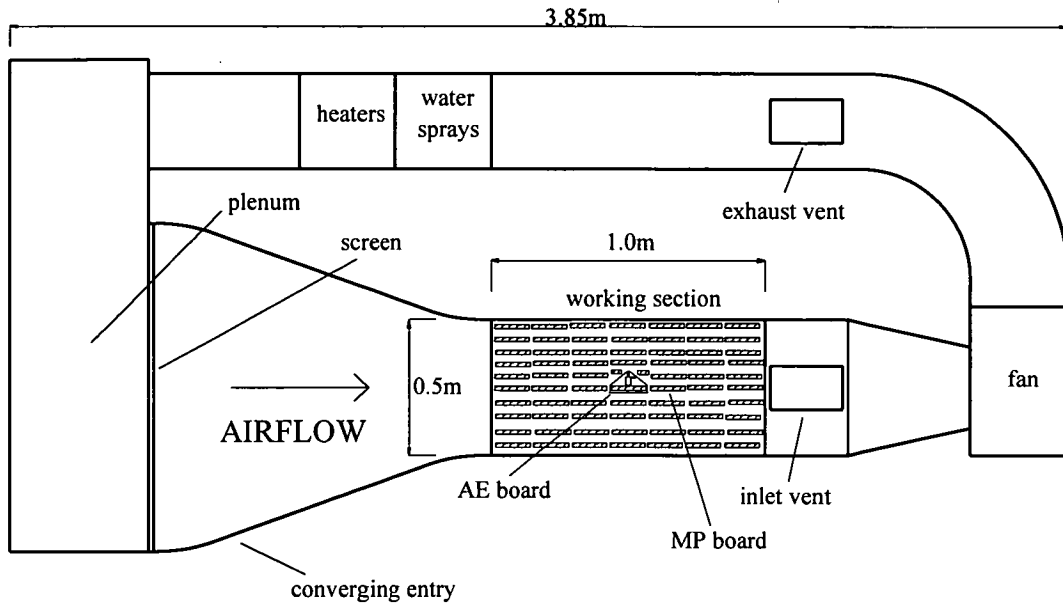


Figure 4.3. Schematic of experimental kiln (racking sticks not shown).

The kiln is of aluminium construction, with a 0.5m x 0.5m x 1.0m long working section. It is a continuous air flow system, with vents in the kiln walls for the inlet and exhaust of air. Air is forced around the kiln by a centrifugal fan. Before entering the kiln working section, the air passes through a plenum, a screen and a converging entry, promoting uniform air flow characteristics at entry to the working section. At very low air speeds, poor mixing of the kiln air caused 'pockets' of hot or humid air to travel around the kiln. Mixing was improved by inducing turbulent airflow at entry to the plenum as a jet of air at about 3 m/s.

The drying boards are oriented perpendicular to the air flow and thus are only 0.5m long. The kiln working section can accommodate approximately seventy 0.12m wide by 0.28m thick by 0.5m long boards, ensuring uniform air flow characteristics throughout the stack. The boards are significantly shorter than the boards dried in industrial kilns. However, the following measures ensured the small research kiln provided a rigorous test for the feasibility of developing an industrial automatic drying system. Longitudinal moisture transport within the boards was prevented by coating the board ends with an impermeable paint, simulating the negligible end drying that occurs in the significantly longer commercially-dried boards. The edges of neighbouring boards were stacked together to reduce edge drying. Moisture loss was then effectively restricted to the wide board faces,

a one-dimensional mode of moisture loss similar to that experienced by significantly longer boards.

The air speed upstream of the stack was measured by placing a vane anemometer through a small hole in the kiln wall. It was not practical to determine the air speed with the anemometer each time a change in air speed was required (the fan speed was adjusted manually with a potentiometer). The drying simulation program used in this study (described in Chapter 5) assumes an instantaneous change in air speed. The relationship between the air speed and fan speed was measured with the working space fully loaded with boards. At various fan speeds measured with a tachometer, the corresponding air speed upstream of the stack was measured, from which the mean air speed between the boards (VEL) was calculated. An air speed - fan speed curve was plotted. Provided the working section was full in subsequent drying tests, changes in air speed were satisfactorily implemented by adjusting the potentiometer until the required fan speed was attained.

Boards lay upon 25mm aluminium equal angle spacers running the length of the working section, providing 16 mm separation between the layers of boards. During a drying trial, the AE Board was regularly observed to determine the time of check initiation (surface check detection is described in detail in Chapter 6). In addition, several boards ('MP Boards') surrounding the AE Board were frequently removed and the ends docked to provide samples for moisture profile measurement (described in 5.7.3). Rather than opening the large kiln door each time a profile was to be measured and introducing excessive ambient air, a small hatch was placed in the kiln door and the AE Board and MP Boards were situated directly behind this hatch. Small spacers were added to the full length spacers in these rows, providing a slightly larger gap around the relevant boards, facilitating their simple removal and replacement.

The height of the transducer and clamp was approximately 70mm so the board that would have laid directly above the AE Board was absent. This gap inevitably increased the air flow across the AE Board, resulting in faster drying. This was overcome by placing packing pieces around the AE Board to maintain as nearly as practicable uniform air flow in the gap. The transducer co-axial cable was placed between the AE Board and its

downstream neighbour, running parallel to the boards and exiting the kiln through the front door, and was unlikely to produce significant airflow disturbances.

The whole batch lay on an aluminium frame suspended from mass transducers and the stack mass was recorded by the kiln control computer. From the mass of the stack frame and aluminium spacers and the measured initial timber moisture content, the stack moisture content was calculated and data-logged continuously throughout the trial.

4.4.1. Kiln hardware

Humidity in the kiln is controlled with mains-pressure water sprays. Heating of the air is provided electrically with heating elements. The vents are used to promote overall stable temperature control with the algorithm described below in 4.4.2. The heaters, vents and sprays are controlled with 0-10V DC signals, initially supplied direct from the analog output channels of the Boston Technology PC30-B Analog to Digital Data Acquisition board ('Analog/Digital Board') in the control computer. An amplification stage was subsequently designed to 'buffer' the Analog/Digital Board from the kiln hardware. Each output channel on the Analog/Digital Board provides only 20mA current whereas the buffer stage allows 250mA capacity per channel. This was desirable because the Clever Kiln Controller® system subsequently developed was a generic product, designed to interface with existing (as yet unknown) hardware in industrial kilns.

Heating of the kiln air is controlled by a SCR (Silicon-Controller Rectifier) unit that powers up the heating elements for a period of time proportional to the DC supply signal. Humidification is controlled with a pulse-width modulated signal proportional to the required spray setting, that is the spray output channel on the Analog/Digital Board is set at 10V for the required period before resetting to zero.

4.4.2. PID kiln temperature control

Dry bulb temperature (DBT) and wet bulb temperature (WBT) are recorded automatically, upstream and downstream of the working space, with Analog Devices 590 two-terminal temperature transducers. The WBT transducers

are enclosed in a cotton wick saturated with water from a reservoir external to the kiln. Sample AE Boards and MP Boards were situated in the centre of the batch of timber but the stack-centre temperatures were not measured directly. These temperatures were taken to be the average measured upstream and downstream temperatures.

Standard Proportional Integral Derivative (PID) control algorithms are employed to control the kiln conditions. The control task is complicated by two facts. Firstly, two input process variables are measured (DBT and WBT) and three output state variables may be utilised to adjust the process variables (Heaters, Sprays and Vents). Secondly, the DBT and WBT are intimately coupled so poor DBT control will be manifested directly as poor WBT control, no matter how sound the WBT control algorithm is in a 'stand-alone' mode. It was decided that the critical output state in DBT control was the heaters whilst the corresponding WBT output state was the sprays (for example, a proportional change in heaters has a far more immediate effect on DBT than either of the other output variables). Therefore, DBT and WBT were controlled independently with separate PID algorithms. The vents were adjusted separately with an 'error function' algorithm described below. Each PID algorithm utilises the current error in process variable, the previous error and the error preceding the previous error. The PID algorithm is based on central differences differentiation and trapezoidal integration (Van de Vegte 1986). The DBT algorithm is as follows :

$$u_k = u_{k-1} + (K_p + \frac{K_i T}{2} + \frac{K_d}{T})e_k - (K_p + \frac{2K_d}{T} - \frac{K_i T}{2})e_{k-1} + \frac{K_d}{T}e_{k-2} \quad (4.1)$$

where

e_k represents the k^{th} error equal to $(\text{DBTSP}_k - \text{DBT}_k)$.

u_k represents the k^{th} output state (heater setting).

K_p represents proportional gain

K_i represents integral gain

K_d represents differential gain

The WBT algorithm incorporates the same algorithm but DBT errors are replaced with WBT errors and the output state corresponds to the spray setting.

The values of K_p , K_i and K_d are adjusted by the kiln operator to optimise the kiln transient response and steady state control. The relative gain values are totally dependent on the particular kiln in operation.

The vent 'error function' is based on the sum of DBT and WBT error. That is,

$$error = (DBTSP_k - DBT_k) + (WBTSP_k - WBT_k) \quad (4.2)$$

and

$$u_k = u_{k-1} + error \quad (4.3)$$

where

u_k represents the k^{th} output state (vent setting).

When this error is positive and relatively large, meaning both the DBT and WBT are above the setpoint, the vent setting increases to reduce the kiln temperature and humidity (assuming the ambient temperature and humidity are below the setpoint settings). Conversely, a negative error results in the vents closing to increase the kiln temperature and humidity. Changes in vent setting reduce to zero as the steady state DBT and WBT errors reduce to zero. In this manner, the vents act to assist the heaters and sprays in controlling the kiln temperatures. Furthermore, the vents close with slightly positive DBT error (at nominally zero WBT error) and thus act to reduce heating costs at all times.

Typical temperature control and the corresponding kiln hardware settings are presented below in Figure 4.4.1 and 4.4.2 respectively.

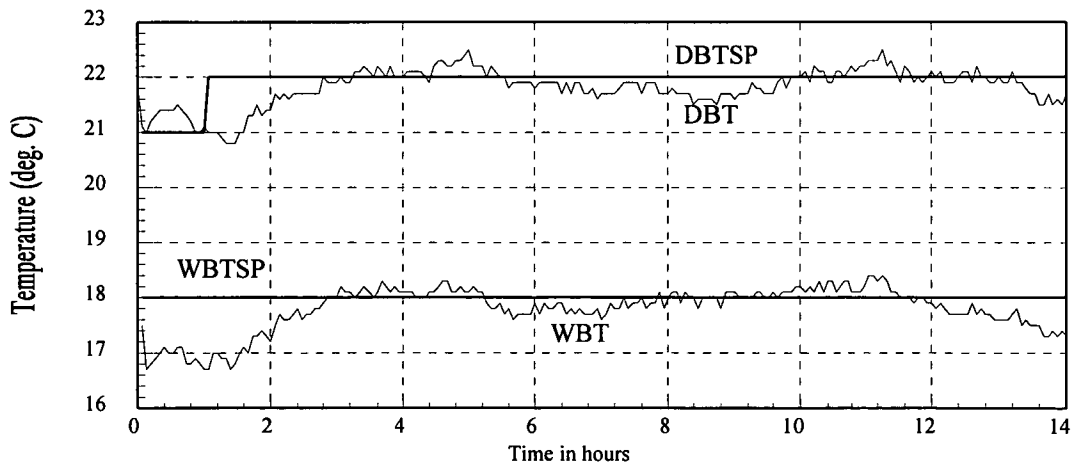


Figure 4.4.1. Typical kiln temperature control in the research kiln

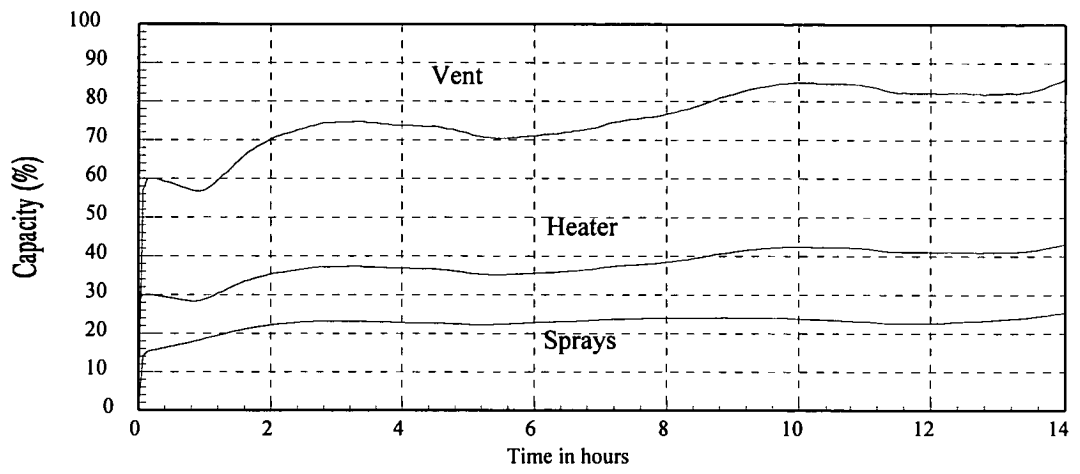


Figure 4.4.2. PID-controlled hardware settings

Chapter 5

One-dimensional drying model for Tasmanian eucalypt and related bulk material property tests

This chapter presents the fundamental heat and mass transfer theory and stress~strain theory upon which the nonlinear drying program KILNSCHED is based. KILNSCHED simulates an arbitrary number of drying conditions, allowing the user to experiment with different kiln schedules and grasp the fundamental process of timber drying. The chapter concludes with a description of the methodology employed to determine bulk properties such as basic density and unconfined shrinkage. These are required as user-input data to KILNSCHED.

5.1. Introduction

KILNSCHED is a computer program based on a nonlinear model of timber drying developed by Oliver (1991). KILNSCHED evolved from the nonlinear drying simulation program DRYWOOD, also developed by Oliver (1984). A literature review revealed that the drying models published prior to KILNSCHED were based on elastic or viscoelastic principles and thus were primarily restricted to linear material behaviour. Linear models are not applicable to the seasoning situation because board surfaces progress well into the nonlinear range of material behaviour before surface checking occurs. Linear stress~strain curves generally lead to unrealistic estimates of stress and strain. KILNSCHED has been shown to predict the time of onset of surface checking to within 10%, Wu (1989), because it incorporates nonlinear material behaviour.

In KILNSCHED, an ideal board is considered to comprise a discrete number of equal thickness wafers lying parallel to the wide board surfaces (these theoretical wafers are analogous to the wafers in the moisture profile measurement technique described in 5.7.3). The thickness of each wafer and the time-step employed in KILNSCHED are determined by numerical stability constraints and these in turn are dictated by the thickness of the

board and the material diffusion coefficient (discussed below). The number of wafers or grid-points increases with increasing board thickness and decreasing diffusion coefficient.

KILNSCHED is restricted to modelling boards experiencing one-dimensional flow of heat and moisture from the centre to the wide surfaces since sufficient data on 'edge-drying' is not yet available. KILNSCHED assumes symmetrical drying and thus models one half-board thickness only. Strictly, KILNSCHED should only be applied to wide boards that are either wholly backsawn or wholly quartersawn and cut far from the centre of the tree. The material is considered to be homogeneous, with the physical properties the same at all points across the board. In this sense, the model is concerned with the macroscopic structure of the board and not concerned with discontinuities at the growth ring level for instance. Despite the inhomogeneity of the material at the microscopic level, it appears that material specimens may be considered to be homogeneous when they are significantly larger than the individual material components such as fibres and vessels. As reported in 3.4, the nominal fibre dimensions in Tasmanian eucalypts are 600 μm long by 15 μm external diameter (Hasan 1994).

Collapse shrinkage tends to be restricted to 'pockets' of fibres beneath the board surface with the requisite cell lumen diameter and fibre wall thickness (collapse shrinkage is described in detail in 6.5). Interestingly, if collapse shrinkage could be induced in all fibres, green material could be dried at higher temperatures without inducing seasoning degrade. The localised nature of collapse means collapse shrinkage is not accurately modelled with a one-dimensional model such as KILNSCHED. Therefore accurate agreement between measured and calculated drying behaviour will only be attained when the timber does not experience collapse shrinkage. This is attained by drying at temperatures in the vicinity of 20°C to maintain relatively high cell wall stiffness and thus increased resistance to collapse.

5.2. Heat and mass transfer

The drying process is intimately related to the temperature, humidity and velocity of the air causing the drying. These factors directly affect the boundary layer at board surfaces and this controls the surface drying rate. Oliver (1991) reported that the best model for the transfer of heat and mass

across a boundary layer in air flowing over the extremely rough surface of a rough-sawn board is the Reynold's analogy (Rohsenow and Choi 1961). This assumes that the transports of momentum, heat and mass water vapour through the air are by similar mechanisms and leads to the conclusion that the distributions of air velocity, temperature and vapour concentration should be similar, that is :

$$\frac{\overline{U}}{(T_m - T_w)} = \frac{\overline{(c_m - c_{vw})}}{(c_m - c_{vw})} \quad (5.1)$$

where u = local air velocity (m/s)

U = free stream air velocity outside boundary layer (m/s)

T = local temperature (°C)

T_w = temperature of air in contact with wood (°C)

T_m = air temperature at mid-stream (°C)

c_v = local moisture concentration in air (kg/m³)

c_{vw} = moisture concentration of air in contact with wood (kg/m³)

c_m = moisture concentration in mid-stream (kg/m³)

A small 'laminar sub-layer' is often assumed to be present in boundary layer theory (eg Rohsenow and Choi 1961) but Wu (1989) was unable to detect such a layer in his boundary layer investigation of a small timber stack. On this basis, the heat flux from the air to the wood, h_e , is given by :

$$h_e = \frac{1}{2} f U \rho c_p (T_m - T_w) \quad (5.2)$$

where f = friction factor

U = local air speed (m/s)

ρ = air density (kg/m³)

c_p = specific heat (kJ/kgK)

By the same arguments, the mass flux of water vapour from the wood to the air, h_m , is given by :

$$h_m = \frac{1}{2} f U (c_{vw} - c_m) \quad (5.3)$$

The heat flux from the air to the wood is taken to be consumed in evaporating the water and heating the wood. Both processes are assumed to

occur at the surface of the wood. The wood surface temperature is equal to the temperature of the air in contact with the surface.

In KILNSCHED, above FSP, wood is assumed to behave as a free water surface, so that the vapour pressure of the moisture in the surface fibres equals the vapour pressure of air saturated with vapour at the surface temperature. These are the conditions for equilibrium between the moist wood and the air. When the moisture content of the wood falls below FSP, the vapour pressure is less than at higher moisture contents, because the remaining moisture is bound to the wood and thus more energy must be applied to break these bonds.

5.2.1. Movement of moisture within wood

In eucalypt material, it appears virtually all of the free water is held within fibres because any free water in the vessels and medullary rays soon drains out after sawing (Oliver 1991). The fibres overlap longitudinally and the free moisture passes rapidly from one cell to its neighbour through pits in the walls. However, when these pits are occluded water vapour must diffuse across fibre walls. The moisture follows complicated paths to the surface before being evaporated and convected away from the surface by boundary layers in the air.

Schaffner and Doe (1981) and Wu (1989) showed that moisture transport in eucalypt material is dominated by diffusion and can be adequately described by Fick's Law i.e.

$$\frac{\partial m}{\partial t} = D \frac{\partial^2 m}{\partial y^2} \quad (5.4)$$

where D is the diffusion coefficient (m^2/s), m is the moisture concentration (kg/m^3), t is time (s) and y is the distance from the surface (m).

Oliver (1991) developed KILNSCHED to monitor moisture *loss* from internal points and thus determined moisture distributions by solving for moisture deficiency, q , from the initial value m_0 at each point rather than absolute moisture concentrations. Therefore, the diffusion equation used in KILNSCHED is actually

$$\frac{\partial q}{\partial t} = -D \frac{\partial^2 m}{\partial y^2} \quad (5.5)$$

where $q = m_0 - m$.

Solutions to this differential equation are linearly added until the appropriate boundary conditions are satisfied. The solution for moisture deficiency is divided into 2 parts, one that satisfies the moisture distribution but leaves the surface value unchanged and one that allows for changes at the surface. The first part of the solution solves for the change in moisture distribution due to the internal moisture gradients, the second solves for changes caused by the heat and mass transfer at the material surface.

The diffusion coefficient within a board is considered to vary with local temperature but not with moisture concentration or stress. That is,

$$D = D_0 e^{\frac{T_k}{T_0}} \quad (5.6)$$

where T_k is the local temperature (K) and D_0 is the reference diffusion coefficient.

Wu (1989) used KILNSCHED to obtain close agreement between measured moisture distributions and calculated distributions using this approach. However, Oliver (1991) states that '...species other than eucalypts might well, because of differences in structure, exhibit a dependence of the diffusion coefficient on other factors beside temperature such as moisture content and stress or their gradients'.

5.2.2. Movement of heat within wood

The Fourier equation describing the conduction of heat in solids is

$$\frac{\partial T}{\partial t} = \alpha \frac{\partial^2 T}{\partial y^2} \quad (5.7)$$

where the thermal diffusivity, α , is defined by

$$\alpha = \frac{k}{\rho c} \quad (5.8)$$

and the material properties remain constant. T is temperature (K), t is time (s), k is the thermal conductivity (kW/mK), c is the heat capacity (kJ/kgK), y is the depth beneath the surface (m), and ρ is density (kg/m³).

Whilst this equation is of the same form as the diffusion equation, the thermal diffusivity in the eucalypt material is approximately three orders of magnitude greater than the diffusion coefficient. The effect of a change of surface moisture concentration affects only the first two points beneath the surface in the first hour but a corresponding proportional change in surface temperature affects the full board thickness. This means a different form of solution is required. However, the general approach is the same, with one part of the solution satisfying the internal temperature distribution while leaving the surface unchanged and the other part allowing for changes at the surface. The general solution to this problem is a Fourier Series (Carslaw and Jaeger, 1959).

Changes in surface temperature are propagated like a wave through the board. When the temperature of the air in contact with the wood surface changes rapidly, the Fourier series converges slowly because the peak of the wave is very near the surface. However, for the majority of the drying process, little change occurs at the surface and the first term in the Fourier series describes the temperature distribution at an arbitrary time to within 0.1°C. Under these circumstances, the Fourier series sine curve is replaced with a simpler parabola.

5.3. Strain components

The model assumes that the net strain, ϵ_n , observed in a board during drying is the resultant of four separable and separately measurable components. These components are unconfined shrinkage strain (ϵ_u), instantaneous strain (ϵ_i), mechanical creep strain (ϵ_c) and mechano-sorptive strain (ϵ_m).

$$\epsilon_n = \epsilon_u + \epsilon_i + \epsilon_c + \epsilon_m \quad (5.9)$$

Each component is dependent upon different variables, but they are added linearly to produce the overall strain since strain is a purely geometrical quantity and components are linearly additive under all conditions.

When the surface stress is tensile and the surface fibres are shrinking, the instantaneous strain acts in the opposite direction to the unconfined shrinkage strain. The creep strain is always in the same direction as the stress so in the initial stages of drying when the surface is under tension, creep offsets the shrinkage strain. Similarly, the mechano-sorptive strain is initially a tensile strain and adds a third component in offsetting the shrinkage strain.

5.3.1. Unconfined shrinkage strain, ϵ_u

Unconfined shrinkage is the shrinkage strain fibres would experience during drying if they were not restrained by the bulk of the board.

In Tiemann's (1906) model, there is no shrinkage in drying specimens until the moisture content attains FSP (nominally 30% in Tasmanian eucalypts). In practice, in Tasmanian eucalypt materials the measured unconfined normal shrinkage curve usually contains a sharp 'knee' at about 0.5% shrinkage and a moisture content between 35 and 40%. This shrinkage above FSP may be attributed to the removal of bound water from the walls of vessels (and medullary rays) whilst the fibres still contain free water. Free moisture is removed easily from vessels and rays under the influence of partial pressure gradients in water vapour between the board centre and the surface. Figure 5.1 depicts typical unconfined normal shrinkage and collapse shrinkage (shrinkage measurement is described in 5.7.4)

Between FSP and EMC, the relationship between moisture loss and shrinkage is very nearly linear. Typically 1 or 2% additional shrinkage occurs when the samples are oven-dried from EMC down to zero moisture content.

The measured unconfined shrinkage curve (Figure 5.1) is replaced in the drying program by an hyperbola defined by three points:

- zero shrinkage at the initial (green) moisture content
- shrinkage and moisture content values at the FSP knee
- shrinkage and moisture content values at the EMC knee

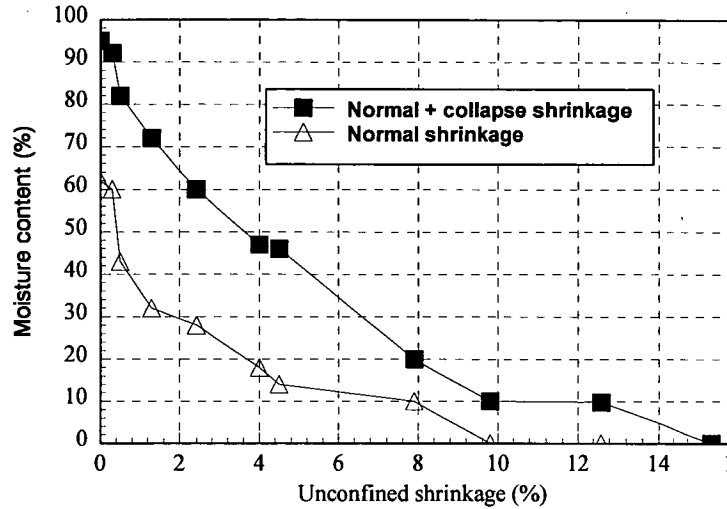


Figure 5.1. Unconfined tangential shrinkage curves

5.3.2. Instantaneous strain, ϵ_i

This component represents the immediate effect of a change of stress. This is the measured strain corresponding to the applied stress in a standard short term loading test in a laboratory testing machine. The material is assumed to behave in a linear elastic manner until the instantaneous strain exceeds the proportional limit of 0.005 - published results seem to lie entirely within the range of 0.004 - 0.006 (Oliver 1991). Surface checking occurs when the surface stress exceeds the ultimate stress. However, the manner in which the nonlinear stress~strain curve is incorporated into KILNSCHED means the calculated stress is asymptotic to this ultimate stress so an ultimate strain is used as the criterion for the onset of surface checking. Eucalypt materials dried in the vicinity of 20°C are taken to experience surface checking when the instantaneous strain attains 0.02 or 2%, a value determined in laboratory trials (Schaffner 1981).

5.3.3. Mechanical creep, ϵ_c

Mechanical creep strain is the progressive strain which occurs in specimens at constant moisture content under constant applied stress. Oliver (1991) reports 'that the most comprehensive set of data for this component has been presented by Kingston and Clarke (1961) for beam tests on the species *E. regnans*'. Creep varies markedly with temperature but is almost independent of moisture content provided that is held constant. Long-term creep is

known to exist but is not incorporated into KILNSCHED because of the lack of suitable quantitative data.

5.3.4. Mechano-sorptive effect, ϵ_m

The mechano-sorptive effect is the deformation in wood resulting from bending, compressive or tensile loading during simultaneous changes in moisture content, as reported by Armstrong and Kingston (1962). They determined that separate sets of eucalypt beams showed linear variation of mechano-sorptive effect with moisture content when dried from different initial moisture contents at different rates. Wu (1989) measured two apparently separate effects above and below FSP in 'peppermint' eucalypt samples strained across the grain. In each case, the mechano-sorptive effect was linear with moisture content. Above FSP, the mechano-sorptive effect is highly dependent on temperature (Wu 1989).

The mechano-sorptive effect is poorly understood. KILNSCHED uses the best available data, with ϵ_m taken to be linearly related to moisture loss. Different values are used when the stress acts in the same direction as the shrinkage caused by moisture loss and when it acts in the opposite direction.

5.4. Stress~strain curve

KILNSCHED employs a nonlinear stress~strain curve (Figure 5.2) based on numerous laboratory compression and bending tests (Oliver, 1991). Such tests are rather more representative of stress and strain behaviour in seasoning than a tension test where a minor defect causes catastrophic failure. Innes (1992) measured load-deflection behaviour in Tasmanian eucalypt specimens subject to slow tension loading, at varying moisture contents and temperatures, and reported that the stress~strain curve in KILNSCHED appeared to be a satisfactory approximation to the actual material behaviour.

The curve is linear up to a nominal proportional limit strain (ϵ_{pl}) of 0.005. The slope of the linear stress~strain curve below the proportional limit is Young's Modulus, E , dependent upon both temperature and moisture content. Above 20% moisture content, E is taken to be linearly dependent on temperature and independent of moisture change. Below 20%, it is taken as

linearly dependent on moisture content as well as temperature. The straight line describing modulus below 20% moisture content crosses zero and this creates computational problems, especially in this situation where iterative solutions are required. An hyperbola with asymptotes defined by the two straight lines is used to describe Young's Modulus in KILNSCHED.

The stress~strain curve is taken to be exponential in form beyond the proportional limit up to an ultimate stress equal to a fixed fraction of the Young's Modulus. This assumption is based on the nearly linear relationship between Young's Modulus and ultimate stress, σ_u (Oliver, 1991). This relationship exists because density is largely a function of the ratio of cell wall thickness to cell diameter and variation in either parameter markedly affects the Young's Modulus of the cell wall. Taking the ultimate stress to be a fixed fraction of the Modulus allows for variation of ultimate stress with moisture and temperature at failure.

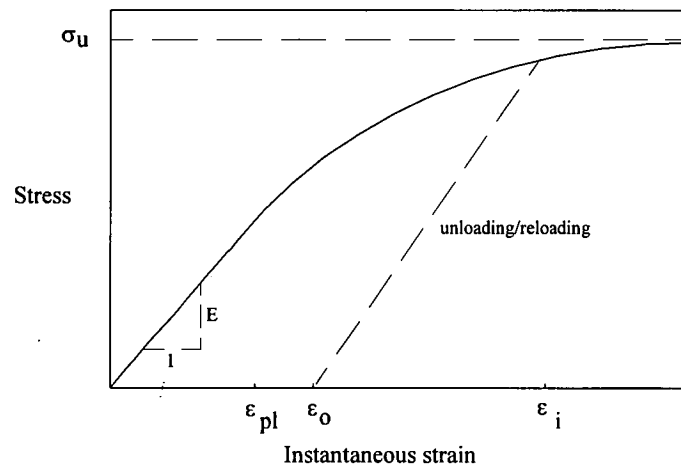


Figure 5.2. Nominal stress~strain curve in KILNSCHED

During drying, every section through the board thickness is at a different temperature and moisture content so E is different at each point. The ultimate stress is different at each point so every section lies upon a different stress~strain curve. This requires a number of stress~strain curves equal to the number of grid-points used in the program. This introduces major computational problems because as the material dries, sections continuously cross other stress~strain curves.

Oliver (1991) overcame this computational hurdle by normalising the stresses to create a non-dimensional stress~strain curve. In the non-

dimensional curve, the stresses are considered as fractions of the ultimate stress. The stress~strain curve is asymptotic to the reference value σ/σ_u . The ultimate stress is taken as a constant fraction of the local linear Young's Modulus, E , so a change in local Modulus affects the ultimate stress proportionately. When the material is loading nonlinearly, the stress is independent of the linear Young's Modulus and is defined by the shape of the exponential curve relating stress and strain. When strain release occurs at a board surface (due to humidification of the drying air for example), the material is assumed to unload along the straight line defined by the local linear Young's Modulus. If the severity of the drying conditions are then increased again and the material surface commences to reload, changes in Young's Modulus affect both the ultimate stress and stress proportionately, so the material returns to the same point at which unloading commenced on the non-dimensional stress~strain curve before loading nonlinearly.

Using the nondimensional curve, the material stress~strain behaviour is modelled with a single curve, vastly simplifying the task of monitoring the stresses and strains when the material is repeatedly loading and unloading due to frequently changing conditions. The non-dimensional curve is used to define a relationship between stress and instantaneous strain that is satisfied at all times, independent of the history of loading. The dimensional curve requires a description of paths followed from a point on one curve at the start of the time step to a point at the end of the time step. On the dimensional curve, the residual strain or set must be recalculated whenever Young's Modulus changes. On the non-dimensional curve, the set need only be recalculated when the material is loading nonlinearly.

This description involves several simplifications which must be considered only as rough approximations introduced for computational reasons rather than scientific precision. However, the final result seems to agree with the AE measurements to within 20% right out to the prediction of failure (refer to 7.2 for comparisons between measured AE rate and calculated surface instantaneous strain). This degree of agreement compares favourably with predictions of failure of many materials with less variability than timber.

5.5. Solving stresses and resulting strain components.

The model is restricted to one-dimensional behaviour and plane sections normal to the board surface are assumed to remain plane during drying, simplifying the stress~strain calculations. Then the net shrinkage is the same at all points across the board thickness. There can be no net force across any section, i.e.

$$\int_{-T_b}^{T_b} \sigma dy = 0 \quad (5.10)$$

where T_b is the board thickness.

At each time step, the program calculates moisture and temperature distributions within the wood as determined by the applied air temperature, humidity and velocity and the current internal moisture and temperature distributions. The new moisture distribution gives a distribution of unconfined shrinkage across the board thickness and thus values of changes in shrinkage at each grid-point. These are ultimately responsible for changes in the stress distribution. The change in stress at each grid-point is determined with simple iteration; although points within the board near the surface are behaving nonlinearly, the majority are below the proportional limit and operate in a linear, reversible manner. For the majority of the drying, the rate of change of instantaneous strain is very small, so the previous calculated change in strain is used as a trial value in the new time step. This new strain allows the calculation of a corresponding stress from the stress~strain curve. The stresses across the board are integrated according to Equ. 5.10, leading to the calculation of a net strain. However the trial instantaneous strain at each point is invariably wrong, leading to a non-zero right hand side in the stress equation. Corrections are then made to the stresses at each point based on the contribution of that point to the new net strain. This process is repeated and usually converges within three iterations.

5.6. Material variability effects

Modelling timber drying is made difficult by the inherent variability of the material. Mechanical properties vary markedly not only from tree to tree but

even within the same tree; 30% variation in mechanical properties between the butt log and the head log from the same tree is common.

Much of this variability has effectively been removed in KILNSCHED by following Commonwealth Scientific Industrial Research Organisation (CSIRO) practice and using dimensionless ratios. The mechano-sorptive effect and creep are calculated with reference to the instantaneous strain, ϵ_i . Using the instantaneous strain as reference value succeeds because variations in density are the most critical factor in producing variability in test results and Young's Modulus varies nearly linearly with density.

Young's Modulus in the radial and tangential directions are taken as fractions of that value in the longitudinal direction, rather than absolute values. In this manner, errors in estimation of Young's Modulus have little effect that can be checked, since the errors appear only in calculated estimates of stress in the board, which can not be measured. However, the relative values are important, since these stresses are used in calculating the relevant strains.

5.7. Bulk material property tests

Various timber properties such as basic density, initial moisture profile, unconfined shrinkage and diffusion coefficient are required as input parameters to KILNSCHED. All but the diffusion coefficient are determined at the commencement of the drying trial.

Boards were selected from a log off the saw at the sawmill, block-stacked and wrapped in plastic. This batch was immediately transported to the laboratory and the board ends were painted with an impermeable bituminous coating to inhibit longitudinal moisture transport. These measures prevented as much natural drying as possible before the commencement of controlled kiln drying. Several boards were used as samples to determine the basic density, initial moisture content and propensity for shrinkage of the saturated timber. These were removed and once again wrapped in plastic in preparation for the tests described below. The remaining boards were placed in the experimental kiln and the drying trial commenced.

The tests described below are relevant to 120 x 28 mm cross-section boards.

5.7.1. Initial moisture content

Approximately 30mm long cross-section specimens were cut from near the centres of sample boards and weighed as soon as practicable. The mass and an identifying number of each specimen were recorded. The specimens were then oven-dried at a temperature of approximately 103°C until no further decrease in mass was observed. The initial average moisture content of each sample was described as the ratio of the initial mass of water present to the oven-dry mass of wood.

5.7.2. Basic ('green') density

The Initial Moisture Content samples were also used to determine the timber basic density prior to oven-drying. The green volume of each specimen is determined using the water displacement method with a Sartorius balance. Once the initial sample masses had been determined as above, the samples are fully submerged in a container nearly filled with water by pressing them below the surface with a sharp pointer. The green material is so nearly saturated that it is assumed that no absorption of water occurs in the short time the specimens are submerged. The difference in the mass readings before and after each specimen is submerged represents the mass of the volume of water displaced by the specimen. The sample volume is then determined from the density of the water. Basic density is defined as the ratio of oven-dry mass of wood to the green volume of wood.

5.7.3. Initial moisture distribution

A specimen measuring approximately 30 x 28 x 30 mm was cut from the centre of an MP Board. Commencing at a wide board surface and progressing into the sample centre, a purpose-built microtome (Figure 5.3) was used to cut about 1mm slices or wafers parallel to the wide surfaces of the board. After approximately ten wafers had been cut, the sample was rotated 180° and wafers cut traversing in from the opposite surface. This process produced approximately 20 wafers and one larger centre piece. Each wafer was weighed and the wafer thickness measured with vernier callipers. The wafer masses were monitored during oven drying and when no further

moisture loss was measured, the wafers were placed in a desiccator before determining the oven-dry mass on a Projecta $\pm 0.001\text{g}$ beam balance. The desiccator was necessary because buoyancy effects caused significant error in the mass readings when the specimens were weighed hot. The moisture content of each wafer was determined as above.

Figure 5.3. Microtome used to prepare wafers for unconfined shrinkage and moisture distribution tests

The feedscrew for the microtome knife had 1.6mm pitch and thus 0.8mm wafers were obtained by rotating the feedscrew one half turn during the slicing process. However, the first wafer thickness could only be estimated because the pressure of the sample riding against the knife varied significantly in the first instance.

The thinner the measured wafers, the more accurate the determination of moisture distribution, provided the weighing is accurate. The surface moisture concentration can not be calculated directly but is extrapolated from the parabola passing through the natural logarithms of the measured average moisture contents of the 3 wafers directly beneath the surface, on the grounds that the analytical solution to Equ. 5.4 is a sum of error functions. Thin sections are particularly desirable for this surface calculation because

the moisture gradient is generally extremely steep in the first stages of drying and large errors are possible in extrapolating the surface value. However, when the sections are cut too thin, they fall apart on slicing and are extremely delicate in the oven-dry state making it easy to lose material scards during handling.

Once a profile had been measured, the moisture in the board was plotted as a function of board thickness using the computer program MCPROFILES, developed by Oliver (1991). The slice thicknesses varied and the sum of the slice thicknesses invariably exceeded the measured thickness of the board. MCPROFILES adjusted the slice thicknesses so that the sum equalled the board thickness. The corresponding measured moisture concentrations of the original slices are shifted to the centroids of the area under the curves. The resulting interpolated moisture distribution is plotted at uniform spacing equal to the grid-spacing used in KILNSCHED to allow simple comparison with calculated drying behaviour.

5.7.4. Unconfined shrinkage

A cube is cut from the centre of a board cross-section sample. Nominal 1 mm wafers are cut parallel to the wide board surfaces with the microtome as in the moisture distribution tests. The slice thicknesses used in measuring unconfined shrinkage are small to ensure the moisture content is very nearly uniform when dried at room temperature. This ensures each specimen does not experience differential shrinkage effects and is thus free of restraint.

The samples are placed in wire frames to prevent distortion out of the specimen plane without restraining shrinkage in the plane. Each specimen is numbered and two marks sharp to $\pm 0.3\text{mm}$ are made approximately 25 mm apart on each specimen face with a felt pen. The specimens are allowed to dry naturally in the laboratory and thus small temperature and humidity fluctuations may occur. At regular intervals, the samples and frames are weighed and the separation between the marks is measured with a travelling microscope (Figure 5.4 depicts a shrinkage specimen in a wire bridle and the travelling microscope). Once no further loss in mass is detected, the samples and frames are placed in the oven.

Figure 5.4. Unconfined shrinkage measurement

Shrinkage is described as the ratio of the measured movement of the pen marks to their initial separation. The moisture content of each specimen is determined from the initial masses and the oven-dry masses as described above. In this manner, curves relating unconfined shrinkage to moisture content are plotted.

The unconfined shrinkage specimens were initially sliced parallel to the wide board surfaces to maintain compatibility with KILNSCHED which effectively models the board as comprising a number of such wafers. Collapse shrinkage was thought to be prevented by ensuring the specimen thicknesses were less than 1mm, thereby significantly increasing the probability that most of the fibres were damaged during sample preparation. However, private communication with Ilic (1992) revealed that the orientation of the fibres with respect to the wide specimen face determines the propensity for collapse shrinkage. Slicing the samples parallel to the board surfaces results in the fibres lying parallel to the cuts and thus the majority are not damaged and remain collapse-susceptible. Only when the specimens are oriented so that the fibres lie perpendicular to the microtome cut is collapse prevented.

Shrinkage measured in wafers cut parallel with the fibres represents the maximum shrinkage the material would experience during drying at that temperature. When the unconfined shrinkage is measured in both planes, the difference in shrinkage between the curves provides a predictive measure of the collapse that would occur during drying. Figure 5.1 presents unconfined shrinkage measured in longitudinal and transverse wafers cut from a sample board.

5.7.5 Diffusion coefficient

Schaffner (1981) determined the diffusion coefficient prior to drying by measuring the steady state moisture transfer rate through thin wood samples exposed to different relative humidities at each specimen surface. Using thin specimens makes this measurement suspect because it introduces permeability affects and these are likely to dominate the moisture transport rate by moisture diffusivity, resulting in spurious high values of diffusion coefficient. This error was avoided in this study by determining the diffusion coefficient during drying by regularly measuring through-thickness moisture profiles in the MP Board(s) with the slicing technique discussed in 5.7.3 and utilising MCPROFILES, also discussed in 5.7.3. MCPROFILES inherits the drying model functionality of KILNSCHED (without the stress~strain functionality).

After measuring an initial profile and a second profile (typically 24 hours later, depending on the severity of the conditions), MCPROFILES was used to simulate drying under the datalogged drying conditions. With an arbitrary 'trial' value of diffusion coefficient, the calculated profile was compared with the measured profile. The author adjusted the diffusion coefficient in MCProfiles until the profiles were accurately matched. The diffusion coefficient value was checked further by ensuring the calculated average moisture content agreed with the average moisture content calculated as in 5.7.1.

Further moisture profiles were measured at intervals dependent on the severity of the drying conditions; the first 3 points in a given moisture profile must be reasonably different from the corresponding points in the preceding profile to accurately extrapolate the surface concentration value. When the next slicing was performed too soon after the preceding slicing, the moisture

gradient was not sufficiently different to refine the diffusion coefficient value. The value of diffusion coefficient was refined after each slicing measurement. Experience revealed that when drying was commenced at temperatures in the vicinity of 22°C, slicing measurements at 0, 24, 72, 120 hours followed by weekly and fortnightly slicings provided sufficient data.

Chapter 6

Determining the AE checking threshold

The following chapter describes the development of a method to determine the characteristic acoustic emission parameter (the 'AE checking threshold') related to incipient surface checking in backsawn and quartersawn eucalypt boards. Incipient surface checks were detected visually with a 10 times magnifying glass. The chapter includes a detailed description of surface check detection because incipient surface checks are particularly small (typically 1mm in length) and the direction of check propagation is directly dependent on the orientation of the growth rings.

It must be realised that seasoning degrade was considered to have occurred in this study even when surface checks were visible only with the magnifying glass. Drying conditions such as 24°C DBT, 20°C WBT and 1m/s airspeed typically caused surface checking in green material within 24 hours and thus are considered 'harsh' in this study.

More than 200 green boards were dried under harsh conditions to induce surface checking in approximately 24 hours. The AE rate and cumulative counts were measured during each trial. It was determined that incipient surface checks formed in backsawn and quartersawn eucalypt material at a very nearly constant AE rate (Booker 1994b). This meant that the acoustic emission was independent of the direction of sawing and thus independent of the bulk material properties. This was strong support for the hypothesis that acoustic emission was due to crystalline slips within cell walls. The AE sensor is caused to ring by the cumulative effect of a massive number of tiny, crystalline slips occurring in the immediate vicinity, not by relatively large, individual stress release events.

This hypothesis was tested further by measuring acoustic emission in drying radiata pine and myrtle boards but the results were generally inconclusive. The hypothesis regarding acoustic emission and crystalline slips was extended to include a description of surface check initiation.

As a prelude to this discussion, it must be realised that localised stress release due to crystalline slips and the macroscopic surface checking phenomenon are quite distinct. Descriptions of the former process consider timber to comprise individual fibres in a matrix of 'cementing' substances while the latter considers the material to behave as a continuum. Inevitably some material behaviour is not adequately described by both arguments.

6.1. Surface check detection and propagation in backsawn boards

No matter how small an incipient surface check, the stress concentrations at the sharp tips and the bottom of the check drive it along and into the board with further drying; it is impossible to remove further moisture without generating sufficient local stress to cause it to grow. Surface checking must be avoided when drying furniture grade material and thus detection of check *initiation* is critical if acoustic emission is to be used in an automatic kiln control system. Oliver (1991) predicted that surface checks would be of the order of only 1 to 2 millimetres long and 0.1 millimetres wide at initiation. Observations during early trials confirmed this. Incipient surface checks were not visible to the naked eye and were differentiated from the rough sawn board surface only with a 10 times magnifying glass. Surface checks large enough to be visible to the naked eye are relatively 'old' and do not provide an accurate measure of the time of check *initiation*.

Several automatic check detection systems were reported in the literature review in Chapter 2. Noguchi et al. (1987) applied a monitor voltage to a ring of conducting material painted on *Zelkova serrata* disks during drying trials. Surface check formation was detected when the electric circuit was broken by an underlying fracture. The dimensions of the checks were not reported but it is likely the conducting paint would stretch slightly and would not break until the checks had grown somewhat. Quarles (1992) used a video camera to record the growth of surface checks during the drying of Californian Black Oak. Checks typically appeared to be of the order of 4 to 5mm long before they were detected. The resolution of a video camera alone without a high resolution or magnifying glass was expected to be insufficient to differentiate incipient 1mm checks in the rough board surface. These techniques automate surface check detection, which is useful in its own right, but neither are sufficiently sensitive to detect check *initiation*.

Observation of surface checks in air-dried backsawn material at a sawmill revealed that the checks generally propagated deep into the boards in a direction perpendicular to the surface. Schaffner (1981) examined drying checks in samples of *E.delegatensis* with an electron microscope and reported that the checks propagated in the radial direction, parallel to rays but not necessarily along them. Surface checks initiate in the radial direction because the radial-longitudinal plane is the weakest plane in the timber structure (for this reason, internal checks are also aligned in the radial direction). High stress concentrations form at the tips and the base of an incipient check. The perpendicular to grain tensile stresses that caused the incipient check increase with further drying. These act parallel to the wide board surface and combine with the stress concentrations to drive the check directly into and along the board with further drying.

In a perfectly backsawn board, the radial direction of check initiation coincides with the subsequent radial check propagation and the stress concentrations at the check tips readily promote further check growth. Incipient checks in backsawn boards are detected relatively easily by looking directly perpendicular at the surface with the magnifying glass. The problem of surface check detection in quartersawn boards is discussed in 6.7.

6.2. AE rate and cumulative count

The two most common time domain acoustic emission parameters reported in the literature are ringdown counts and cumulative count. As discussed in 4.1, Kline (1983) reported that ring-down counts (AE rate) was related more closely to the energy of the acoustic emission than any other parameter. Hence the cumulative count represents, qualitatively, the total acoustic energy generated by the material. This author intended to relate surface checking to the strain energy absorbed by a board and therefore AE rate and cumulative count were 'desirable' acoustic emission parameters. However, cumulative count was expected to be dependent on the history of loading. It is expected that during drying, the material constantly experiences minor, insignificant stress release events that simply redistribute the local stress field with little effect on the overall stress field. Material dried relatively slowly would experience numerous minor stress release events, each generating acoustic emission and contributing to an ever-increasing cumulative count.

Intuitively, the same material dried rapidly would generate less cumulative AE. Therefore AE rate was thought to be the more likely reliable measure of material failure and the following tests concentrated on AE rate. Noguchi et al. (1987) and Quarles (1992) reported that cumulative counts were not a useful measure of the propensity for surface checking, but differences in data acquisition hardware means caution must be applied when comparing results obtained in different studies.

In preparatory trials, perfectly backsawn green boards were deliberately dried under harsh constant conditions (typically 24°C DBT, 20°C WBT and 1m/s VEL) to induce surface checking. A typical AE rate response measured in the early stages of this study is shown in Figure 6.1. The outstanding feature of the response is the presence of the intermittent, energetic acoustic emission 'bursts' or peaks interspersed between periods of low activity (presumably corresponding to the 'insignificant' stress release events mentioned above). Surface check formation was expected to involve a relatively violent rearrangement of the local stress field and would thus correspond to one of these energetic peaks.

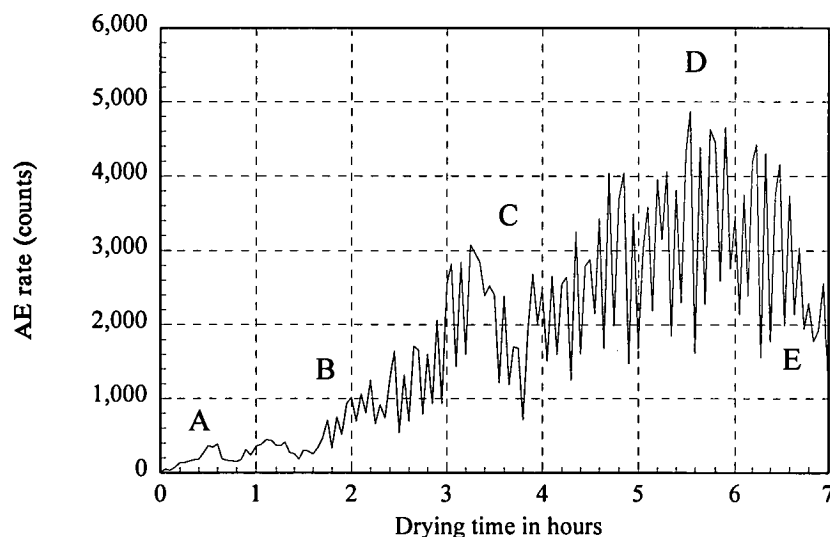


Figure 6.1 Typical AE response from surface checked eucalypt specimens

In terms of the overall shape, the response comprises a gradual increase in the acoustic emission peaks at the commencement of drying (A), leading to the onset of major acoustic emission activity (B), followed by a period of rapidly increasing AE rate (C) to the peak in the curve (D) and reasonably sharp dropoff to low levels (E).

In these preliminary tests, surface checks were always detected once the AE rate had peaked (D). As described in 3.6, incipient surface checks in drying timber do not induce immediate catastrophic failure. The edges of the checks cannot bear any stress so check formation increases the stress on the neighbouring intact fibres. Clearly, the average surface stress continues to increase after incipient surface checking and therefore the acoustic emission continues to increase. The surface stress increases until the surface unloading described in 1.3.1 commences. Clearly, surface checks form before the peak AE rate (D) in Figure 6.1. Noguchi et al. (1987) recorded similar shaped acoustic emission responses in end-checked *Z. serrata* disks and reported that surface checks formed before the peak AE event rate.

It was expected that surface check formation would be manifest as a distinct point in the measured acoustic emission behaviour and thus it appeared surface check initiation corresponded to a peak at one of two points on the AE event rate response : the onset of major acoustic emission activity (B) leading to the peak in the response (D), or an event rate between (B) and (D) - probably where the maximum rate of increase in the AE rate occurred (C). Noguchi et al. (1987) concluded that the AE rate and the average rate of increase of this rate were useful measures of surface checking.

6.3. Backsawn AE checking threshold trials in the laboratory

In this study, the backsawn AE checking threshold was determined before the quartersawn threshold because the former material is particularly prone to surface checking, simplifying the task of detecting 1mm long checks in a rough-sawn board surface. Backsawn boards were obtained from both a regrowth and over-mature tree and cut into 100x28x500mm boards.

The optimum technique to determine the AE checking threshold involves continuous observation of the drying board surface. The kiln working section had no viewing stations so board surfaces could not be observed in situ during the drying process. To facilitate observation of the board surface and visual detection of the first surface check, individual boards were dried in the laboratory. Each board surface was continuously scanned with a 10-times magnifying glass until surface checks were detected. Once satisfactory results were obtained in the laboratory, the results were verified by drying boards in the research kiln.

The AE checking threshold was determined by monitoring the acoustic emission in a single board during drying. When surface checks were detected, the initial 'trial' AE checking threshold was assigned the maximum AE rate measured during the drying test. This trial threshold was progressively reduced in subsequent tests on new green boards when smaller surface checks were detected at lower AE rates. This process was repeated until the true AE checking threshold corresponding to incipient surface checking was determined.

As discussed in 4.2, the AE transducer was initially clamped to a small machined region in the centre of the AE Board. The machined region extended approximately 70mm along the board and across the full board width. The machined surface maintained intimate contact between the transducer wear-plate and the board surface, minimising the risk of acoustic emission signal attenuation. The initial boards were subject to 25°C DBT, 19°C WBT and 5m/s VEL, producing surface checking within 30 minutes of drying.

Teething problems were encountered in the first trials. It proved to be very difficult to detect incipient 1mm checks in the rough sawn board face and the board surface area was simply too large to monitor effectively. The vessels are not perfectly parallel to the board surface so at numerous sites across the surface, the end of a vessel was cut by the saw and resembled a short fracture. As well, extraneous 'noise' generated by the fan was recorded by the transducers.

The noise was removed by relocating the fan and placing the AE Board on vibration-damping rubber strips. The remaining 500mm boards were cut into 150mm lengths to increase the number of available test samples. The ends of these samples were coated to prevent end drying and end checking. Plastic sheet was wrapped around the ends of these samples to restrict the drying (and thus acoustic emission generation) to the small, machined region around the transducer. This vastly simplified the task of detecting incipient surface checks.

In subsequent tests, surface checks were differentiated from the ends of vessels when they were approximately 5 mm long. Check *initiation* had not

been observed so initiation could only be attributed to the peak AE rate recorded. The time of observation of checks, peak AE rate and the cumulative count were recorded. With practice, extremely small checks were observed. Incipient checks often appeared as wet, dark lines. Check formation relieves the local tensile stress field and this effectively adds a compression gradient to the local stress field. This forces free water beneath the surface to migrate towards the check. When incipient checks appeared as dark lines, one could assume with confidence that check formation occurred very recently and therefore a particular AE rate was attributed to check initiation.

After approximately 30 laboratory drying trials, a relationship between surface check initiation and AE rate was determined. When the AE rate exceeded 250 counts per 15 seconds, surface checks approximately 1mm long were observed in the machined surface. Provided the AE rate did not attain 250 counts, surface checking was not detected in the backsawn boards. This AE rate had been defined previously by Booker (1990) as the "onset of major acoustic emission activity leading to the peak [AE rate] in the response".

As reported by Schaffner (1981), checks were generally observed to originate at vessels. From a stress analysis viewpoint, a vessel constitutes a large notch around which drying stresses concentrate. The checks form at the end of a vessel and then run along the surface and into the board, lying in the radial-longitudinal plane.

This characteristic acoustic emission parameter in backsawn eucalypt boards was then tested during drying in the research kiln.

6.4. Backsawn AE checking threshold trials in the kiln

Verifying the AE checking threshold during kiln drying proved difficult because it was not possible to observe the sample board surface in situ. Removing the AE Board and inspecting the surface with the magnifying glass generated 'noise' that saturated the acoustic emission signal generated within the wood so acoustic emission was not recorded during inspection time. Incipient surface checks are so small that board surfaces must be inspected for at least 5 minutes to positively determine whether checks were

present. It was possible that surface checks might form *during* board observation whilst the AE transducer was not connected.

In the initial trials, the drying conditions were relatively severe to induce rapid surface checking and rapid verification of the AE checking threshold. This was satisfactory initially, but as the 'trial' AE checking threshold reduced with progressively smaller surface checks detected at lower AE rates, the harsh drying conditions became a hindrance. This was primarily due to the rapid growth of surface checks after initiation and more specifically the occurrence of high magnitude acoustic emission peaks after check initiation. In other words, once the AE rate exceeded the current 'trial' AE checking threshold, it was almost impossible to remove the AE Board from the kiln and inspect the surface before at least one peak in the AE signal greater than the trial checking threshold was measured. This effectively made the test results redundant because surface check initiation could only be assumed to correspond to the highest peak measured. Hence, as progressively smaller checks were detected, the drying conditions were modified to reduce the rate of growth of surface stress (and acoustic emission) and allow more time to observe the AE Board after the AE rate exceeded the 'trial' AE checking threshold.

In each trial, a green AE Board was situated in the centre of a full batch of previously dried timber, simulating the air flow patterns in commercial drying. The transducer was clamped to the machined region of the AE Board. Plastic wrapping was not employed so observation of the surface was restricted to the region immediately surrounding the transducer. The initial drying conditions used were 22°C DBT, 20°C WBT and 1.5 m/s VEL.

During inspection of board surfaces, those points where vessels 'ran out' on the board surface were observed first with the magnifying glass, for these constituted natural stress raising sites and were thus the most likely check initiation sites. As in the laboratory trials, observation of wet, dark checks allowed check initiation to be confidently associated with a recent acoustic emission peak.

The AE checking threshold was reduced to 220 counts after the first trial. A peak in the acoustic emission response occurred at 220 counts, but the AE Board was not inspected until the AE rate attained the 250 count checking

threshold. The board was immediately removed from the kiln and inspected with a magnifying glass. Very thin, 3 to 4 millimetre long checks were observed. Experience had shown that the checks could not have grown to that size in the short time between the 220 count and 250 count peaks. Check initiation was attributed to the 220 count AE peak and the AE checking threshold was decreased accordingly. In the subsequent trial, surface checking was observed in the machined surface after 24 hours when the peak AE rate attained was 200 counts.

Run 3 lasted 12 days and the average moisture content in the AE Board dropped from 100% to 75%. The 200 count AE checking threshold was not exceeded during the trial. After 12 days, no visible checking was observed in the machined surface but 50 and 60 mm long checks were present in the rough sawn surface of the AE Board. It was immediately clear that clamping the transducer to the machined region 'masked' the state of the stresses in the rough sawn surface. The machined surface was considerably stronger than the surrounding rough sawn material. In the preceding trials, a lack of experience resulted in small surface checks being observed in the machined region without detection of (presumably larger) checks in the rough material; had the trials been performed over a longer period, the checks in the rough surface would have been apparent.

Several short drying trials revealed that clamping the AE transducer directly to the rough board face, using the grease transmission couplant under the wear-plate to reduce signal attenuation, provided satisfactory acoustic emission transmission characteristics. Trials in the research kiln to determine the AE checking threshold with the transducer applied directly to the rough face were commenced.

In the first of these trials, the AE checking threshold was reduced to 140 counts. The acoustic emission response recorded in Run 8 is seen in Appendix A. The AE Board was inspected immediately the 132 count AE peak was recorded. Large (4-5mm) checks were detected so the checking threshold was reduced to 100 counts. In Run 9 (Appendix A), a peak was obtained at 98 counts and small surface checks were detected so the checking threshold was reduced to 80 counts.

The AE Board was inspected 28 hours after the commencement of drying in Run 11 (Appendix A) and no definite checking was observed. The peak AE rate measured in this trial was 72 counts. Herein lay an inherent problem in inspecting boards before they had checked; checks were initially so small it was difficult to rapidly ascertain that none were present. When a check was found after inspecting the board for 10 minutes, say, it was not known whether it was present initially and had simply been overlooked or formed subsequently during the time out of the kiln. It became common practice to scan a board surface for 5 minutes at a time. If no checks were detected the board was immediately wrapped in plastic to ensure no further drying occurred. The board could then be inspected for short periods as often as desired without inducing surface checking during the observation.

The peaks in the acoustic emission response recorded in Run 11 lay very nearly along a straight line, within the variability of the material. Similar behaviour was reported by Booker (1990) in drying tests performed with backsawn and quartersawn eucalypt boards under constant drying conditions, except much higher AE rates were measured in those tests. Inspection of the Run 8 and 9 acoustic emission responses also revealed approximately linear increase in the peaks to the peak AE rate. The slopes of the lines passing through the acoustic emission peaks agreed remarkably well. In Runs 8 and 9, the line passing through the acoustic emission peaks with this slope passed through an AE peak of 95 counts at 28 hours. When the line passing through the peaks in the Run 11 response was extrapolated beyond the 72 count rate recorded, it passed through 100 counts. Had the drying been allowed to continue in this trial, it appeared an AE peak would have occurred at 100 counts.

An AE peak occurred at 98 counts in the next trial. The AE Board was immediately inspected but the possible check sites were so small that they could not be positively identified without marking the sites and allowing further drying. These possible checks subsequently extended along and into the board with drying in the laboratory. In Run 14 (Appendix A), the AE Board was removed daily from the kiln and inspected. No surface checking was observed after 92 hours of drying. Upon replacing the AE Board in the kiln at this time, the AE rate rose immediately to 96 counts and subsequently to 136 counts. Tiny surface checks were immediately detected upon removing the AE Board from the kiln.

The 100 count AE rate represented incipient surface checking in this batch of rough sawn backsawn eucalypt boards at temperatures in the vicinity of 20°C. Provided the AE rate generated in a sample board did not attain 100 counts during drying, surface checking did not occur. Examination of the cumulative count at failure in these trials revealed that the cumulative count was not representative of the development of surface checking. The cumulative count at failure appeared to be dependent on the drying history. The cumulative count was higher in those boards that dried for longer times before surface checking, as predicted in 6.2. Table 6.1 presents a summary of the AE checking threshold trials. Trials 1 to 12 represent summary data for the backsawn material.

This 100 count backsawn AE checking threshold was then verified in more batches of backsawn material dried at temperatures in the vicinity of 22°C. The basic density of these batches varied from 510 to 670 kg/m³. The 100 count AE checking threshold appeared to be independent of basic density and thus was independent of bulk material stiffness, since stiffness is nearly linearly related to basic density. This suggested that the acoustic emission was a fundamental property of the material and independent of the bulk material properties. The AE checking threshold appeared to be constant for Tasmanian backsawn eucalypt material dried near 20°C. This precluded the tedious process of determining the AE checking threshold for every batch of backsawn timber dried and made the acoustic emission-based kiln control system far more feasible.

Table 6.1. AE checking threshold results.

Trial #	Basic Density (kg/m ³)	¹ Growth ring angle, θ (°)	² Drying time (hours)	peak AE rate (counts/15sec)	³ Cumulative Counts (counts)	Surface checking	No surface checking @ AE rate
1	670	0	28	135	21000	✓	
2			28	96	25000	✓	
3			28	72	29000	✗	
4			92	105	90000	✓	
5	515	0	24	82	50000	✗	82
6			160	45	9000	✗	45
7	560	0	14	190	33000	✓	86
8			130	190	90000	✓	86
9			9	115	42000	✓	
10	540	0	30	140	116000	✓	86
11			23	130	54000	✓	80
12			190	60	280000	✗	60
13	600	45	10	180	56000	✓	
14			9	100	30000	✓	
15			13	100	50000	✓	
16			34	85	170000	✗	
17	590	45	4	98	24000	✓	
18			4	80	19000	✗	
19			3	86	13000	✗	
20	630	45	75	120	84000	✓	80
21	630	45	75	100	45000	✓	
22	600	80	1.5	120	16000	✓	
23			0.4	112	16000	✓	
24			0.3	96	3000	✓	
25			4	110	3000	✓	
26			0.5	80	6500	✗	
27	620	80	15	145	52000	✓	
28			30	105	64000	✓	
29			8	104	17000	✓	
30			21	92	28000	✓	
31			70	95	180000	✓	
32	620	90	43	90	65000	✗	90
33			1	200	7500	✓	
34			3	180	13000	✓	
35	580	90	2	170	10000	✓	
36			2	170	12000	✓	
37			1	130	6000	✓	

¹ Angle subtended from board surface to incident growth rings. $\theta=90^\circ$ corresponds to a perfectly quartersawn board, $\theta=0^\circ$ corresponds to a perfectly backsawn board.

² When surface checking occurred, drying time refers to the drying time at which the AE rate exceeded 100 counts, otherwise drying time refers to the total test time.

³ When the peak AE rate exceeded 100 counts, cumulative counts corresponds to the total counts at that 100 count AE rate, otherwise the cumulative counts corresponds to the total counts measured.

6.5. AE checking threshold and collapse

The AE checking threshold was then tested at higher temperatures to investigate a relationship between acoustic emission and temperature. Another batch of backsawn regrowth boards was obtained from the sawmill and kiln trials were conducted at elevated temperatures.

Various trials were performed at 30°C DBT, 24°C WBT and 1.5 m/s VEL. Peak AE rates were obtained at 95, 95, 90 and 96 counts respectively. The AE Board was inspected immediately these peaks occurred and small surface checks were detected. The checks were rather localised, confined to a narrow band running the length of the AE Board. The check interiors appeared dark and wet due to the exposure of moisture below the board surface, implying the fractures had formed very recently.

Drying was then performed at 40°C DBT, 28°C WBT and 1.5m/s VEL. In the first trial, surface checks were observed on the AE Board after a peak AE rate of only 74 counts. Further high temperature trials revealed surface checks formed before the AE rate attained 62 counts. Once again, the surface checks were confined to a narrow region rather than across the whole face. In several trials, large localised checks (60mm long and 2mm wide) passed directly under the AE transducer and the AE rate did not exceed 60 counts. Severe collapse, represented by grossly distorted board sections and slight washboarding, was evident.

The AE checking threshold appeared initially to be dependent on drying temperature. However, detailed qualitative analysis of the localised differential shrinkage induced by collapse revealed that the AE checking threshold was directly dependent on the occurrence of collapse shrinkage and only indirectly dependent on temperature. When a localised region of fibres beneath the surface experiences collapse, the surface fibres directly above are subject to normal shrinkage due to surface drying and shrinkage induced by the underlying collapse shrinkage. This causes premature surface checks in these highly stressed surface fibres well before the remainder of the surface approaches the ultimate stress. The localised nature of the surface checking observed on boards subject to collapse supported this argument. Collapse propensity is dependent on drying temperature and

thus the indirect relationship between the AE checking threshold and temperature.

At these elevated temperatures, it appears the majority of surface fibres are significantly below the ultimate stress when premature surface checks induced by underlying localised collapse form. The transducer is caused to ring by the numerous stress release events occurring in a region surrounding the transducer and not by individual flaw extension processes. The measured AE rate represents the cumulative 'ringing' effect of the AE transducer. Clearly, when the majority of surface fibres are well below the failure criterion, the measured AE rate will represent the level of crystalline slip activity in these less highly-stressed fibres, not the slip activity of a localised region of fibres. It is important to re-emphasise that acoustic emission represents crystalline slip activity and not surface check formation directly. Hence surface checks due to collapse shrinkage may occur (and even initiate very near the AE transducer) without causing the AE rate to attain the AE checking threshold.

The fact that surface 'macro-checks' passed directly underneath the transducer (and surface checks passed very near the transducer in many other trials) without causing high AE rates is further evidence that the transducer is not caused to ring by intermittent micro-cracks (which presumably generate significantly lower energy stress waves than the macro-cracks). Nor is the acoustic emission representative of stress release events caused by surface check extension, since the position of surface checks in the preceding tests at low temperatures had no effect on the measured AE checking threshold. This is further evidence that the AE transducer is caused to ring by the numerous, tiny intermittent crystalline slips in fibres surrounding the transducer.

The propensity for collapse shrinkage in Tasmanian eucalypts means acoustic emission cannot be successfully related to surface checking at elevated drying temperatures. Localised collapse shrinkage beneath the surface induces localised surface checking directly above when the AE rate is significantly lower than the AE checking threshold. Collapse shrinkage must be avoided if acoustic emission is to be used as the feedback measure of surface check development in an optimal kiln control system.

6.6. Quartersawn AE checking threshold

Backsawn eucalypt timber experienced surface checking when the AE rate exceeded the 100 count AE rate. This level was determined to be independent of material density and bulk properties in general, as predicted by the hypothesis relating acoustic emission to slips within crystalline cellulose regions described in 3.6. Naturally, the next line of investigation involved verifying that the 100 count backsawn AE checking threshold also applied to quartersawn eucalypt material.

A batch of near perfect quartersawn boards was obtained from the sawmill, with the grain angle only slightly off 90 degrees to the surface. In turn, single AE Boards were dried in the centre of the existing dry batch of boards in the kiln and when the AE rate exceeded 100 counts, the AE Board was immediately inspected. It was even more difficult to differentiate fractures from vessels and upturned fibres in the quartersawn material than in the backsawn material. Using the magnifying glass, surface checking was not detected in these first boards when the AE rate attained 100 counts. Indeed, surface checks were not detected in boards where the AE rate had attained 300 counts. It was suspected that the check detection technique employed in backsawn material was not directly applicable to the quartersawn material. This suspicion was confirmed when incipient checks were observed by looking at an angle to the (quartersawn) face of boards previously considered to be free of surface degrade. Board surfaces must be viewed directly radially when searching for incipient surface checks in quartersawn material. This is a major finding in the study and is discussed below in 6.7.

Once this was understood, further checking threshold trials were performed on batches of green quartersawn boards obtained from the sawmill. Scanning board surfaces radially with the magnifying glass revealed incipient surface checks at an AE rate of 100 counts. There appeared to be no significant difference in AE rate measured at failure due to direction of sawing (Booker 1994b). As expected, the AE rate generated at the onset of surface checking in both backsawn and quartersawn Tasmanian eucalypt material was very nearly constant. The acoustic emission is related to the fundamental structure of the cell walls and this is effectively constant.

6.7. Detecting incipient surface checking in quartersawn material

Initial trials revealed that the AE rate was attaining values as high as 300 counts in apparently intact quartersawn material. This was quite surprising and resulted in a thorough qualitative analysis of the behaviour of incipient surface checking in quartersawn material.

As described in section 6.1, incipient surface checks propagate radially in the first instance since the radial plane is the weakest plane in the tree. It was realised that when quartersawn boards were inspected before significant check propagation had occurred, the checks may still be lying in the radial direction; that is the surface stress parallel to the wide face had not acted for a sufficiently long period to drive the checks directly into the board. With this in mind, the quartersawn boards dried in the original trials were inspected again. However, the boards were deliberately oriented so that one was looking directly radially at the surface (see Figure 6.2). This immediately revealed that the boards that were thought to be free of surface checks actually contained numerous small checks. These lay in the radial direction and were thus invisible when viewed from directly above.

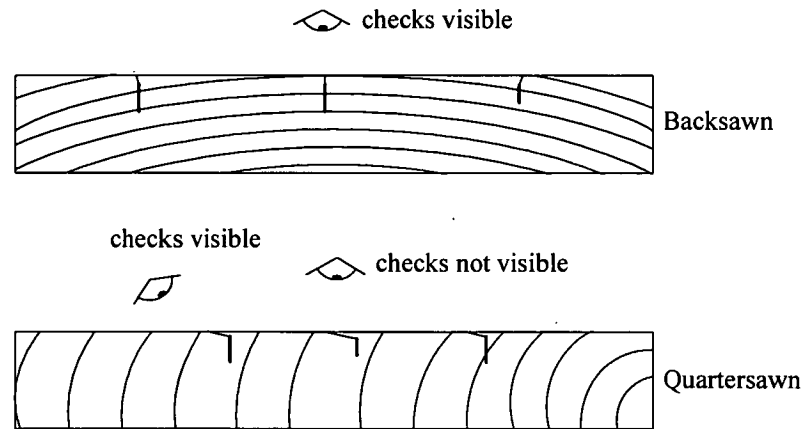


Figure 6.2. Surface checking in backsawn and quartersawn boards.

Inspections at the sawmill subsequently revealed a proportion of surface checked quartersawn boards contained large checks (greater than 300mm long) running directly perpendicular to the wide face while other boards contained similar size checks running radially into the boards (that is the checks had not changed direction since initiation). Further investigation

revealed the former boards were invariably kiln dried whilst the latter boards had been air-dried. This behaviour is related to the relative magnitude and 'time of action' of the surface tensile stress. Air-dried boards are typically dried slower and with lower peak surface stress than kiln dried boards. Thus incipient surface checking is exposed to lower parallel to the surface tensile stress and the direction of check propagation may not necessarily be turned around from the radial direction to that perpendicular to the surface.

In non-backsawn boards, the directions of check initiation and propagation are not aligned (see Figure 6.2). In the extreme case of a perfectly quartersawn board, the directions are perpendicular. It was originally thought that incipient checks in non-backsawn boards would propagate in the radial direction and immediately be arrested. The checks would not be visible, even with the magnifying glass, until the tensile stress field parallel to the surface drove the check into the board perpendicular to the surface.

In the perfectly quartersawn board, check initiation would occur directly parallel with the surface and not propagate into the board at all. In boards with growth rings ranging from nearly perfectly quartersawn to say 45°, a check initiates radially but rapidly strikes sound wood and is halted. The check only propagates into the board perpendicular to the surface when the stress field turns the check around. It appeared that the checks did not change direction as rapidly as expected.

Communication with an experienced sawmiller revealed quartersawn boards which are apparently free of degrade often tear and rip while being moulded. It is proposed that the boards are in fact surface checked but the checks had propagated radially rather than perpendicular to the board surface and were not visible to the naked eye unless the board was oriented correctly. It was also predicted that surface checks in quartersawn material may well change direction beneath the surface, that is initiate radially but change direction beneath the surface. Such behaviour was observed and would explain problems incurred when machining material apparently free of surface degrade.

As in the backsawn boards, the checking threshold was tested and proved in quartersawn boards cut from another two trees and dried near 20°C. The

results of the AE checking threshold tests performed at low temperatures are summarised in Table 6.1. At the time of this discovery, check development had been successfully related to a repeatable acoustic emission parameter but the acoustic emission had not yet been related to a failure stress or strain. KILNSCHED was used to relate acoustic emission to the instantaneous strain in backsawn and quartersawn material in this study, as discussed in Chapter 7.

6.8. Backsawn radiata pine AE checking threshold

The AE checking threshold was determined to be substantially independent of the direction of sawing in eucalypt boards of different basic density and was thus independent of bulk stiffness. Assuming the acoustic emission was due to intermittent slips within the crystalline cellulose of cell walls, it was predicted that the very nearly constant proportion of crystalline cellulose in both hardwoods and softwoods reported by Siau (1984) would result in the same AE rate at failure in different timber species. This hypothesis was tested first in plantation radiata pine (*Pinus radiata*) boards.

The first test was performed in the research kiln but subsequent drying tests were performed in the laboratory with a fan heater at approximately 40°C DBT and 1.5m/s VEL. Such conditions were not expected to produce seasoning degrade, since radiata pine is commonly dried from green at temperatures exceeding 100°C without damage. In the first test, the acoustic emission exceeded 2000 counts, that is twenty times the 100 count AE checking threshold measured in eucalypt boards, but no surface checking was observed. Figure 6.3 depicts typical acoustic emission behaviour measured in the radiata pine boards. In subsequent tests, the acoustic emission suddenly increased from very low levels to several thousand counts without warning. This behaviour was significantly different from the manner in which the acoustic emission increased in eucalypt boards. Such high count rates were attained when drying eucalypt boards only under extended periods of harsh conditions with serious surface checking forming.

The acoustic emission behaviour was measured under different drying temperatures to investigate whether the acoustic emission was due to a thermal expansion effect or perhaps cavitation, as reported by Tyree and Dixon (1983). After several minutes drying with the fan heater turned on,

the fan was turned off. The acoustic emission immediately decreased, and upon reapplication of the heat, the acoustic emission increased dramatically. This rapid response meant the acoustic emission was indeed due to stress redistribution occurring at the surface.

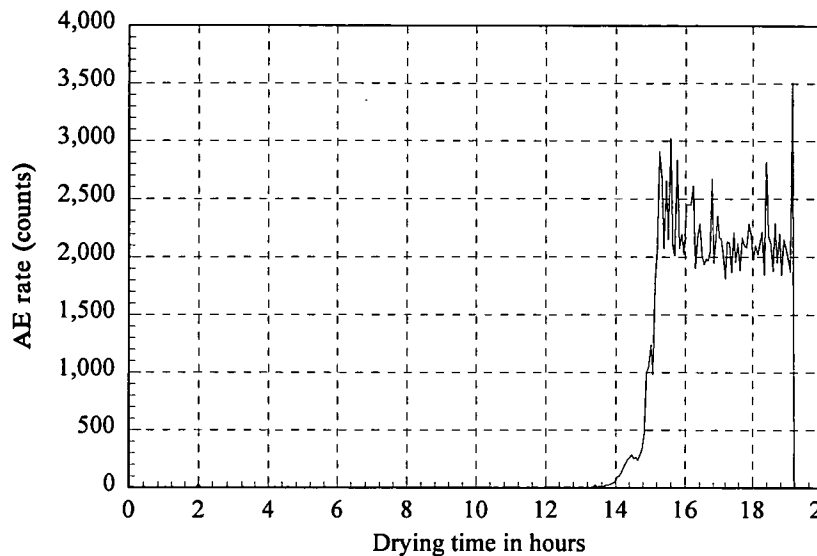


Figure 6.3. Typical AE response measured in *radiata* pine at 25°C.

A green specimen was entirely coated in paint to retard moisture loss and dried at 50°C, approximately 10°C hotter than the previous drying conditions. The sudden increase in AE rate was postponed several hours (the paint did not completely retard moisture loss). Therefore the sudden increase in AE rate was not due to temperature and thermal stresses alone but was inherently related to moisture loss.

The 'explosive' nature of the acoustic emission response in pine appears to represent brittle material failure, although surface checking was not present so the brittle failure did not correspond to ultimate material failure. Elements within the pine structure suddenly generated 'massive' levels of acoustic emission without warning. Reference to the texts mentioned in Chapter 3 describing the cellular structure of softwoods revealed the most likely candidate for such brittle failure was the resin canals, structural elements not present in the Tasmanian eucalypt. In the green state, the walls of the canals at the surface are saturated, but upon drying it is plausible that the moisture is removed rapidly, causing the canals to become stiffer and more brittle. At a critical combination of surface tensile stress and stiffness, it appears the canals commence to experience brittle failure. It is plausible that

the stress redistribution events themselves are crystalline slips within the canal walls.

6.9. Backsawn myrtle AE checking threshold

As a result of the spurious acoustic emission behaviour measured in the pine boards, a non-eucalypt hardwood species was studied. It was hoped that the structure of this hardwood would be rather more similar to the eucalypts already studied and would thus produce more conclusive results.

Boards were obtained from a myrtle (*Nothofagus cunninghamii*) tree. These trials were initially performed in the laboratory.

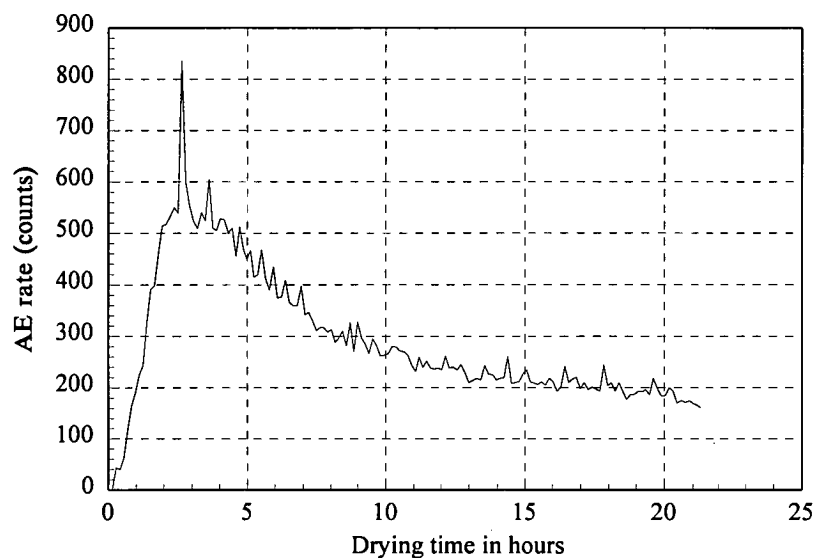


Figure 6.4. Typical AE response measured in myrtle at 25°C.

In the first trial, drying was induced with the heater and the AE rate increased rapidly to several thousand counts before gradually decreasing to approximately 100 counts. Typical acoustic emission behaviour measured in the myrtle boards is depicted in Figure 6.4. This response resembles the familiar distribution curve measured in this study (Figure 6.1) and reported by Noguchi et al. (1987). The acoustic emission did not increase in the 'explosive' manner encountered in the pine boards. In subsequent trials under forced drying in which the acoustic emission had attained several thousand counts after only a matter of minutes, turning off the heater resulted in a dramatic decrease in acoustic emission to very low levels before returning to the previous AE rates when the heater was turned on again.

This showed that, as with the pine, the high acoustic emission signal was generated by surface stress release activity and was not due to internal events.

Examination of photomicrographs of myrtle specimens revealed the material contained significantly more vessels than the eucalypts and the vessels were significantly smaller. It is hypothesised that crystalline slips occur in the thin-walled vessels. The much lower proportion of vessel to fibre wall means the signal is dominated by stress redistribution events within the fibre walls.

It is likely that movement of the vessels does not generate sufficient shrinkage to cause material failure. Subsequent tests involved maintaining very low temperatures initially to maintain high vessel wall stiffness. Stress redistribution events in the form of crystalline slips still occur. When the AE rate attained 60 counts, the fan was turned off and the acoustic emission immediately decreased. Later, the fan was turned on again and the acoustic emission immediately rose to 180 counts. The AE peaks decayed to a 40 count 'background' level over a period of several hours before the AE Board was inspected. The bottom 'chain-sawn' surface contained reasonably uniformly spaced surface checks running the full specimen length. The top surface contained several end checks that had progressed towards the transducer and some possible small check sites near the transducer. The next test was commenced and again the acoustic emission rose dramatically when the fan was turned on. The peak AE rate was 150 counts, with large checking on the bottom surface (chain sawn surface) and small 3-4 mm checks near the transducer. One large end check ran past the transducer and a 15-20 mm check resided near the transducer.

When the fan is turned off after forced drying, the air surrounding the AE Board is immobile and the partial pressure in the air attains equilibrium with the partial pressure in the surface fibres. The moisture concentration in the air surrounding the electric heaters is much lower. When the fan is operated, the boards are suddenly exposed to a band of air at significantly lower moisture concentration. The transient effect is a sudden increase in the drying rate and corresponding increase in the surface stress.

It appears the AE checking threshold was near the predicted 100 count rate. This is only attained by maintaining a low drying temperature so as to

maintain high stiffness in the weak vessels. The large surface checks running past the transducer did not produce spurious high count rates. Similar behaviour occurred in samples subject to localised collapse shrinkage (as discussed in 6.5). Despite the strain energy (discussed in Chapter 8) released by macrocrack extension, it appears that the duration of the extension process is so short that the transducer output decays exponentially below the DC threshold very rapidly and relatively few counts are recorded. Despite the length of the crack, the only source of acoustic emission is at the tip; there can be no stress acting on the sides of the crack.

6.10 Summary

The acoustic emission generated in Tasmanian eucalypt boards at the onset of surface checking appears to be independent of the timber bulk material properties. Therefore the acoustic emission is considered to be related to the structural composition of the fibre walls. It appears that radiata pine contains structural elements (such as resin canals for example) which experience sudden failure of a brittle nature and generate 'massive' AE rates. The eucalypts studied do not appear to experience such failure. Myrtle is more similar in bulk structure to the eucalypts than the radiata and rather more similar acoustic emission behaviour was observed. It is plausible that timber species with a cellular structure similar to the Tasmanian eucalypt genus will generate similar acoustic emission behaviour.

Chapter 7

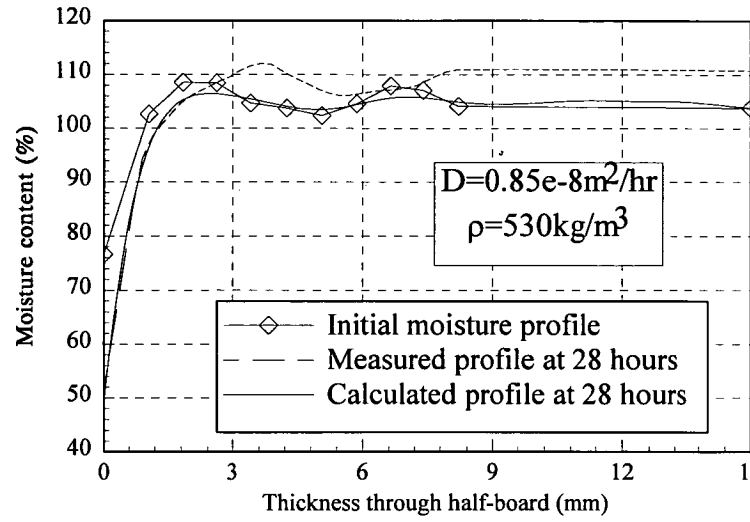
Relationship between surface instantaneous strain, AE and drying conditions

This chapter compares measured drying behaviour with drying behaviour calculated with KILNSCHED. The diffusion coefficient in KILNSCHED was inferred by matching calculated half-thickness moisture profiles with those regularly measured in a sample MP Board during drying. The calculated surface stress and instantaneous strain were then compared with the acoustic emission measured in an end-matched AE Board. The AE peaks closely correlate with surface instantaneous strain (Booker 1994a). The acoustic emission and surface instantaneous strain are both intimately related to the difference in moisture concentration between the surface fibres and the free stream air and to the surface stiffness. Acoustic emission and surface instantaneous strain are not directly related to drying temperature or relative humidity alone. This chapter concludes with a basic control strategy for an automatic kiln control system that adjusts the drying conditions in response to the measured acoustic emission in sample boards.

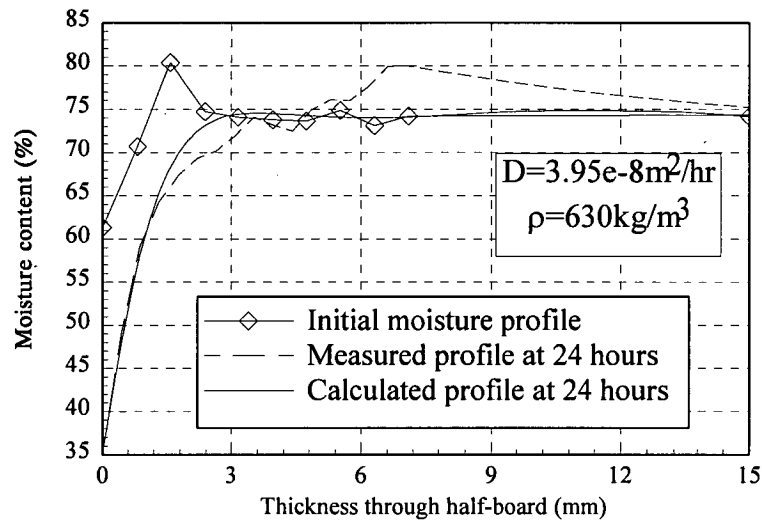
7.1. Calculated and measured moisture profiles

Figure 7.1a represents measured and calculated half-thickness moisture profiles in a perfectly backsawn 30mm thick MP Board after 28 hours drying. Figures 7.1b and 7.1c represent measured and calculated profiles in two separate quartersawn boards.

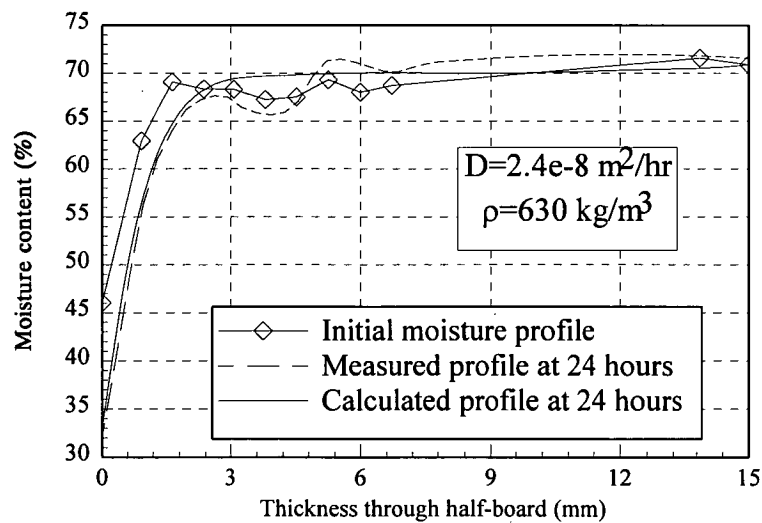
Figure 7.1 presents typical examples of the non-uniform nature of initial moisture profiles measured in this study. Significant surface drying occurred whilst the green timber was transported from the sawmill (despite the timber being wrapped in black plastic during this period). The eucalypt material appears to be particularly prone to 'wet patches', localised regions of higher than average moisture concentration beneath a board surface (Figure 7.1b reveals such a region 2mm below the board surface). Such initial moisture profiles are not satisfactorily approximated by assuming a uniform moisture content within the board. KILNSCHED was modified by this author to allow for an arbitrary initial moisture profile.



(a)



(b)



(c)

Figure 7.1. Calculated and measured moisture profiles in green eucalypt boards showing the variations of initial moisture content.

As discussed in 5.2.1, KILNSCHED originally calculated internal moisture distributions by fitting parabolas to the natural logarithms of the deficiencies in moisture concentration at three neighbouring points. Clearly, computational problems arise when the calculated moisture concentration at a particular point *increases* (causing a negative deficiency), as might occur when the board centre is at a lower concentration than surrounding wet patches. KILNSCHED was modified by the author to calculate the drying behaviour based on the absolute moisture concentration at each point through the board thickness.

The half-thickness moisture profiles in Figure 7.1 are well matched in the first millimetres beneath the surface but differ somewhat through the board interior. The initial moisture profile in Figure 7.1b contains a wet patch 2mm below the surface. The profile measured 24 hours later in a sample only 30mm away from the initial sample does not contain this wet patch but does contain a separate wet patch 7mm below the surface. In this situation, it is clearly not possible to fit the 'apparent' centre drying behaviour and the surface drying to the calculated drying behaviour with a single diffusion coefficient. The diffusion coefficient used in such cases was always selected to produce close agreement between the measured and calculated profiles near the surface for this moisture gradient controls the surface stresses (Figure 7.1 reveals excellent surface moisture gradient agreement in each case). At this early stage of drying, the centre regions are significantly above FSP and have experienced no tendency to shrink. At such high internal moisture contents, the actual magnitude of the centre regions has little effect on the calculated stress and strain profiles, provided the gradient is accurate.

7.2. AE related to surface instantaneous strain

Figure 7.2.1 shows the drying conditions at the centre of the kiln stack measured in the test corresponding to Figure 7.1a. Figure 7.2.2 shows the calculated surface σ and surface ϵ_i and measured AE rate. Figure 7.2.3 represents the moisture concentration of the air in equilibrium with the surface fibres (c_{vw}) calculated with KILNSCHED, the moisture concentration in the free stream air outside the boundary layer (c_m) and the moisture concentration differential between the surface of the wood and air ($c_{vw}-c_m$). Refer to 5.2 for the relevant boundary layer equations.

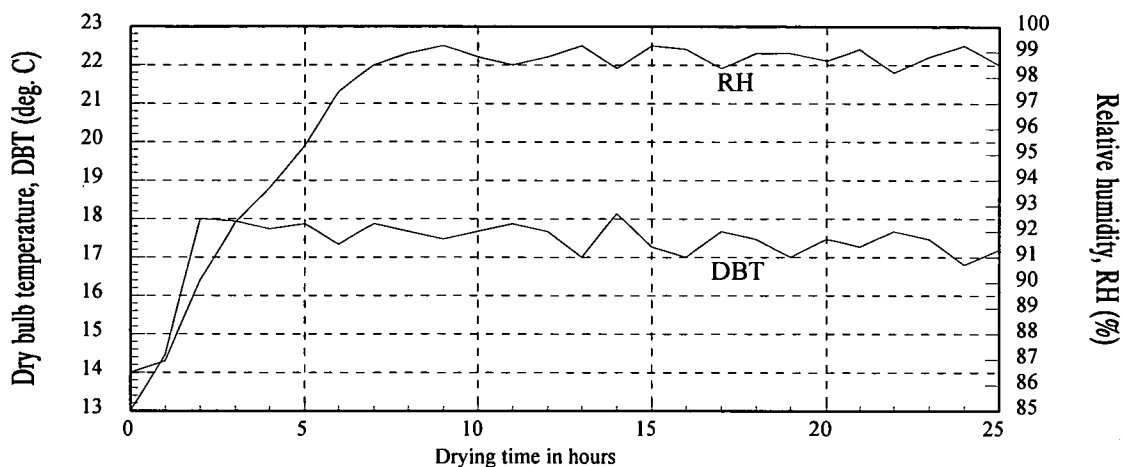


Figure 7.2.1. Measured centre-stack dry bulb temperature and relative humidity.

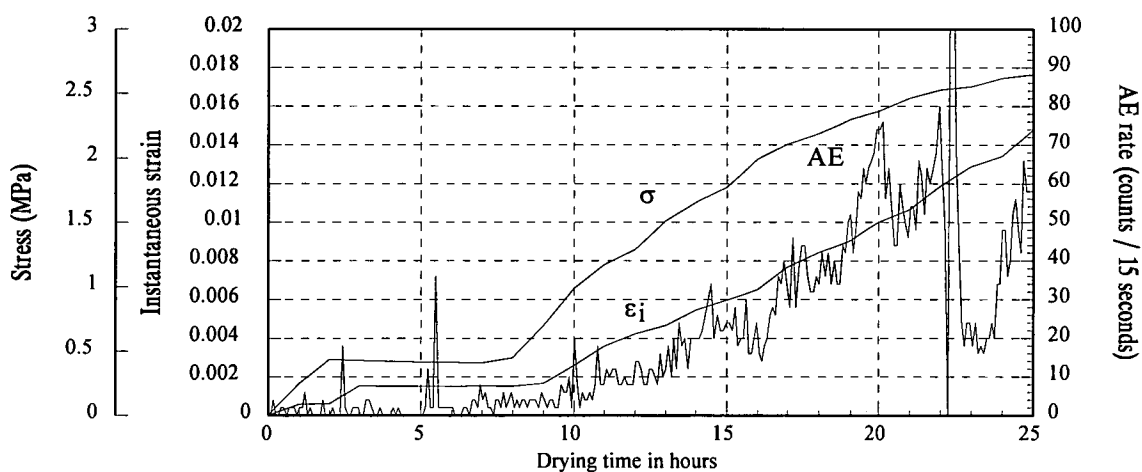


Figure 7.2.2. Measured AE rate and calculated surface stress (σ) and instantaneous strain (ϵ_i).

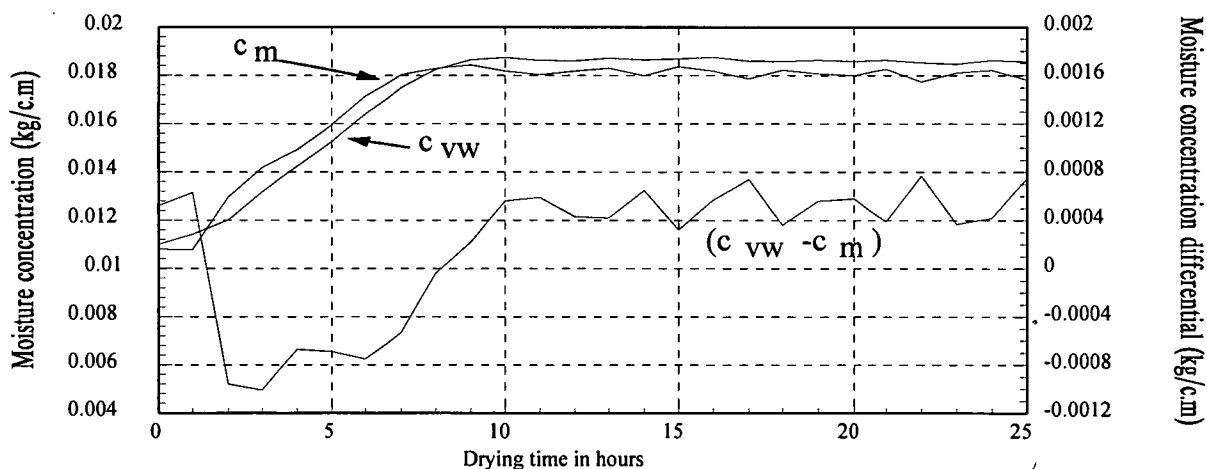


Figure 7.2.3. Surface moisture concentration (c_{vw}), moisture concentration in air (c_m) and moisture concentration differential ($c_{vw} - c_m$).

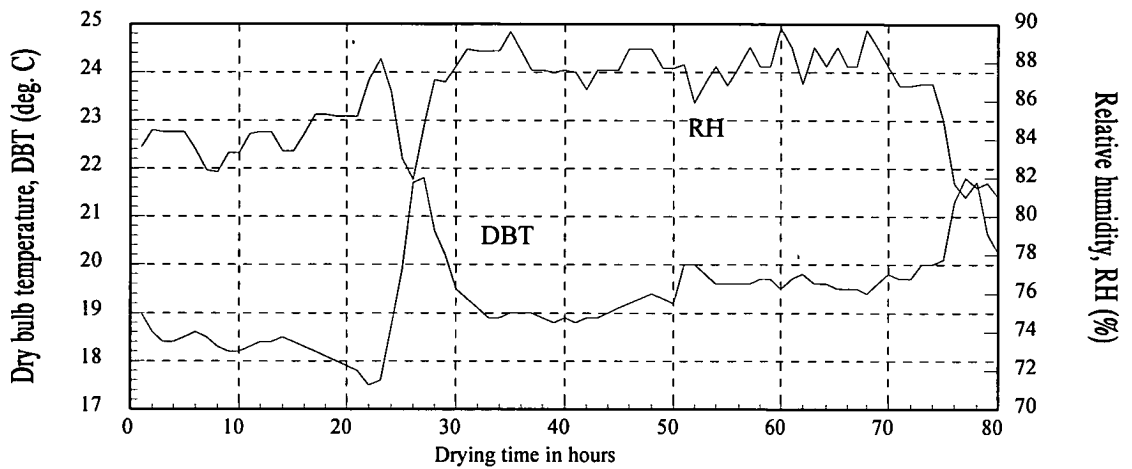


Figure 7.3.1. Measured centre-stack dry bulb temperature and relative humidity.

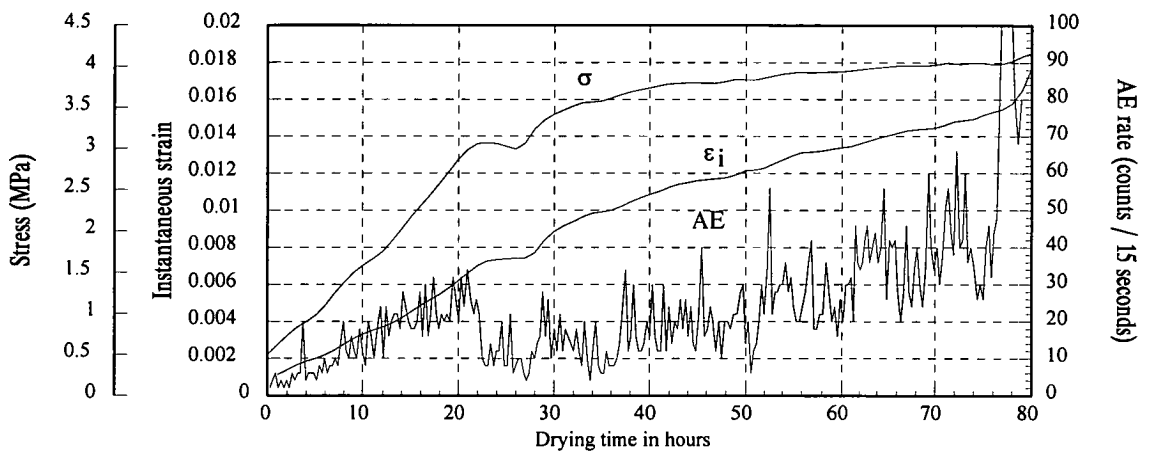


Figure 7.3.2. Measured AE rate and calculated surface stress (σ) and instantaneous strain (ϵ_i).

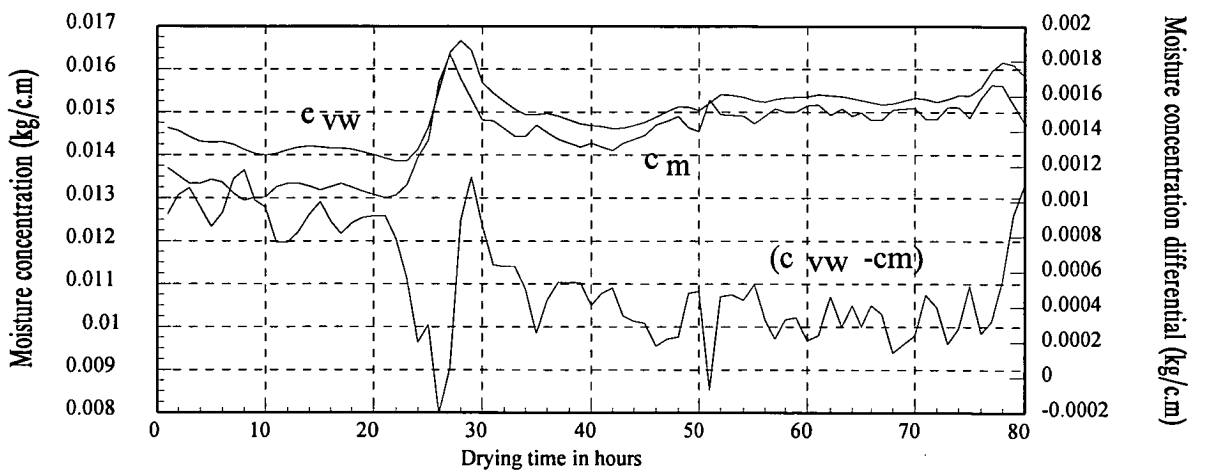


Figure 7.3.3. Surface moisture concentration (c_{vw}), moisture concentration in air (c_m) and moisture concentration differential ($c_{vw} - c_m$).

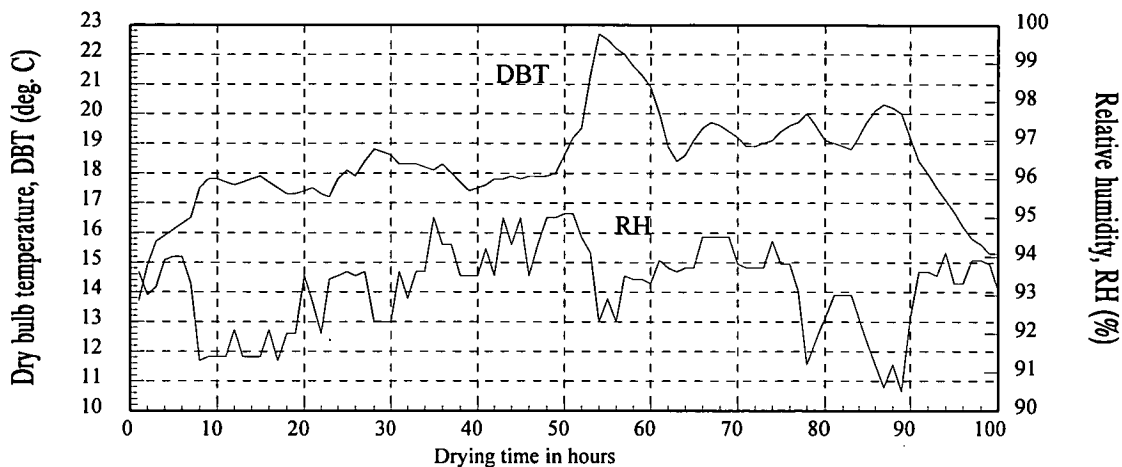


Figure 7.4.1. Measured centre-stack dry bulb temperature and relative humidity.

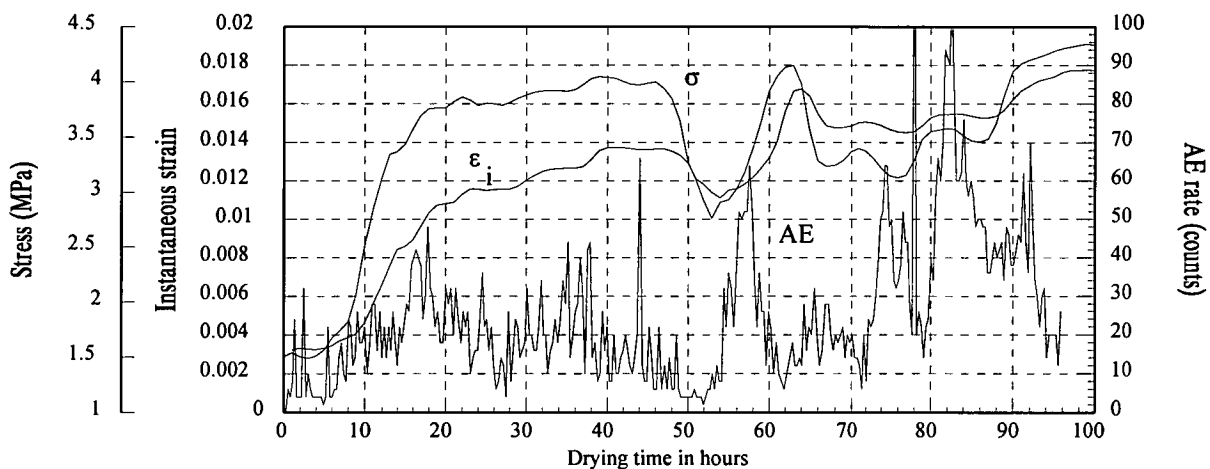


Figure 7.4.2. Measured AE rate and calculated surface stress (σ) and instantaneous strain (ϵ_i).

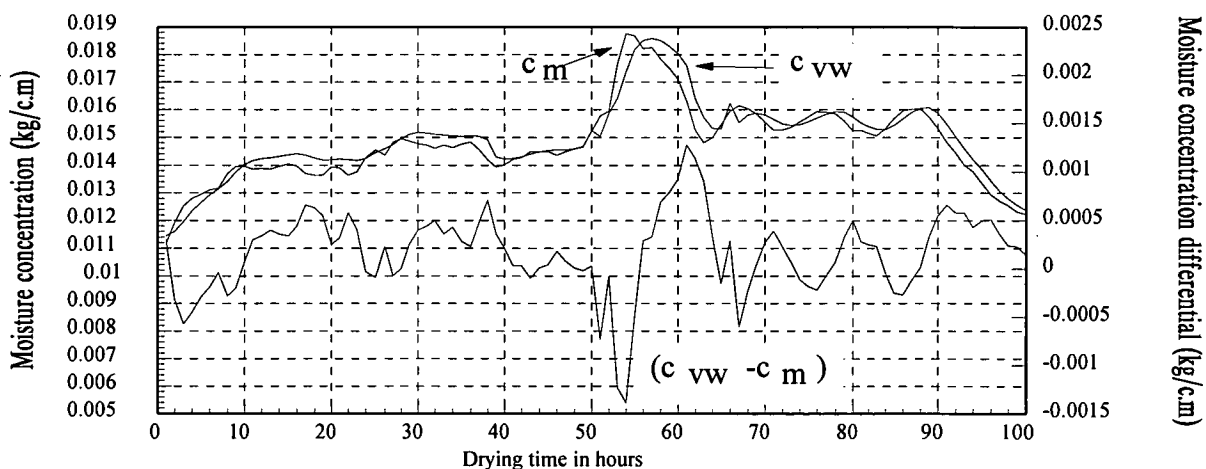


Figure 7.4.3. Surface moisture concentration (c_{vw}), moisture concentration in air (c_m) and moisture concentration differential ($c_{vw} - c_m$).

Figures 7.3 and 7.4 correspond to the moisture profiles presented in Figures 7.1b and 7.1c respectively.

The AE spike at 22.5 hours in Figure 7.2.2 occurred whilst the AE Board was being removed from the kiln for inspection. The AE spikes at 3 and 6 hours in the same figure are assumed to be due to crystalline slips in a localised region of fibres with walls particularly contorted around rays or vessels. The sudden change in direction of the fibre constitutes a natural stress-concentration site. A microfracture may form but its growth is halted because the ends of the fracture strike the surrounding material of much higher stiffness. As discussed in 3.6, such a microfracture simply redistributes the local stress field without significantly affecting the overall stress pattern. The uniformity of the stress field in a specimen strained in a testing machine means the same microfracture may lead to catastrophic failure.

Young's Modulus or stiffness in the radial direction is nominally twice the tangential value in the Tasmanian eucalypts and the stiffness defines the surface stress at a particular instantaneous strain. Figures 7.2.2, 7.3.2 and 7.4.2 reveal that the magnitude of the calculated surface stress is significantly higher in the quartersawn material but the calculated surface instantaneous strain and measured AE rates are of the same order in the backsawn and quartersawn material. Acoustic emission is related to the surface instantaneous strain but not the surface stress (more specifically the AE *peaks* are related to the surface instantaneous strain, as discussed below). The repeatable 100 count AE checking threshold in backsawn and quartersawn boards corresponds to the 0.02 ultimate strain in KILNSCHED and appears to be independent of the basic density and stiffness (Booker 1994a). Surface stress is directly dependent on stiffness.

7.2.1. AE and surface fibres

It appears that the acoustic emission is primarily generated at the surface of a drying board. This is evidenced by the close relationship between the measured acoustic emission and the *surface* instantaneous strain and the fact that the acoustic emission responds so rapidly to relatively small changes in drying conditions; it is envisaged that at least one hour would be required before the stress conditions in regions more than 1mm below the surface

would be affected by such small surface changes. In addition, KILNSCHED was used to simulate the drying of boards of different thicknesses and diffusion coefficients over extended periods and in each case only a very thin region beneath the board surface (less than 2mm) exceeded the proportional limit during the entire simulation. Acoustic emission represents irreversible stress release events and ideally is not generated in regions below the proportional limit. Finally it is expected that attenuation of stress waves generated relatively deep within a board would preclude significant acoustic emission being measured from that region. Therefore acoustic emission can be attributed to stress release events occurring within the surface fibres with some confidence.

This relatively thin section of a given board producing measurable acoustic emission is closely related to the repeatable AE checking threshold. The AE rate measured is not due to the cumulative ringing effect of events occurring within variable thicknesses of a drying board but rather surface stress redistribution events alone, and appears to be relatively independent of the drying conditions. Bernatowicz and Militzer (1992) and Quarles (1992) reported that AE activity was not a function of specimen size provided specimens were properly end-coated to prevent end drying, which seems to confirm this proposition. Whilst the majority of AE checking threshold trials described in Chapter 6 were performed on nominal 30mm thick boards, thicker boards were occasionally tested and the AE rate at failure lay very near the 100 count AE checking threshold.

Figures 7.2.2, 7.3.2 and 7.4.2 (and the AE responses in Appendix A) reveal the intermittent nature of the AE. The responses comprise a burst of AE (an 'AE peak') followed by minimal AE activity before another peak. Each peak represents very effective stress redistribution in a large number of fibres around the transducer (that is the peak represents the *average* state of stress redistribution at the board surface). No further widespread stress redistribution process is required (represented by the extended periods of low AE generated by localised stress release events) until the localised stress builds up sufficiently. This behaviour seems closely related to the concept of intermittent crystalline slips that increase the local material strength, resulting in the low AE periods, whereas microfractures are stress concentration sites that reduce the local strength and might be expected to cause continued acoustic emission.

7.2.2. AE and the proportional limit

Adams (1969) reported a rise in the rate of microfailures at the proportional limit during bending in Douglas-fir, western Hemlock and western red cedar beams. He reported that the proportional limit was at least in part associated with microfailure development. Porter et al. (1972) reported a rise in the rate of microfailures near the proportional limit in Douglas-fir beams loaded in flexure. The three AE responses presented in this chapter all contain a sudden, discernible burst of AE which appears to herald the onset of increasing AE peaks (corresponding to point 'B' in Figure 6.1). At 14 hours in Figure 7.2.2, 14 hours in Figure 7.3.2 and 10 hours in Figure 7.4.2 the AE rate suddenly increases from 'background' AE comprising small bursts interspersed between extended periods of minimal activity to energetic peaks of increasing amplitude. Similarly, the AE responses presented in Appendix A all contain a discernible burst of AE that represents the commencement of major AE activity. These bursts in Figures 7.2.2, 7.3.2 and 7.4.2 coincide with a surface instantaneous strain very near the nominal proportional limit of 0.005 used in KILNSCHED. This repeatable burst of AE in all boards tested is strong evidence that a significant change in material properties occurs when the surface attains the proportional limit. It is important to realise that the concept of a proportional limit in timber is rather arbitrary, much like FSP in the discussion of free and bound moisture. The variability of the material means there will be no clear delineation between elastic and inelastic behaviour, however it is a useful tool in simplifying the discussion of the behaviour of the timber during seasoning.

If the material were truly elastic below the nominal proportional limit, no sudden, irreversible deformations that might cause the transducer to ring would occur so no AE would be detected. The AE responses presented in this chapter and in Appendix A reveal that acoustic emission was invariably generated from the commencement of drying (the boards tested were always 'wet to the touch', meaning the surface was initially well below the proportional limit). Dinwoodie (1968) detected crystalline slips in spruce compressed parallel to the grain at stresses less than 25% of the failing load and predicted the slips may be present at even lower stress levels. Adams (1969) recorded acoustic emission in Western white pine specimens tested in bending at around 2% of the ultimate stress. Clearly, irreversible stress

redistribution processes do occur in timber below the proportional limit. These might be due to crystalline slips in prestressed fibres; for example, small diameter trees are often subject to higher than usual growth stresses. The growth stresses are not the longitudinal stresses usually considered but the transverse growth stresses emanating from the weight of the tree and Poisson's effects. A quite separate potential acoustic emission source below the proportional limit is due to the strain energy imparted to a board surface and this is discussed in detail in 8.5.

7.2.3. AE peaks

Beyond the proportional limit, the AE peaks are directly related to the surface instantaneous strain. Because both the AE and ϵ_i curves are plotted against relevant failure criteria (100 counts and 0.02 ultimate strain respectively), they represent the proximity of material failure. The AE rate is representative of the average strain across the board only when an AE peak lies near the ϵ_i curve, meaning the strain energy at the board surface has been entirely consumed by slips and the generation of AE and some heat (strain energy concepts are discussed in detail in Chapter 8). When the AE peaks are significantly lower than the ϵ_i , the acoustic emission represents localised stress release events. The surface instantaneous strain does not decrease with the AE after each AE burst for the AE represents localised stress release events that affect the local stress field only. These events redistribute the local stress on the neighbouring fibres, maintaining the average surface instantaneous strain.

The rate of change of instantaneous strain is related to the rate of change of the AE peaks and is further evidence that the instantaneous strain determines the AE rate. When the instantaneous strain remains nearly constant for some period, the previous maximum AE rate is not exceeded. Precisely this behaviour is seen between 22 and 28 hours in Figure 7.3.2. The ϵ_i was nearly constant during this period whilst the AE decreased. This means the measured AE rate is not representative of the state of surface stress during extended periods of unloading. This is discussed further in 7.3.

The correlation between the AE peaks and the ϵ_i improves with increasing strain. The instantaneous strain is calculated from local stresses averaged over a finite width near the middle of the board. Below the proportional

limit, the AE rate represents localised microfailures and crystalline slips occurring in the relatively small number of highly prestressed fibres and the AE peaks and the ϵ_i are poorly matched. Beyond the proportional limit, progressively more fibres experience crystalline slips so the AE rate becomes a more accurate representation of the instantaneous strain acting across the whole surface. This improving correlation between AE rate and ϵ_i with increasing strain and the very nearly constant proportion of crystalline cellulose in normal wood is closely related to the repeatable AE checking threshold. The correlation between the peaks in the AE response and the surface instantaneous strain is effectively a correlation between the number of active slip planes at a board surface and instantaneous strain.

7.2.4. AE and relative humidity (RH)

Relative humidity appears to have been considered more meaningful than the absolute humidity in previous AE studies. When viewing Figures 7.2, 7.3 and 7.4 for the first time, one tends to rationalise the AE rate and ϵ_i with the corresponding DBT and RH history. The literature contains numerous references to an inverse relationship between the measured level of AE activity and relative humidity of the drying conditions (Becker 1982, Noguchi et al. 1987). This has naturally lead to the misconception that acoustic emission generated during drying is related to humidity. The following description reveals acoustic emission (and ϵ_i) are intimately related to the drying temperature and the air *absolute humidity*.

In Figure 7.3.1, the DBT suddenly increased 4.5°C and the relative humidity decreased 6% over a three hour period (between 23 and 26 hours drying). The coupled effect of increased temperature and reduced humidity might have been expected to result in a sudden increase in the measured AE rate. Figure 7.3.2 reveals the AE rate *decreased* significantly during this time and the rate of growth of ϵ_i decreased. Similar DBT and RH behaviour after 52 hours in Figure 7.4.1 produced decreased AE activity and ϵ_i in Figure 7.4.2. Clearly, the AE is not simply related to temperature or relative humidity.

7.2.5. AE, absolute humidity and temperature

Noguchi et al. (1983) dismissed temperature as a significant factor in AE generation by increasing the drying temperature in green specimens and not

recording increasing AE until the RH was decreased (at constant temperature). Such testing ignores the state of surface stress and strain in the specimens and leads to misconceptions.

The material is extremely sensitive to slight changes in drying temperature; changes of 0.2°C were sufficient to cause sudden changes in the AE and ϵ_i . The thermal diffusivity is approximately 1000 times the magnitude of the diffusion coefficient in the eucalypts studied. A sudden increase in temperature increases the vapour pressure differential between the board surface and the free stream air, increasing the moisture concentration differential. The relatively high thermal diffusivity means the temperature change affects the surface (and a region within approximately 0.5mm below the surface) very rapidly whereas it is estimated that it would take of the order of 2 hours for a change in air absolute humidity at the surface to affect the material 2mm beneath the surface when the material diffusion coefficient is of the order of $1e-8 \text{ m}^2/\text{hr}$. More moisture is removed from this thin region than can be replaced from interior regions since the diffusion coefficient is so low. This immediately affects the surface stress and instantaneous strain.

At temperatures in the vicinity of 20°C, the drying rate is controlled by the moisture concentration differential between the relatively saturated surface fibres (c_{vw}) and the moisture concentration of the drying air (c_m) (refer to 5.2 for the relevant boundary layer equations). Figures 7.3.3 and 7.4.3 reveal that the sudden coupled increases in DBT and RH described above resulted in the absolute humidity of the air increasing significantly and rapidly. The diffusion coefficient is relatively low so the surface moisture concentration cannot change rapidly, leading to the decreased moisture concentration differential ($c_{vw}-c_m$). This results in a decrease in the surface drying rate, and thus the surface stress ceases to increase. Effectively no new stress release sites are created at constant stress so the AE gradually decreases.

The complex nature of the relationship between the drying conditions and board surface behaviour is highlighted by the AE and ϵ_i behaviour after 77 hours in Figure 7.4.2. Whereas the previous sudden increase in DBT and reduction in RH caused a decrease in AE, this time the AE and surface ϵ_i increased. Reference to Figure 7.4.3 reveals the moisture concentration differential increased and hence the surface drying rate increased.

The interaction between AE and drying conditions is complicated further by the effect of temperature on the stiffness of a board surface. When c_m decreases during drying (as the result of an increase in DBT at constant WBT for example), the surface drying rate immediately increases and we would expect increased surface stress. However, the increased air temperature almost immediately increases the local material temperature and thus the local material stiffness decreases. Hence the surface stress and instantaneous strain may tend to decrease, despite the effect of increased surface drying rate.

7.2.6. Conclusions

The preceding sections in this chapter revealed that the AE peaks are directly related to the surface instantaneous strain calculated by KILNSCHED, provided accurate density, diffusion coefficient and shrinkage data are incorporated into the drying program. This relationship is strengthened by the repeatable occurrence of a sudden AE burst near the 0.005 strain proportional limit calculated with KILNSCHED. This enables the user to say with great confidence, prior to the AE rate attaining 70 counts for example, that the surface is below the '70% of failure condition'. In terms of the AE-based optimal kiln control system referred to in Chapter 1, the kiln conditions may be ameliorated at a preset strain below the ultimate strain rather than at an arbitrary 'safe' AE values in systems implemented by Honeycutt et al. (1985) and Noguchi et al. (1987).

7.3. Preventing surface checking by measuring AE

Skaar et al. (1980) reported that it should be feasible to adjust the drying conditions in a kiln in response to the AE measured in boards during drying. An optimum kiln control system incorporating AE as a non-destructive feedback measure of surface stress was discussed in 1.5. The literature review in 2.3 reveals that researchers such as Honeycutt et al. (1985) and Noguchi et al. (1987) implemented AE-based kiln control systems with moderate success. It appears the inherent variability of timber and the lack of a suitable correlation between AE and stress or strain (due to the absence of an accurate nonlinear drying model such as KILNSCHED) has prevented the development of a fully automatic kiln control system that optimises the

seasoning process. However, the AE checking threshold trials discussed in Chapter 6 revealed that AE is explicitly related to surface check development. Provided the AE rate is below the 100 count AE checking threshold and collapse has not occurred, board surfaces are free of surface checks. It appears previous researchers have considered incipient surface checks to be rather larger than the checks considered in this study. The existence of the constant AE checking threshold is a necessary condition for the development of an optimum kiln control system.

Acoustic emission must be used in a continuous manner when it is incorporated into an optimal kiln control system. Figures 7.2.2, 7.3.2 and 7.4.2 reveal that the AE generally decreases after an AE peak, since the peak represents very effective stress redistribution. The surface instantaneous strain may remain reasonably constant after the peak since the AE represents only localised stress redistribution and the average state of surface strain is not much effected by the localised stress release events. Extended drying trials have revealed that the AE may decrease gradually over periods of many days when relatively moderate drying conditions are applied. Clamping an AE transducer to a board at regular stages of the drying process only would present a quite erroneous measure of the current state of surface stress and instantaneous strain.

Quarles (1990) reported that an inherent disadvantage of AE control is the fact that transducers must be attached to representative boards selected from the kiln charge. Timber properties can vary quite widely, even in material cut from one tree; 30 % variation in mechanical properties between the butt log and head log are commonly measured. One would expect this phenomenon to cause problems when controlling relatively large industrial kilns with thousands of drying boards. However, it appears the AE behaviour is strictly related to the crystalline cellulose component in the wood structure. Provided the wood is normal wood (as opposed to tension wood or compression wood), clear boards will experience surface checking at very nearly the same AE rate.

Therefore it is not necessary to clamp AE transducers to a large number of boards. It is envisaged that an AE transducer at stack inlet, stack centre and stack outlet should provide an adequate representation of the stresses in the boards through the stack, provided uniform airflow constraints are satisfied.

It is important to realise that the vast majority of industrial drying is performed with no measure whatsoever of the drying stresses in boards. Measuring the AE behaviour in several boards provides substantially more information on the state of stress in the drying boards than is presently available.

The Tasmanian eucalypts are particularly prone to collapse at elevated temperatures (section 9.3 reveals material in this study collapsed at 24°C but not at 22°C). Therefore we may expect AE to be generated by stresses resulting from simultaneous normal surface shrinkage and collapse shrinkage beneath the surface. Booker (1990) and Parsons (1989) detected AE generated in timber experiencing collapse and found the AE response to have the same form as that generated by surface checking. This strengthened the likelihood that collapse checking results from the same differential shrinkage processes that produce surface checking. Section 6.5 revealed that AE is not representative of surface check development when collapse shrinkage occurs. Therefore, a means of differentiating between surface generated AE and internally generated AE must be available if the AE is to be used to prevent surface checking during drying. Alternatively drying temperatures must be maintained below collapse-inducing temperatures until the centre board moisture content attains the nominal 30% FSP value. The latter approach was adopted in this project due to a lack of quantitative data on collapse shrinkage. Further research currently being conducted at the University of Tasmania aims to address this gap in knowledge.

The AE-based kiln control strategy in the Clever Kiln Controller® described in Chapter 10 is referred to as the 'AE Controller'. The AE Controller adjusts the drying conditions based on the measured AE rate in a sample board (Clever Kiln Controller actually employs three AE sensors, but the following discussion is restricted to the AE measured in a single board). When the AE rate exceeds 'ControlAE', a maximum allowable AE rate set by the user, the drying conditions are ameliorated. When the AE is relatively low for an extended period, the drying conditions are made more severe. The user effectively selects a 'safety factor' by selecting how low to set ControlAE with respect to the AE checking threshold. The greater is ControlAE, the more rapid the drying conditions must be adjusted to prevent the AE rate exceeding the AE checking threshold. Therefore it is envisaged that a relatively conservative ControlAE should be used in large kilns.

Unlike the rather arbitrary control levels employed by Honeycutt et al. (1985) and Noguchi et al. (1987), ControlAE is set at a particular fraction of failure since the AE rate is directly related to surface instantaneous strain. In other words, selecting ControlAE equal to 70 counts is equivalent to preventing the surface instantaneous strain from exceeding 70% of the 0.02 ultimate instantaneous strain.

82

Chapter 8

AE and strain energy

It is hypothesised that acoustic emission is generated by intermittent crystalline slips within surface fibre walls subject to high tensile stress. These irreversible stress release events consume strain energy. The surface stress and instantaneous strain calculated by KILNSCHED in the trials discussed in Chapter 7 were used to determine the strain energy imparted to the material surface during drying. The relationship between the cumulative count (representing indirectly the total acoustic energy released during drying as discussed below) and surface strain energy is investigated in this chapter. The cumulative count is related to the unrecoverable strain energy rather than the recoverable or elastic strain energy. The cumulative count is shown not to be a useful measure of the propensity for surface checking.

8.1. Strain energy in homogenous materials

In studies based on the deliberate propagation of a single crack in solid materials, researchers have employed the theory of fracture mechanics to relate the measured AE to the energy involved in crack extension. Elastic strain energy was considered as the source of the AE because fracture mechanics theory assumes the material immediately surrounding the crack tip unloads linearly elastically during crack extension (Gordon 1968).

Ravenhall (1977) used a stress wave emission (SWE) or AE technique to characterise the growth of a single crack in a metal specimen loaded at constant strain rate. Ravenhall reported that some portion of the stored elastic strain energy in a material under load is emitted in the form of a stress wave when a crack propagates in incremental steps. The energy processes involved in crack formation and propagation during a typical test were summarised simply by the equation :

$$E_{in} = E_p + E_\gamma + E_{AE} \quad (8.1)$$

where E_{in} is the total input strain energy, E_p is the work of plastic deformation, E_γ is the energy consumed in the formation of new surfaces and

E_{AE} is the strain energy released as AE. Crack extension was assumed to cause the material to unload linearly elastically. The ideal (theoretical) stress wave energy emitted increased monotonically with time as the crack length increased in constant strain rate tests. The cumulative count was measured during the loading tests and was determined to have definite limitations in its use as an aid to prediction of failure.

Rotem and Altus (1979) induced a single crack in various fibrous composite laminates. The AE energy was assumed to be due to the release of strain energy. Within the same material, a constant relationship between acoustic energy and the fracture energy released by an increment in crack size was determined. The relationship was reported to be different for different materials and probably different for different geometries.

Gerberich and Hartbower (1967) investigated the energy released by the small extension of a single crack in high-strength aluminium, titanium and steel alloys. The number and size of the stress waves generated appeared to bear a unique relationship to the amount of crack growth. The energy of the AE waves was hypothesised to be a proportion of the available elastic energy and the energy of an individual wave was taken to be proportional to the square of the wave amplitude. Using elasticity theory, a semi-empirical relationship between the energy of the stress wave and the available elastic energy was derived.

In studies involving the deliberate propagation of a single crack, the AE rate is effectively directly related to the magnitude and energy of the AE wave; the greater the energy released by crack extension, the greater the magnitude of the elastic stress wave and the higher the measured count rate. It was thought similar concepts might be applicable to seasoning of timber. However, during seasoning, the AE transducer is triggered by the cumulative effect of numerous coincident stress redistribution events such as crystalline slips. Therefore, the energy relationships involving the extension of individual flaws derived above are not directly applicable to the AE generated in the seasoning situation. While the AE rate represents the 'instantaneous' strain energy released in a short period, the cumulative count represents the total energy released in the form of crystalline slips and AE. This author thought it was likely that the cumulative count during drying might be related to the total strain energy imparted to the material. During

seasoning, board surfaces progress well beyond the proportional limit and AE results from *irreversible* stress release events. Therefore the author did not expect elastic strain energy to be the source of the AE in this study.

8.2. Recoverable and unrecoverable strain energy.

The strain energy imparted to a specimen under load is the area under a curve of force, F , versus displacement, s . In other words,

$$\text{Strain Energy} = \int Fds = \int A\sigma d(\epsilon l_0) = Al_0 \int \sigma d\epsilon \quad (8.2)$$

where A = specimen cross-sectional area

ϵ = strain

σ = stress

l_0 = original specimen length prior to deformation

Thus strain energy results from the interaction of a stress and an associated strain. During seasoning, four separate strain components exist but the instantaneous strain is the strain component directly related to the stress. Board surfaces absorb strain energy when the surface stress and instantaneous strain increase with differential shrinkage between the board surface and core. Creep, mechano-sorptive effect, unconfined shrinkage and net shrinkage are related only indirectly to the stress through the controlling strain equation (Equ. 5.9); a change in unconfined shrinkage with moisture affects the applied stress only indirectly through its affect on instantaneous strain.

The strain energy per unit volume imparted to the material surface during drying, W_{in} , (distinct from the surface energy required to generate new surfaces at the tip of a propagating crack) is given by :

$$W_{in} = \frac{\text{strain energy}}{\text{unit volume}} = \frac{\int \sigma d\epsilon}{Al_0} \quad (8.3)$$

As discussed in 7.2.1, the AE appears to be predominantly generated at the surface of drying boards and the AE is directly related to the surface instantaneous strain. On this basis, the calculated strain energy in the following discussion is considered to be entirely due to the surface stress and instantaneous strain. The very low diffusion coefficients in the Tasmanian

eucalypts induce very steep stress and strain gradients within a board so the stress and strain at internal points are expected to contribute negligible strain energy compared with the surface strain energy.

Surface strain energy is hypothesised to comprise the recoverable strain energy, U_r , and the unrecoverable strain energy, U_u . The recoverable energy is the potential energy that would be wholly regained if the material unloaded to a state of zero stress (and surface set ϵ_0). This energy is not consumed by preceding irreversible stress release events (as represented by AE). The unrecoverable energy represents the strain energy consumed by irreversible phenomena such as crystalline slips, plastic flow processes and AE. The stress release processes also release a small amount of heat. Therefore, we may write

$$U_u = E_{AE} + E_{slips} + E_{heat} \quad (8.4)$$

where E_{slips} is the energy associated with the change in geometry within fibre walls caused by localised crystalline slips and E_{heat} corresponds to the temperature change associated with the structural redistribution. It is not possible to determine E_{slips} or E_{heat} separately.

As discussed in detail in 5.4, KILNSCHED employs a dimensional and a nondimensional stress~strain curve, the latter using ultimate stress as a reference value for the stresses. The nondimensional curve represents all stress~strain behaviour with a single curve because changes in Young's Modulus with moisture content and temperature affect the calculated stress and ultimate stress proportionately. Significant computational advantages are gained by using the nondimensional curve to calculate surface strain energy and these are discussed further below.

We define W_{in}^* , U_u^* and U_r^* as the non dimensional strain energy, unrecoverable strain energy and recoverable strain energy respectively (Figure 8.1). The non dimensional strain energy per unit volume imparted to the material, W_{in}^* , is calculated by integrating the area under the non dimensional stress~strain curve. The non dimensional recoverable energy, U_r^* , at a given stress and strain is the area of the triangle beneath the unloading line defined by the current value of linear Young's Modulus. The unrecoverable strain energy is the residual strain energy component.

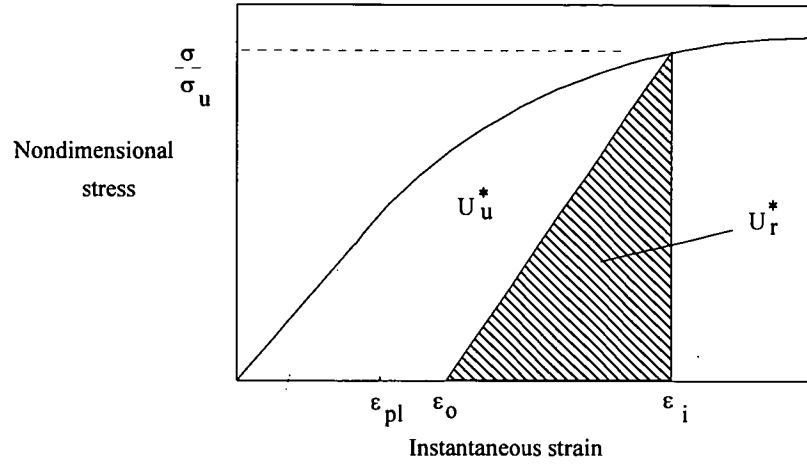


Figure 8.1 Nondimensional recoverable and unrecoverable strain energy.

$$W_{in}^* = U_u^* + U_r^* \quad (8.5)$$

$$\text{Now, } W_{in} = \int \frac{\sigma_u}{\sigma_u} d\epsilon_i \text{ and } U_r = \frac{\sigma_u^2}{2 \sigma_u E} \quad (8.6)$$

$$\text{so } U_u = \int \frac{\sigma_u}{\sigma_u} d\epsilon_i - \frac{\sigma_u^2}{2 \sigma_u E} \quad (8.7)$$

Whereas net shrinkage, creep, unconfined shrinkage and mechano-sorptive effect indirectly affect the stress field, a change in temperature affects the stress field directly and instantaneously at the surface, independent of the instantaneous strain. This introduces a quite separate thermal strain energy component due to the interaction between board temperature changes and stress. Thermal strain energy is not included in this discussion because preliminary calculations revealed that the effect is negligible when drying is performed at nearly constant temperature in the vicinity of 20°C.

8.3. Cumulative count and acoustic energy

The transducer output signal is representative of the ringing characteristics of the sensor. As discussed in 4.3, the transducer appears to be 'triggered' by the cumulative effect of numerous 'events' occurring within the immediate vicinity of the sensor rather than the extension of individual flaws. For this reason, a traditional energy analysis of the transducer output, based on the direct relationship between the square of the amplitude of a wave and the wave energy (Kline 1983), is not applicable in the seasoning situation. However, Kline (1983) reported that the AE rate (ringdown counts) was probably more closely likened to the energy of an AE event than any other physical parameter. Then the cumulative count (the cumulative AE) is

likened to the total acoustic energy generated within a drying board. Difficulties in determining the acoustic energy explicitly were overcome by this author by assuming the magnitude of the strain energy released by individual crystalline slips is constant and a given AE rate corresponds to an explicit strain energy release.

This means an increasing AE rate is due to an increasing number of crystalline slips (of equal energy) within a data period. At the commencement of drying, localised regions of surface fibres only are subject to sufficient stress to experience irreversible crystalline slips. With further drying, the surface stress becomes less localised and progressively more slips occur.

This author hypothesised that the cumulative count was related to the unrecoverable strain energy, that energy available for irreversible stress release events.

8.4. Cumulative count and unrecoverable strain energy

Noguchi et al. (1987) and Quarles (1992) reported that the cumulative count was not a useful measure of failure. Cumulative count was shown to be dependent on the history of loading in Chapter 6. The longer the drying time, the greater the cumulative count since the timber surface experiences numerous stress release events that are insignificant on their own but do contribute to the overall stress field. Conversely, when surface checking is induced rapidly, less cumulative counts will be measured. In the AE checking threshold trials described in Chapter 6, single boards from a given log were dried under the same drying conditions in order to induce rapid surface checking. The measured cumulative count at failure was often very similar within the batch of boards. Ansell (1982) reported nearly constant cumulative counts from pine specimens which failed in tension at constant cross-head speed. It appears there is a *minimum* number of crystalline slips that must occur before ultimate material failure (surface checking). Cumulative count is a useful failure criterion only in cases where timber specimens are subject to exactly the same rate of loading.

Figures 8.2, 8.3 and 8.4 represent the drying conditions and surface stress and instantaneous strain in the drying trials discussed in Chapter 7 as well as the

corresponding cumulative count and calculated strain energy at the board surface. Initially, cumulative count and unrecoverable strain energy were to be normalised. However, closer examination revealed a lack of relevant reference parameters since cumulative count and strain energy (and thus unrecoverable strain energy) are dependent on the history of loading. Cumulative count is not a failure criterion; when the material is dried particularly slowly, many more cumulative counts will be recorded before surface checking occurs. Cumulative count represent the history of loading, whereas surface checking is related to the current stress and strain and is quite independent of the manner in which these formed. Similarly, total strain energy is not a failure criterion. Therefore, cumulative count and nondimensional strain energy were compared directly.

Referring to Figures 8.2, 8.3 and 8.4 it is clear that the cumulative count increases during periods when the unrecoverable strain energy is constant (corresponding to linear unloading at the surface). In metals, the AE during repeated loading and unloading behaves according to the Kaiser effect (Kaiser 1950); when a specimen is loaded to a particular stress and then unloaded, AE is not detected until the previous maximum stress is attained. As discussed in 7.2.3, AE continues to be generated during periods of constant (and even decreasing) surface stress and instantaneous strain because the AE represents localised stress. AE is an accurate measure of the surface stress and strain only during loading, that is whilst the surface is progressing towards failure, and not during unloading. When the material surface unloads, the recoverable strain energy decreases at the same rate as the input strain energy since the surface unloads along the straight line defined by the current stiffness, and thus the unrecoverable strain energy is constant. The cumulative count is not related to the unrecoverable strain energy during unloading and thus the correlation between the cumulative count and unrecoverable strain energy would be improved by only accumulating counts while the surface was loading.

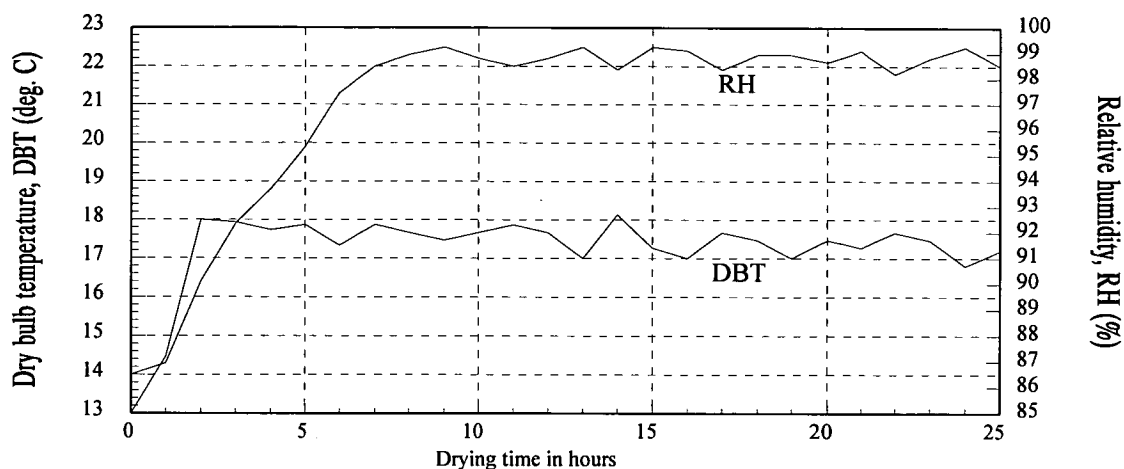


Figure 8.2.1. Measured centre-stack dry bulb temperature and relative humidity.

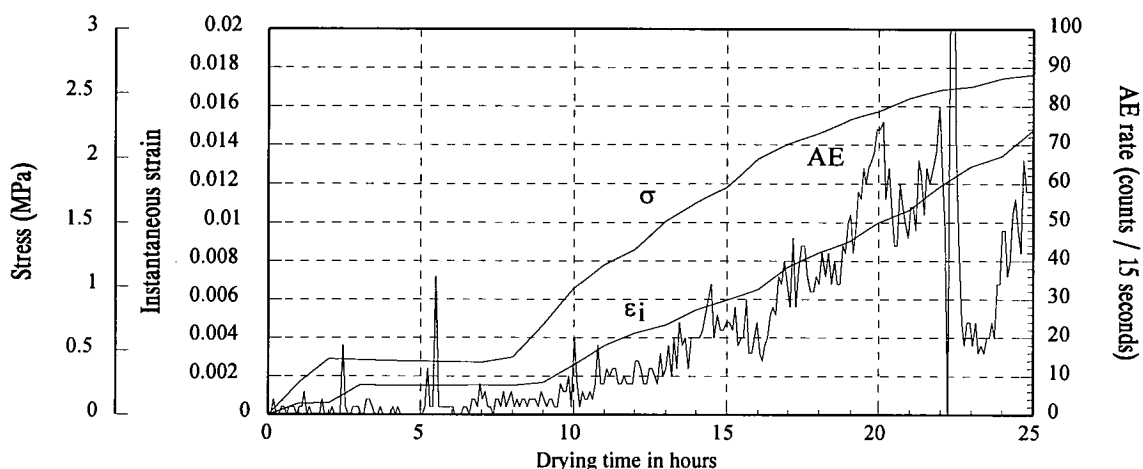


Figure 8.2.2. Measured AE and calculated surface stress (σ) and instantaneous strain (ϵ_i).

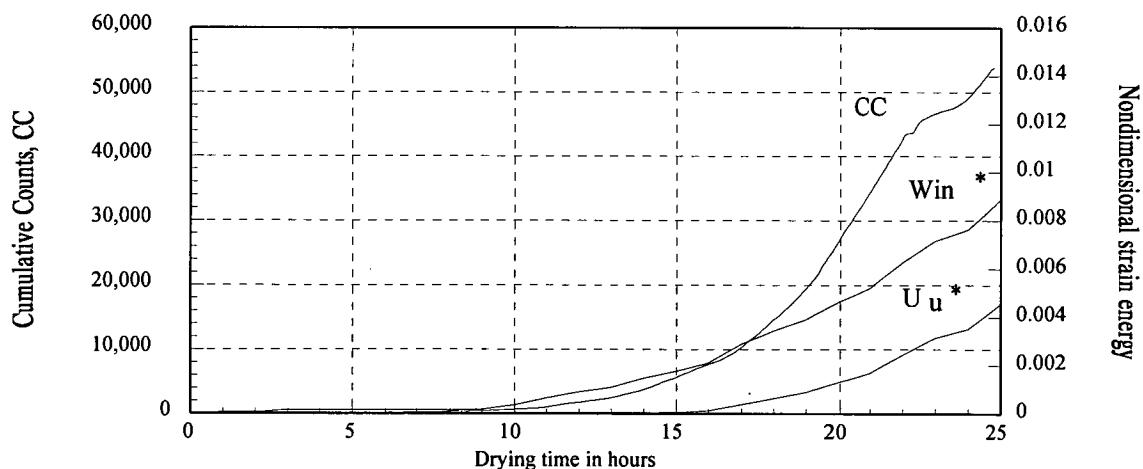


Figure 8.2.3. Cumulative count (CC), nondimensional strain energy (W_{in}^*) and nondimensional unrecoverable strain energy (U_u^*).

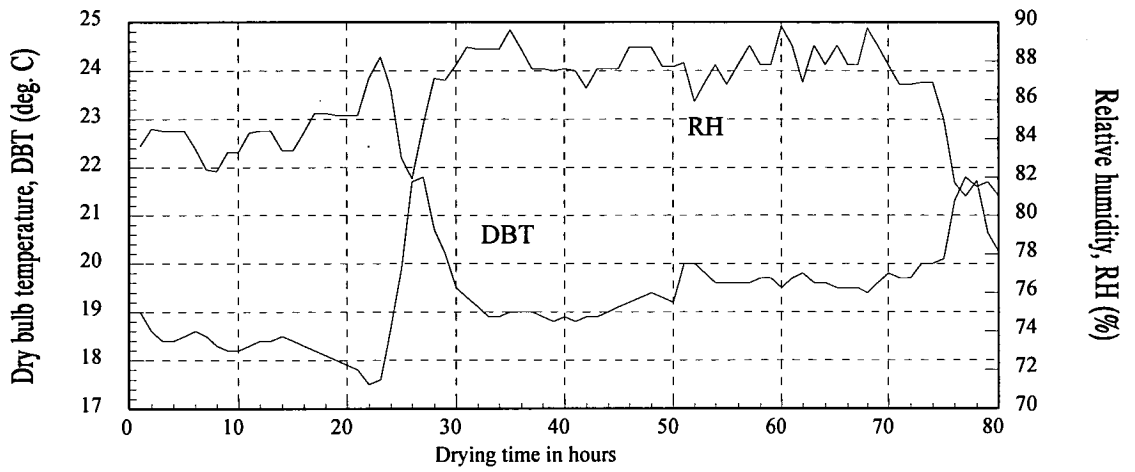


Figure 8.3.1. Measured centre-stack dry bulb temperature and relative humidity.

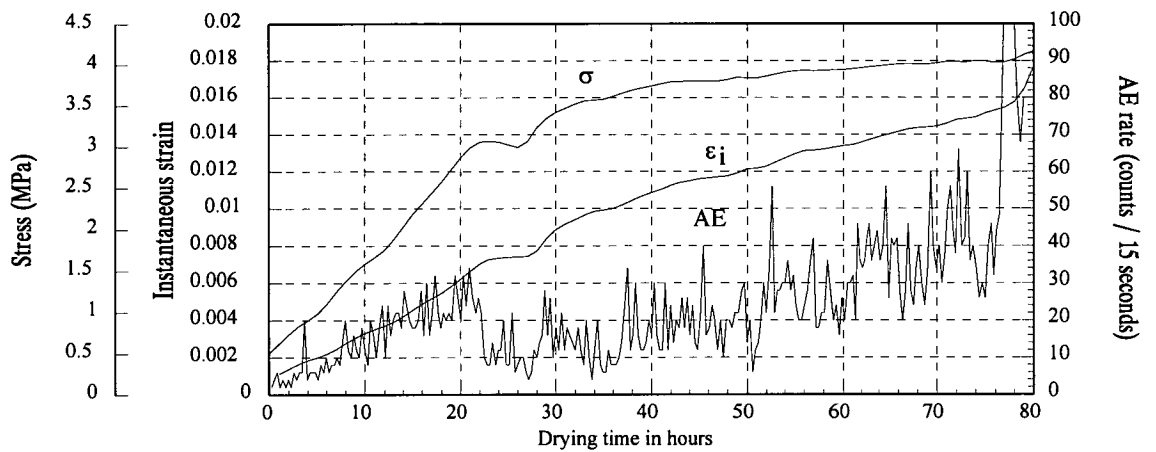


Figure 8.3.2. Measured AE and calculated surface stress (σ) and instantaneous strain (ϵ_i).

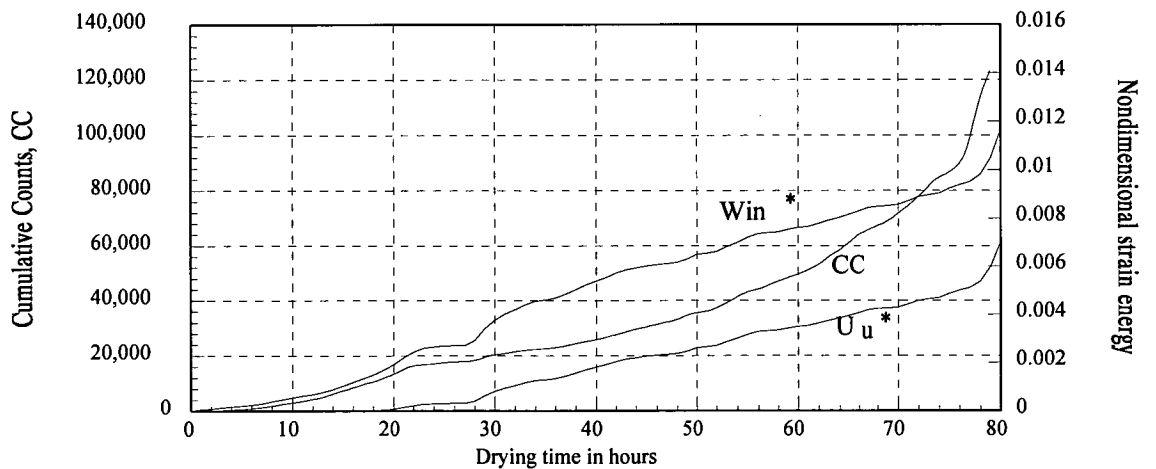


Figure 8.3.3. Cumulative count (CC), nondimensional strain energy (W_{in}^*) and nondimensional unrecoverable strain energy (U_u^*).

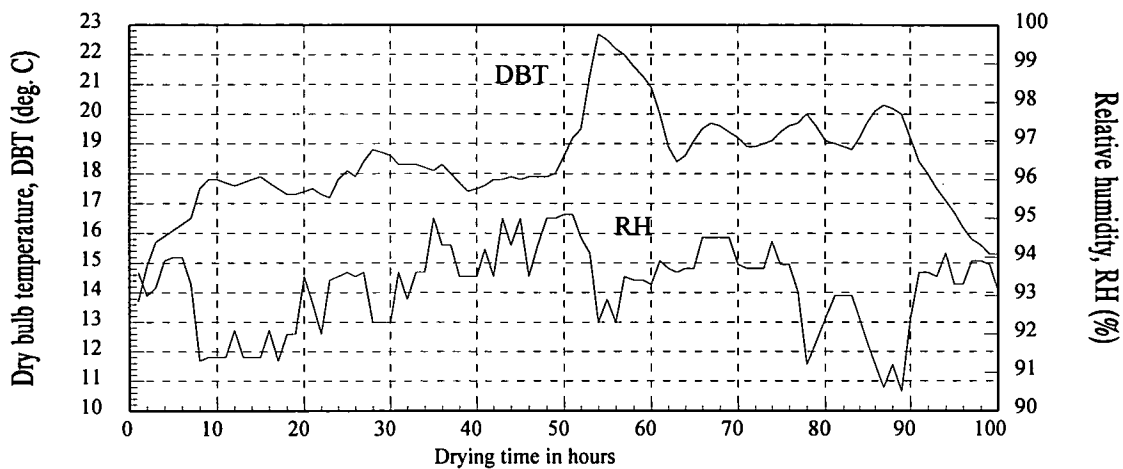


Figure 8.4.1. Measured centre-stack dry bulb temperature and relative humidity.

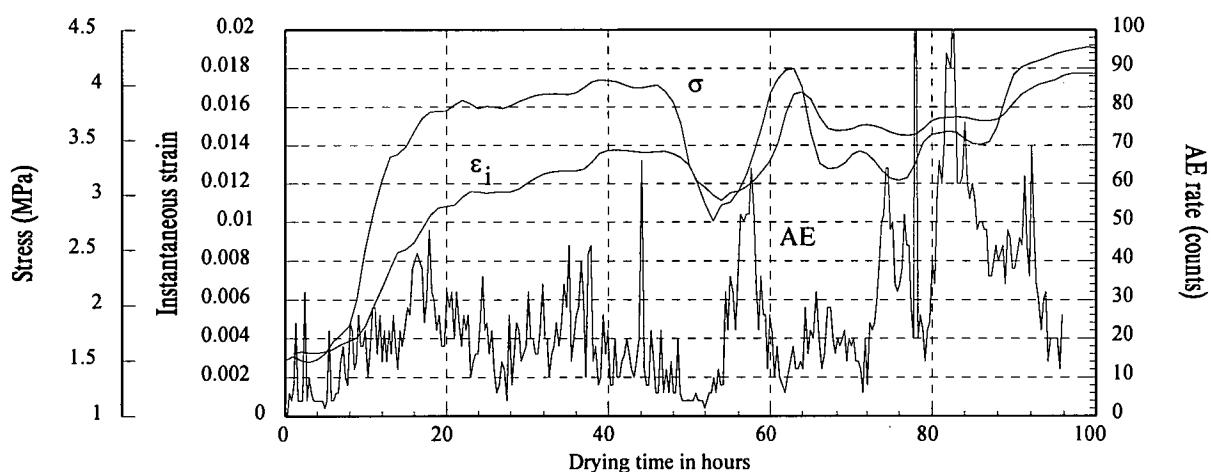


Figure 8.4.2. Measured AE and calculated surface stress (σ) and instantaneous strain (ϵ_i).

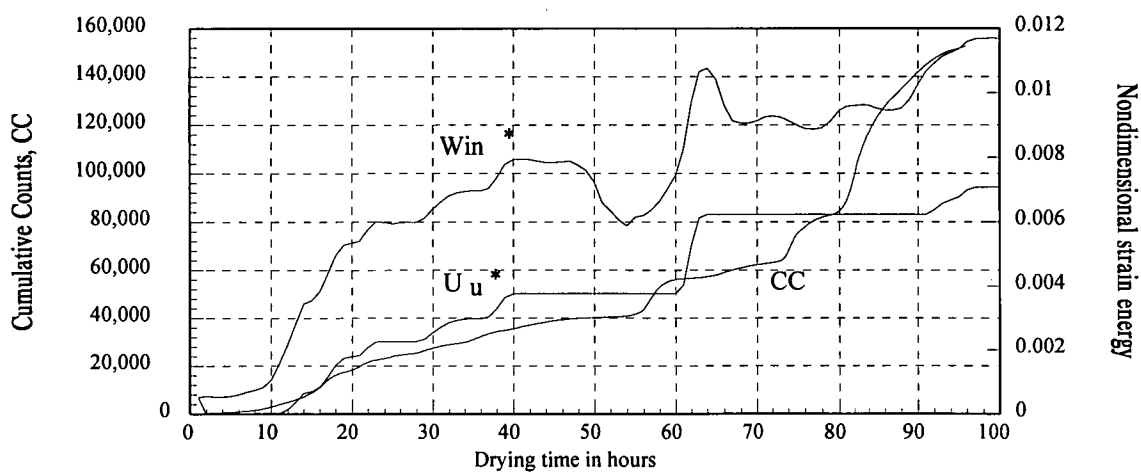


Figure 8.4.3. Cumulative count (CC), nondimensional strain energy (W_{in}^*) and nondimensional unrecoverable strain energy (U_u^*).

Further, the total strain energy per unit volume absorbed by a material during a tension test is given by the area under the stress-strain curve. If the Young's Modulus remains constant during this test, then this area is bounded by the ultimate instantaneous strain and the ultimate stress. In many of the drying tests in this study, surface checking was induced so soon after the commencement of drying that Young's Modulus did not vary significantly from the 'green' value. Then the total strain energy absorbed is not significantly greater than the value calculated using an ultimate stress based on the green Young's Modulus and the unrecoverable strain energy is also limited. The cumulative count on the other hand does not appear to be limited. In various trials performed throughout the study, the AE exceeded the checking threshold with the cumulative count ranging from 1×10^5 to 1.5×10^6 .

AE is generated by irreversible stress release events and thus was thought to be a measure of failure. At constant stress and strain, the material continues to generate intermittent AE bursts, contributing an ever-increasing cumulative count even though the material is no closer to failure. It is plausible that material failure would be independent of the history of loading - when a material is held at constant stress and strain prior to surface checking, the creep and mechano-sorptive effect are acting to reduce the differential stress fields through the material and are thus stalling failure.

Dinwoodie (1968) reported that the propensity for crystalline slips in tracheid walls during longitudinal compression was significantly influenced by the presence of rays in contact with the walls. Dinwoodie reported that there were approximately three times as many dislocations per centimetre of cell wall when the wall was in contact with rays as when it was distant from them. Dinwoodie reported that a considerable proportion of the dislocations occurring at a ray were located towards the outer two or three cells of the ray, at which point the tracheid walls were deflected around it.

The radial orientation of the medullary rays means the wide surface of a backsawn board contains a high proportion of fibres that are adjacent to rays. This preferential development of crystal slips in those parts of the fibre walls that are in contact with rays explains the greater cumulative count at failure measured in backsawn boards than in quartersawn boards.

8.5. AE below the proportional limit

A potential source of the AE below the proportional limit was considered by this author to be high growth stresses causing localised stress release events, as discussed in 7.2.2. A quite separate source is discussed below.

Ansell (1982) reported that in tension tests, 'wood has a close to linear stress~strain curve right up to failure'. As discussed previously, the uniform stress fields in such tests induce premature catastrophic failure while the timber is behaving in an effectively linearly elastic manner. Irreversible deformation processes should not occur when the material is behaving in a linear elastic manner below the proportional limit, since the material loads and unloads along the same line on the stress~strain curve and does not exhibit residual strain or set. Therefore AE should not be detected below the proportional limit. However Adams (1969) detected AE in timber specimens subject to bending at stresses as low as 2% of the ultimate stress. In this study, AE activity was invariably recorded from the commencement of drying of green specimens, well before the calculated instantaneous strain attained the proportional limit. Clearly, AE is generated before the material attains the proportional limit.

Young's Modulus constantly changes with temperature and moisture content during drying. In KILNSCHED, Young's Modulus is taken to be linearly dependent on temperature and independent of moisture content above 20% moisture content and linearly dependent on moisture content and temperature below that figure.

Figures 8.2, 8.3 and 8.4 reveal that the total strain energy, W_{in}^* , increases from the commencement of drying whereas the unrecoverable strain energy, U_u^* , is zero until the nominal proportional limit is attained. On the non dimensional stress~strain curve, the material unloads along the same straight line it loaded on until the proportional limit, regardless of changes in moisture content and temperature. However, on the dimensional stress~strain curve the material unloads along a steeper straight line than the line it loaded on because of changes in stiffness with moisture content and temperature. Figure 8.5 schematically represents the theoretical development of stress and instantaneous strain below the proportional limit during drying. The stress increases linearly to A at which time Young's

Modulus increases due to a decrease in temperature for example. The surface then loads linearly to B. It is clear that some portion of the imparted strain energy is available for irreversible stress release events such as crystalline slips and AE. This component contributes to the AE measured below the proportional limit.

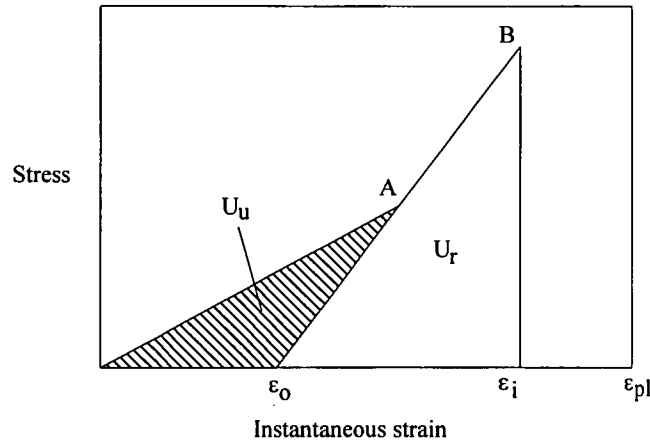


Figure 8.5. Unrecoverable strain energy below the proportional limit.

Thus, the 'background' AE below the proportional limit can be explained by crystalline slips occurring in particularly highly strained fibres *and* crystalline slips occurring as a result of changes in material properties while the spikes are considered to be due to localised microfractures occurring very near the transducer.

Once the proportional limit is exceeded, the local or tangent Young's Modulus decreases and the stress is non-linearly related to the strain. With drying (at constant temperature), the linear Young's Modulus increases due to the decreasing timber moisture content so the material unloads along an ever steeper straight line. Therefore, the proportion of the recoverable strain energy to the total strain energy decreases with drying and the unrecoverable strain energy increases. It is well documented that the ultimate strength of a material is linearly related to Young's Modulus; KILNSCHED uses an ultimate stress equal to a constant fraction of the linear Young's Modulus. When the linear Young's Modulus increases with drying, the ultimate strength increases and the material is further from failure. Crystalline slips strengthen the material by increasing the potential energy of the bonds between the cellulose microfibrils within cell walls.

Reference to Figure 8.4.3 reveals that at higher strains, the material unloaded and reloaded several times. When the linear Young's Modulus changes during unloading, there will be a residual unrecoverable area or a hysteresis loop upon reloading. In addition, the material returns to the nonlinear stress~strain curve at a lower stress, contributing to additional unrecoverable strain energy. This 'unrecoverable area' on the dimensional stress~strain curve (it does not appear on the nondimensional curve) probably represents heat generation.

8.6. Surface checking, crystalline slips and strain energy

Surface checking was discussed in 1.3.1 in terms of differential shrinkage causing the instantaneous strain to exceed the ultimate material strain. We can now describe surface checking in terms of strain energy.

The surface stress and instantaneous strain increase during drying and strain energy is imparted to the material. In an ideal elastic material, strain energy is absorbed without irreversible deformation until the strain attains the proportional limit. In practice, AE is generated below the proportional limit as discussed in the preceding section. Once the nominal proportional limit is attained, crystalline slips within the cell walls consume strain energy by suddenly redistributing the local stress field. AE forms as a by-product of these energetic events. 'Increments' in strain energy due to increasing surface stress and instantaneous strain are effectively consumed by crystalline slips and the associated stress waves and generated heat. However, there is a limit to the strain energy that can be released instantaneously by slips. If the increment exceeds an energy represented by 100 counts, slips alone are not sufficient to release the increment in strain energy and a 'massive' stress release mechanism is required : the macroscopic surface check.

The instantaneous strain energy release rate through slips is limited by the fact that the number of potential crystalline slips is also limited. The slips appear to occur below the level of the light microscope and therefore it is envisaged that a very large number of crystalline slips may occur before material failure. The material satisfactorily consumes strain energy as crystalline slips for the duration of the drying run (weeks, months or years) without surface checking until there is a dramatic increase in the rate at

which strain energy is imparted to the material. If this increment is sufficiently large, the slips alone are not sufficient to release the stress and the surface check forms.

The inability for crystalline slips to consume strain energy is not the only requisite for surface checking. The material has to be reasonably near failure in the first instance, that is the surface strain must be near the failure strain. This is equivalent to saying that the timber has to have experienced some minimum number of slips before surface checking occurs. When a particular increment in strain energy is imparted to the surface when the instantaneous strain is relatively high, surface checking may result. When the same strain energy increment is imparted near the proportional limit, surface checking does not occur, just a burst of AE. In this study, a minimum number of counts at failure is obtained by comparing the cumulative count at failure in those boards that were deliberately dried rapidly, precluding the formation of insignificant stress release events. Table 6.1 reveals the cumulative count in backsawn boards dried rapidly was typically higher than the corresponding value in quartersawn boards dried rapidly.

Chapter 9

SMARTKILN

SMARTKILN, a drying program based on KILNSCHED, was developed by this author to develop optimum drying schedules based on the calculated surface instantaneous strain. Whereas KILNSCHED simulates arbitrary drying conditions selected by the user, SMARTKILN iterates 'optimum' drying conditions at every stage of the drying simulation to maintain the calculated surface instantaneous strain at a preset 'Control Strain'. Simulations with SMARTKILN revealed that drying time is reduced by inducing steep moisture gradients as soon as practicable after the commencement of drying. The nonlinear shape of the stress~strain curve in KILNSCHED means drying time is not significantly reduced by increasing Control Strain towards the ultimate instantaneous strain (Booker 1995b).

This chapter concentrates on optimising the physical process of seasoning timber. Economic factors contribute significantly to the actual drying process employed but an economic analysis is a large study beyond the scope of this thesis. SMARTKILN would prove an invaluable tool in such a study.

9.1. Optimum drying and surface stress

Optimum drying was defined broadly in Section 1.5 as the removal of the moisture in the minimum time with minimum degrade. We must now analyse optimum drying in more detail in order to practically implement the process. At a given air absolute humidity, the drying rate will increase with drying temperature, since the diffusion coefficient is dependent on absolute temperature (as discussed in 5.2.1). However, localised collapse shrinkage was found to cause localised surface checking and collapse propensity increases with temperature (discussed in 6.5). Degrade must be avoided when seasoning furniture grade material so drying temperature is restricted by this constraint. At a given temperature, how is the drying rate maximised?

Rapid drying in the long term (as opposed to transient moisture loss effects when green timber commences to dry) is governed by the magnitude of the

moisture gradient at a board surface. The moisture gradient between the relatively dry surface fibres and the saturated internal fibres controls the moisture flux rate; the steeper the gradient, the greater the relative drying rate. As discussed earlier, the moisture gradient at the surface also controls the differential shrinkage between a board surface and internal regions and thus governs the surface stress and instantaneous strain; the steeper the gradient, the greater the surface stress and strain. Optimum drying involves maximising the surface drying rate and the surface stress by accurate moisture gradient control (clearly, when drying is performed with low surface stresses, significant potential for faster drying is available).

The complicated relationship between surface drying rate, surface stress, air conditions and surface stiffness was discussed in detail in 7.2.5. The material surface was determined to be very sensitive to temperature fluctuations, due primarily to the low mass diffusivity of the eucalypt material. This sensitivity can be used to control the surface moisture flux rate and thus the surface moisture gradient and surface stress.

Various studies based on AE measured in drying boards reported that the AE activity decreased when the relative humidity increased and increased when the relative humidity decreased (Noguchi et al. 1983, Honeycutt et al. 1985, Noguchi et al. 1987). More precisely, surface stress development is related to changes in the absolute humidity of the air rather than the relative humidity, as discussed in 7.2.5. At an arbitrary stage in the drying process the DBT and WBT and the air density define the absolute humidity in the free stream air and the corresponding moisture concentration (c_m). At constant VEL, the moisture concentration differential ($c_{vw}-c_m$) between the moisture concentration at a board surface (c_{vw}) and the moisture concentration in the free stream air fixes the mass flux rate, h_m (Equ. 5.3). This differential thus also fixes the moisture concentration gradient at a board surface and the surface stress and instantaneous strain. Therefore the board surface behaviour can be directly controlled with appropriate changes in DBT and WBT.

In the low diffusivity Tasmanian eucalypt material, a small change in c_m has a significant effect on the surface stress because that change is not effectively propagated through the board but rather concentrated in the surface fibres. The AE generated at the surface of drying eucalypt boards is seen to be

sensitive to temperature changes as small as 0.2°C in Figures 7.2, 7.3 and 7.4. When the surface stress is increasing towards the ultimate stress, surface checking is prevented by reducing the moisture concentration differential ($c_{vw}-c_m$) with an appropriate change in DBT or WBT. This immediately decreases the surface drying rate and thus reduces the growth of surface stress. Conversely, the surface stress may be increased by increasing the differential ($c_{vw}-c_m$). Airspeed changes may also be employed to moderate surface stress behaviour but VEL is not adjusted in the following simulations.

Drying rate is maximised throughout the drying process by maintaining the air temperature as high as practicable. The temperature is limited by the constraint that collapse shrinkage must be prevented, as discussed in 9.3. Therefore the rate of growth of surface instantaneous strain should be controlled by changing ($c_{vw}-c_m$) without decreasing the DBT. In other words, surface instantaneous strain should be controlled with a constant DBT or increasing DBT rather than by decreasing DBT. As explained in 7.2.5, a sudden *decrease* in air temperature directly affects the surface stress and strain due to its effect on stiffness and may cause rapid surface checking.

It should be possible to 'juggle' the drying conditions at every stage of the drying process to maintain the surface at a particular instantaneous strain. The complexity of the relationship between the moisture concentration differential and the surface temperature means a computer program is required.

9.2. SMARTKILN

SMARTKILN is a computer program written by this author, based on KILNSCHED, which generates a theoretical schedule to maximise drying rate whilst holding the surface instantaneous strain at a preset level below the ultimate strain. SMARTKILN automatically humidifies the air condition to prevent the surface instantaneous strain exceeding Control Strain during a simulation. Conversely, SMARTKILN detects when the surface strain is falling below Control Strain and adjusts the drying conditions to increase the surface drying rate and thus the surface strain.

At any arbitrary stage in the simulation, SMARTKILN simulates one full hour of drying using the DBT, WBT and VEL successfully employed in the

previous hour of the simulation. SMARTKILN compares the calculated surface strain with Control Strain. When the surface strain lies beyond particular bounds around Control Strain, SMARTKILN returns to the start of the hour and changes the DBT or WBT as appropriate (VEL remains unchanged in the results reported here). 0.1°C steps are employed in the iteration process as these are considered to be the smallest practical setpoint temperature change that may be applied in an industrial kiln. In those simulations where the material is assumed to be susceptible to collapse, the DBT is restricted to a preset arbitrary temperature and surface strain is controlled through changes in WBT only. Changes in both DBT and WBT are implemented when simulating material assumed to be resistant to collapse. The basic program source code is seen in Appendix B.

In each of the drying curves presented below, the only setpoint conditions selected by the user are the initial DBT, WBT and VEL. The DBT and WBT remain constant until the surface ϵ_i approaches the preset Control Strain. SMARTKILN then automatically humidifies the drying conditions to prevent the surface ϵ_i exceeding Control Strain. SMARTKILN subsequently iterates drying conditions to maintain the surface strain at Control Strain for the remainder of the schedule, producing 'optimum' schedules for boards with the particular material properties selected.

9.3. Optimum schedules for collapse-prone material

Tasmanian eucalypts are particularly prone to collapse shrinkage. Localised collapse shrinkage in fibres just beneath board surfaces induces additional shrinkage in the surface fibres and promotes premature localised surface checking when the 'average' surface instantaneous strain is below the ultimate strain (discussed in detail in 6.5). Collapse also induces internal checking that may remain undetected until the seasoned material is moulded and machined. Whilst we have some qualitative understanding of the mechanism of collapse shrinkage, we do not have the quantitative knowledge to prevent degrade. Therefore, it is imperative that collapse shrinkage be prevented when seasoning furniture grade material.

A batch of green eucalypt material was obtained from a sawmill and dried in an experimental kiln at temperatures ranging from 20 to 30°C. It was found that material dried at temperatures above 24°C experienced collapse

shrinkage while material dried at 22°C did not. Kauman (1964) reported that the propensity for collapse shrinkage is related to the temperature of the wood material. Cell wall stiffness and thus its resistance to sudden deformation due to internal tension decreases with increasing temperature. The colder the material during seasoning, the less susceptible it is to localised collapse shrinkage. A DBT of 22°C was selected as the 'collapse threshold temperature' for the purposes of the simulations reported in this study. Material dried at this temperature was assumed to be resistant to collapse shrinkage. This temperature is somewhat arbitrary but is useful for the purposes of this study.

Occasionally batches of eucalypt material are particularly resistant to collapse, probably due to differences in genetic composition. Such material can withstand higher temperatures throughout the drying process without experiencing collapse. However, it is assumed that even the most resilient material will experience collapse when above FSP and exposed to a critical temperature. This temperature was selected as 30°C in the simulations reported here, again a somewhat arbitrary figure. When SMARTKILN is used to simulate the drying behaviour of collapse-resistant material, the air temperature is allowed to grow exponentially from 22 to 30°C with decreasing centre moisture content from the initial saturated value to FSP.

9.4. Calculated optimum drying schedules

The material properties employed in the drying simulations discussed in this Chapter are presented in Table 9.1.

Table 9.1. Material properties employed in SMARTKILN.

Board Type	Backsawn
Air Velocity	0.5m/s
Diffusion Coefficient	1.7e-7m ² /hr
Basic Density	600kg/m ³
Board Thickness	30mm
Board Width	140mm
Initial Moisture Content	100%
Unconfined Shrinkage @ FSP	1%
Unconfined Shrinkage @ EMC	8%

The simulations represent drying from an initial uniform moisture content of 100% to only 30% at the board centre. Once the centre fibres attain this nominal FSP level, high temperatures (of the order of 80°C and higher) may be applied to the material without inducing collapse since all the free moisture has been removed. Standard final drying treatments may be applied at this time to reduce the centre moisture content to EMC. A lack of numerical data on material properties at high temperatures precludes accurate simulation with KILNSCHED or SMARTKILN. However, SMARTKILN has been employed to develop optimum final drying strategies using the same 'Control Strain' technique and the simulated behaviour appears to accord with known behaviour in a qualitative sense.

Figure 9.1 presents the 'optimum' drying schedule for material nominally assumed to be susceptible to collapse at temperatures above 22°C. This is the maximum temperature employed in the schedule in order to prevent collapse. The initial conditions are 22°C DBT and 20°C WBT, moderate conditions that do not cause the surface ϵ_i to attain the 0.014 Control Strain until after 300 hours of drying.

Figure 9.2 also represents collapse-prone material dried at 22°C DBT. However, the more severe initial drying conditions of 22°C DBT and 14°C WBT cause rapid initial surface drying and generate steep moisture gradients very early in the drying process. SMARTKILN humidifies the drying conditions after only 16 hours to prevent the surface ϵ_i exceeding Control Strain. This schedule reduces the drying time from 1430 hours to 1320 hours compared with the first schedule. Forcing the surface ϵ_i to grow to the 0.014 Control Strain 280 hours earlier reduced the overall drying time by only 110 hours. Clearly the constraining factor in the drying process, in physical terms, is the very slow rate of moisture loss in the intermediate stages of drying.

The temperatures in Figure 9.1 might be typical conditions during the summer months in Tasmania. On first analysis, Figures 9.1 and 9.2 suggest little economic gain is obtained by kiln drying from green rather than predrying the green material in the air for several hundred hours before transferring the partly dried material to a kiln. However, the quality of temperature control in a kiln is significantly better than can be obtained when the material is exposed to the environment (even in curing sheds) so

seasoning degrade is far more likely when the green material is not dried from green in a kiln. Preventing degrade is critical when one is seeking premium prices for furniture grade material because these prices are so much higher than those obtained in other markets and for other end-uses.

Figure 9.3 represents material that is nominally more resilient to collapse, probably due to genetic differences, and thus is assumed to be able to be dried at higher DBT. The calculated schedule reduced the drying time by 250 hours compared with the schedule applied to the collapse-prone material in Figure 9.2, even though Control Strain is unchanged. The drying rate increases with air temperature because the wood temperature increases, causing the vapour pressure in the surface fibres to increase. Thus the moisture concentration in the surface fibres increases and the moisture concentration differential between the air and the surface increases. In addition, the diffusion coefficient increases exponentially with absolute temperature (Schaffner 1981).

The calculated schedule in Figure 9.3 resembles the Continuously Varying Schedule (CVS) developed by Nassif (1983). The CVS comprised increments of the order of 0.1 to 0.25°C in DBT and WBT every hour. The CVS reduced drying times in green *Eucalyptus laevopinea* and *E. agglomerata* to less than one-third of the drying time obtained with a 'conventional' drying regime based on temperature changes at nominal moisture contents. Significant surface checking occurred under all three schedules. The calculated schedule in Figure 9.3 has not achieved such a remarkable improvement in drying time because the maximum allowable temperature was assumed to be constrained by the collapse propensity of the material. Furthermore, the schedules developed by SMARTKILN theoretically prevent seasoning degrade.

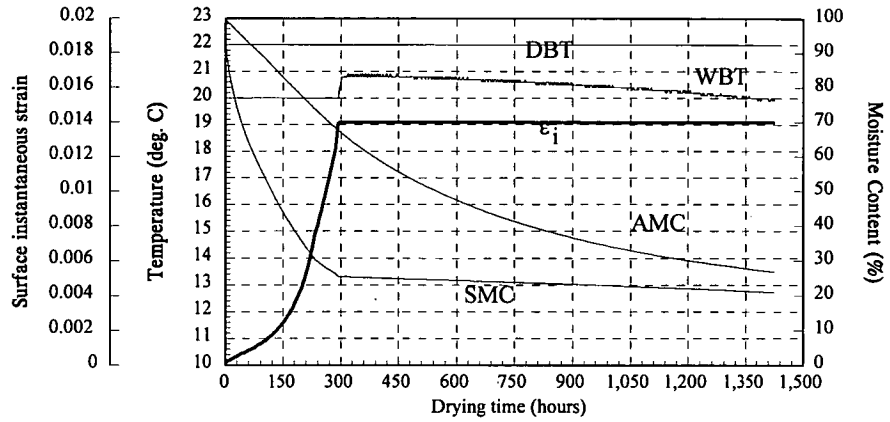


Figure 9.1. Dry Bulb Temperature (DBT), Wet Bulb Temperature (WBT), Average Moisture Content (AMC), Surface Moisture Content (SMC) and Surface instantaneous strain ϵ_i .

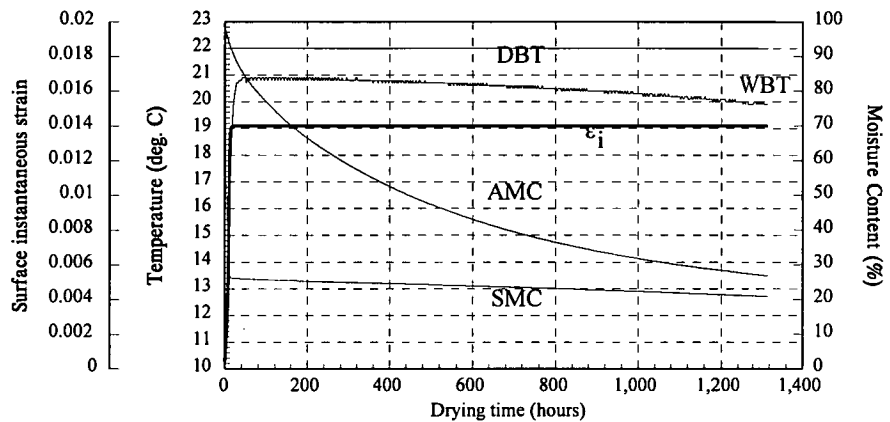


Figure 9.2. Dry Bulb Temperature (DBT), Wet Bulb Temperature (WBT), Average Moisture Content (AMC), Surface Moisture Content (SMC) and Surface instantaneous strain ϵ_i .

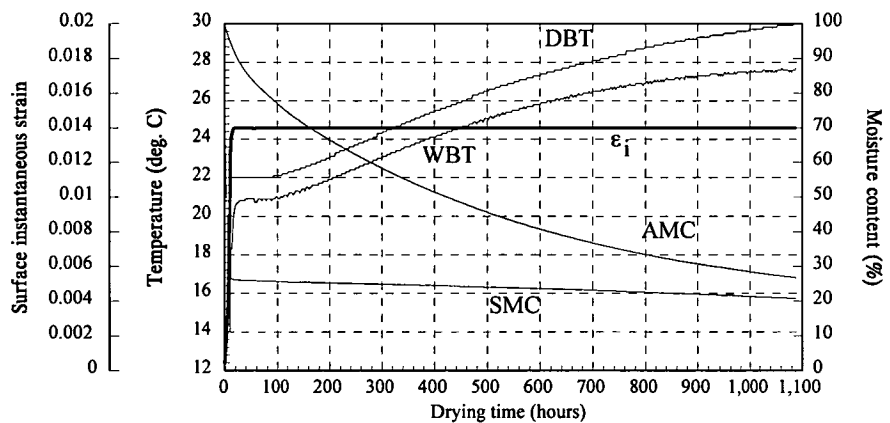


Figure 9.3. Dry Bulb Temperature (DBT), Wet Bulb Temperature (WBT), Average Moisture Content (AMC), Surface Moisture Content (SMC) and Surface instantaneous strain ϵ_i .

The remarkably sensitive nature of the eucalypt material is seen in the overall DBT and WBT curves. Even after 1000 hours of simulated drying, SMARTKILN is employing only 0.1°C temperature changes and the overall WBD increases only marginally. This correlates with results reported by Vanek (1991), who employed a bending moment method and a stress function to continuously measure the size and distribution of drying stresses. He measured a dramatic increase in surface drying stresses after each abrupt climatic change, even during the final stages of drying.

Figure 9.4 reveals drying time from 100% to 30% moisture content appears to be insensitive to the magnitude of Control Strain. This is primarily related to the shape of the stress~strain curve employed in KILNSCHED. Beyond the proportional limit (an instantaneous strain equal to 0.005 or 0.5% based on laboratory loading tests) the stress~strain curve flattens significantly as it increases asymptotically to the ultimate stress. Thus the calculated surface instantaneous strain increases dramatically with relatively small increments in surface stress. Therefore Control Strain increases by 80% when increased from 0.01 to 0.018 for example, but the corresponding surface stress increases far less. This has significant practical applications because a relatively low Control Strain can be employed to generate significantly 'safer' schedules without significantly sacrificing drying time. These 'safer' schedules are more likely to dry particularly refractory boards within a batch of timber without causing seasoning degrade.

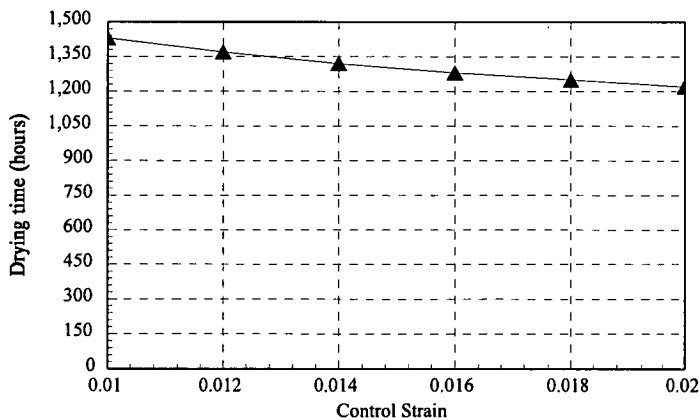


Figure 9.4. Relationship between Drying Time and Control Strain at constant 22°C DBT.

Figure 9.5 presents the relationship between drying time and 'Time to Control Strain' using a Control Strain of 0.014 and material properties listed in Table 9.1. Time to Control Strain is the time from the commencement of

drying to that time at which the surface instantaneous strain attains the Control Strain. This time is directly related to the severity of the (constant) initial drying conditions. It appears that little economic gain in terms of overall drying time is obtained by kiln drying from green rather than predrying the green material in the air for several hundred hours before transferring the partly dried material to a kiln. However, the quality of temperature control in a kiln is significantly better than will be obtained when the material is exposed to the environment or dried in curing sheds. The sensitivity of the material to temperature means seasoning degrade is thus far more likely when the material is not dried from green in a kiln.

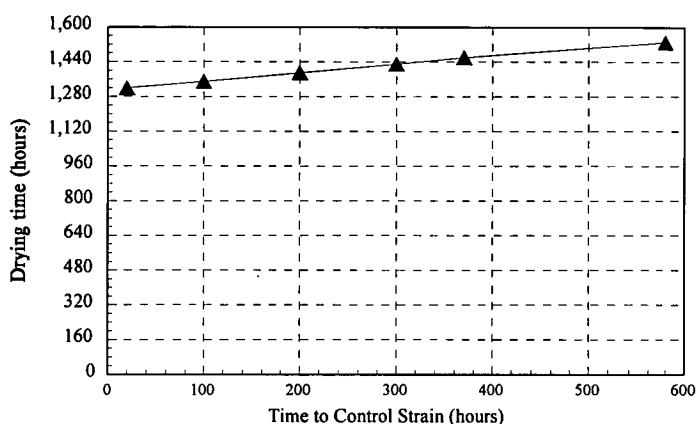


Figure 9.5. Relationship between Drying time T and Time to Control Strain at constant 22°C DBT.

Figure 9.6 represents the relationship between drying time and board thickness using a Control Strain of 0.014 and initial conditions of 22°C DBT, 14°C WBT and 0.5m/s VEL. The material properties used in the simulations are listed in Table 9.1. The cost of drying is essentially related to the time of drying (assuming minimal seasoning degrade occurs). The nonlinear relationship between drying time and board thickness suggests it may be more profitable to season certain thicknesses, although market demands ultimately determine the material thickness.

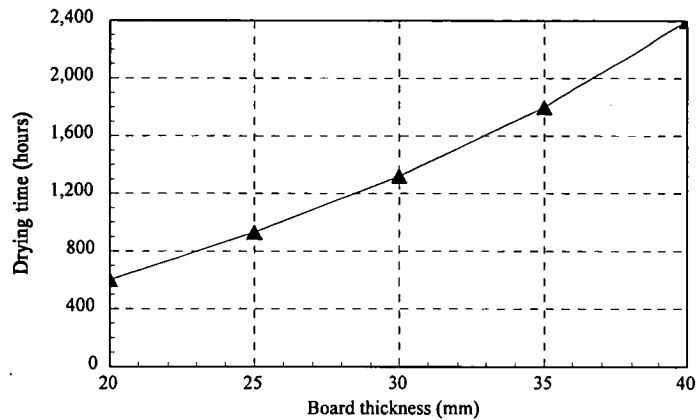


Figure 9.6. Relationship between drying time and board thickness in collapse susceptible material dried at 22°C DBT.

SMARTKILN effectively mirrors the AE Controller philosophy discussed in 10.4 except ControlAE is replaced by Control Strain. The common thread to these processes is adjustment of the drying conditions to maintain the board surface at a preset state of stress for the duration of the drying process.

It is interesting to note that the surface moisture content (SMC) in Figures 9.1, 9.2 and 9.3 does not drop below 20%. This is higher than the figures generally obtained in commercial drying where the SMC is as low as 10-14% when reconditioning is performed. It is generally accepted in the industry that the timber moisture content must be at least 16% or higher for reconditioning to be effective; it appears softening does not occur below this 16% figure. Reconditioning incorporates live steam to re-wet the board surface and force the moisture content above 16% and high temperature air to soften the timber and recover the majority of the collapse shrinkage that has occurred. The optimum schedules calculated by SMARTKILN 'prevent' collapse and maintain a relatively high surface moisture content. Thus it is plausible that such schedules will preclude the need for an expensive boiler plant. Once the centre moisture content attains 30%, it is likely a high temperature treatment alone will be sufficient to equalise residual stresses within boards. Therefore, although the schedules developed with SMARTKILN incorporate low-temperature 'slow' drying, it may well be economically advantageous to avoid collapse.

9.5. Summary

SMARTKILN is an exciting research tool that calculates optimum drying schedules. However, SMARTKILN has even more potential as an online drying simulation program in a kiln control system. Vermaas (IUFRO 1992) reported that "a wide gap existed between drying theory and practical application, despite continuous developments and refinements in drying model theory". "Translating complex drying models into everyday practical application in kiln control has not been achieved to the extent where one could talk of a true synthesis of theory and practice". The close relationship between measured AE and surface instantaneous strain calculated by KILNSCHED, along with the optimum schedules generated by the derivative program SMARTKILN, bridges the gap between theory and practice.

SMARTKILN was modified (in the same manner as KILNSCHED) to simulate drying using datalogged temperatures during a drying trial, before developing the optimum schedule to apply to the timber stack. In addition, KILNSCHED, MCPROFILES and SMARTKILN were modified to run as online drying programs in an optimal kiln control system. The resulting Clever Kiln Controller® system is discussed in detail in Chapter 10.

Chapter 10

Clever Kiln Controller® (CKC)

A predictive, adaptive, real-time kiln control system known as Clever Kiln Controller® (CKC) was developed by the author to dry Tasmanian eucalypt timber in the minimum time with minimum degrade. A professional programmer with experience of C++ in a Microsoft Windows background was employed to develop CKC as a graphical interface application for a personal computer. CKC monitors kiln behaviour, executes online drying simulation programs and plots all relevant parameters.

CKC incorporates three online drying simulation programs and real-time measurement of AE in three sample AE Boards in the kiln. The primary drying program is a modified version of SMARTKILN which uses the datalogged kiln conditions rather than the 'ideal', constant drying conditions entered in the drying schedule. The user compares calculated drying behaviour with measured through-thickness moisture profiles and sensed AE. The user progressively refines the diffusion coefficient to force SMARTKILN to accurately reflect the measured drying behaviour. SMARTKILN then iterates subsequent setpoint temperatures to maintain the calculated surface instantaneous strain at the preset Control Strain and this optimum schedule is applied to the kiln. The system prevents surface degrade by ameliorating the drying conditions and overriding the optimum schedule when the measured AE rate exceeds ControlAE.

10.1. CKC modes of operation

CKC operates in one of three distinct 'modes', each mode incorporating additional 'optimisation' functionality. The basic 'Schedule Setpoint mode' is a simple PID feedback control system (discussed in 4.4.2) that maintains kiln temperatures at preset setpoint temperatures in a schedule defined by the user. In 'AE mode', this user-schedule is over-ridden immediately the AE rate exceeds ControlAE. This mode incorporates the AE Controller discussed in 10.4. In 'SmartKiln mode', CKC inherits the functionality of the AE Controller and develops an optimum schedule with SMARTKILN. When the AE rate exceeds ControlAE (discussed in 7.3), the AE Controller

immediately determines new setpoint temperatures to prevent surface checking and a new optimum schedule is calculated by SMARTKILN.

10.2. Determining the 'collapse threshold temperature'

As discussed in 6.5, AE is not an accurate measure of surface stress when localised collapse shrinkage occurs in the AE Board, since 'premature' surface checking occurs in the neighbouring, highly stressed surface fibres. Furthermore, the drying models incorporated into CKC do not accurately model collapse. Therefore, it is imperative that collapse be prevented when using CKC to produce furniture grade material. As discussed in 9.3, collapse propensity is reduced by drying at low temperatures in order to maintain high fibre wall stiffness. However, drying time increases with decreasing drying temperature so it is important to dry the material at the highest possible *safe* temperature that does not induce collapse. Section 9.3 revealed that a 'collapse threshold temperature' appeared to exist for a given batch of particular material; material collapsed at 24°C but not at 22°C DBT.

Kauman (1964) suggested the best measure for predicting collapse was to oven-dry small sample sections prior to seasoning and observe the collapse produced. The collapse expected during kiln drying could then be estimated from the somewhat higher collapse measured during oven drying.

In fact, the apparent relationship between collapse severity and wood temperature means cross-section samples measuring approximately 100mm long may be removed from boards in the timber batch and oven-dried at a range of different temperatures. The batch should be wrapped in a plastic sheet for the duration of these oven-drying trials to prevent excessive surface drying. Typical drying temperatures might be 15, 20, 25, 30, 35 and 40°C for example. Specimens typically require 24 to 48 hours drying under such conditions to attain FSP (the specimen ends are not end-coated). At the completion of drying, each sample is inspected for collapse and internal checking. The highest temperature sample that did not collapse defines the collapse threshold temperature. This is the maximum temperature that the green material can be dried at without inducing collapse shrinkage. A more conservative approach would be dry the material one or two degrees below this temperature to take into account potential variations in kiln temperatures during drying.

In practice, this simplistic description ignores the effect of drying time on collapse propensity. The greater the drying rate, the faster the free moisture is removed from the cell and the less gradual cell contraction occurs before the compressive stresses in the fibre walls cause collapse. When the drying rate is relatively slow, collapse is postponed by the slow growth of hydrostatic tension forces in the free moisture in the lumen. The compressive stresses in the fibre walls then act for a relatively long time, causing the creep and mechano-sorptive effect to act in the same direction as the shrinkage acting on the fibre wall. Given sufficient time, these phenomena appear to reduce the fibre dimensions sufficiently that the pressure within the free moisture is maintained relatively high, preventing the occurrence of excessive tension in the moisture and thus preventing excessive buckling loads within the cell walls. However, the oven-drying strategy at different temperatures provides sufficient collapse information given the variability of the material.

10.3. Online drying simulation programs

10.3.1. Historical kiln conditions (HKC)

The kiln DBTs and WBTs are datalogged by CKC every 15 seconds for the duration of drying. This data is averaged every 4 minutes and the processed temperatures are referred to as the Historical Kiln Conditions (HKC). MCPROFILES and SMARTKILN use the HKC rather than the user-entered schedule, ensuring the programs are sensitive to the inevitable small oscillations in kiln temperature experienced with varying ambient temperature. Section 7.2.5 revealed that the measured AE during drying and the surface instantaneous strain calculated with KILNSCHED are sensitive to temperature fluctuations of the order of only 0.2°C. Such sensitivity reveals the difficulties faced in commercial drying operations where kiln control is typically no better than ± 2 or 3°C.

10.3.2. Drying simulation programs

Three online drying programs are employed in CKC : KILNSCHED, MCPROFILES and SMARTKILN. MCPROFILES and SMARTKILN are

specialised versions of the base program KILNSCHED with specific functionality described below.

KILNSCHED allows the operator to develop a 'safe' schedule before the commencement of drying, when limited material property measurements have been obtained. This schedule is applied to the green timber when CKC is started.

MCPROFILES is employed to determine the material diffusion coefficient. Moisture profiles are measured at regular intervals during the drying process using the slicing process described in 5.7.3. A typical program of slice times was presented in 5.7.5. MCPROFILES uses the HKC and calculates moisture distribution development with an arbitrary 'trial' diffusion coefficient. The user visually compares the calculated and measured moisture profiles online and adjusts the diffusion coefficient by trial and error until a satisfactory fit between the calculated and measured drying behaviour is obtained (refer to 7.1). After the third profile measurement at 48 hours, the diffusion coefficient is known to within around 3%. The operator refines the diffusion coefficient value each time a new profile is measured. The inferred diffusion coefficient is incorporated into SMARTKILN.

SMARTKILN was discussed in detail in Chapter 9. The calculated optimum schedules in 9.4 comprise constant drying conditions until the surface instantaneous strain approaches Control Strain, at which time SMARTKILN determined the optimum schedule. In CKC, SMARTKILN uses the HKC to ensure the program is sensitive to the variations in kiln temperature experienced by the drying timber and is as accurate as possible. Whilst MCPROFILES is employed to determine the diffusion coefficient, the user employs SMARTKILN to calculate the surface instantaneous strain behaviour. Provided accurate material properties and diffusion coefficient have been incorporated into SMARTKILN, the measured AE and calculated surface instantaneous strain will be satisfactorily matched (as discussed in 7.2). SMARTKILN then develops an optimum drying schedule, as discussed in 9.2. This schedule is revised each time a new hour of HKC is available because SMARTKILN returns to that time and uses the new HKC before determining the new optimum schedule.

10.4. AE Controller

The AE Controller governs the AE (and thus indirectly the surface instantaneous strain) behaviour and prevents surface checking by adjusting the kiln setpoint temperatures (airspeed changes are not employed in CKC). The direct relationship between AE and surface instantaneous strain described in 7.2 means the temperature setpoint 'control strategy' implemented in the SMARTKILN simulations in Chapter 9 are directly applicable when using AE to prevent surface checking.

The most basic AE control strategy incorporates a single ControlAE value (as discussed in 7.3, ControlAE is a preset AE rate, which when exceeded, initiates action to ameliorate the drying conditions and prevent surface checking). Consider the kiln at nominal setpoint temperatures when the AE rate exceeds ControlAE (nominally selected as 70% of the AE checking threshold). The WBTSP is increased by 0.1°C at constant DBTSP to increase the moisture concentration in the free stream air and reduce the moisture concentration differential ($c_{vw}-c_m$), as discussed in 9.1. A 0.1°C change is considered to be the smallest practical setpoint temperature change. The WBT is suddenly below WBTSP and the PID control algorithm in 4.4.2 causes the water sprays to admit more moisture into the air and the vents to close to increase the WBT. Further WBTSP changes are made each time the AE rate exceeds ControlAE. This strategy would prevent surface checking (provided ControlAE is set sufficiently below AE checking threshold) but requires a sudden burst of setpoint changes to retard the surface stress once the AE exceeds ControlAE. Otherwise the AE will attain the AE checking threshold before the temperature changes are effected. It is envisaged that the temperatures in a large industrial kiln could not be adjusted sufficiently rapidly to follow the required setpoint changes. A further problem with delaying temperature changes until the AE rate is relatively near the AE checking threshold is that moisture will probably be re-absorbed by board surfaces during the period of sudden, rapid humidification and thus long drying times will result.

A more robust strategy incorporates an initial ControlAE value ('InitialAE') below the final 70% figure ('FinalAE'). Immediately the AE exceeds InitialAE (40% for example), a WBTSP change is applied to the kiln and ControlAE commences to increase exponentially towards FinalAE. Further WBTSP

changes are applied when the AE exceeds the slowly increasing ControlAE (Figure 10.1 presents typical ControlAE behaviour). This strategy incorporates two major improvements over the single ControlAE strategy. Firstly, CKC moderates the board surface behaviour at a lower stress. A small temperature change has a significant effect at this stage and temperatures in a large kiln are far more likely to follow small, intermittent setpoint changes (due to intermittent AE peaks above ControlAE) than a sudden burst of numerous setpoint changes. Thus rather more smooth temperature control is expected to result from the varying ControlAE strategy. Secondly, when an AE peak greater than InitialAE occurs, ControlAE tends to increase beyond subsequent AE peaks of the same magnitude, thus precluding setpoint changes at constant AE (and thus constant surface instantaneous strain).

This strategy effectively reduces the severity of the drying conditions when the AE rate exceeds ControlAE but has no facility to increase the surface drying rate when the AE rate remains low for a significant period. This is achieved by decreasing WBTSP at constant DBTSP (when DBTSP has attained the collapse threshold temperature discussed in 9.3) or by increasing DBTSP as discussed in 9.1. However, arbitrary setpoint changes cannot simply be applied when the AE rate is relatively low, because the AE is not representative of the surface stress during unloading. At constant or decreasing surface stress and instantaneous strain, the AE gradually decreases since no new stress release events are required (as discussed in 7.2.3 and 7.3). The peak AE rate measured during drying is the true measure of surface stress. A small increase in the severity of the drying conditions when the AE is decreasing is expected to cause the AE to very rapidly return to a level near or above the previous peak AE rate.

This was taken into account by causing ControlAE to decrease back towards InitialAE when the average AE rate decreases below an arbitrary low value (LowAE). The drying conditions are made more severe with a single setpoint change at this time. To avoid numerous changes in drying conditions when the AE rate is low (after a preceding period of high AE), at least one hour must pass before a further condition change is applied (this time is actually selectable by the user). The drying conditions are ameliorated immediately the more severe drying conditions cause the AE rate to exceed ControlAE. This means the drying conditions are ameliorated

before the AE exceeds the previous maximum ControlAE value. Measured ControlAE and setpoint temperature behaviour are presented below in Figure 10.1.1 and 10.1.2 and discussed in detail in 10.7.

10.5. Selecting AE Boards

Localised knots or burls on a board surface act as stress concentration sites from a stress analysis viewpoint. Surface checks initiate near these natural 'defects' before they occur elsewhere on the surface. If a batch of wood contains a high proportion of such defects and it is desirable to prevent surface checking in such boards, then the AE Boards should contain such defects and the AE transducer should be placed near the defect. However, when a small proportion of boards contain defects, the transducers should be placed on clear boards.

Backsawn and quartersawn boards experience surface checking at the same AE rate, so on first analysis the transducers may be clamped to either board type. However, backsawn boards are prone to cupping. This induces additional tensile strain at the surface since the growth rings tend to straighten out during drying. The effect is more pronounced on the surface containing the 'tight' growth rings. Therefore the AE Board and MP Boards must be cut far from the centre of the tree to minimise cupping. Of course, the ever-decreasing diameters of regrowth logs entering the sawmill may make it difficult to prevent cupping. When AE is measured in a backsawn board, the transducer should be clamped to the surface closest to the centre of the tree, as this surface experiences greater cupping and thus higher surface stress.

In summary, the AE Boards should simply be selected as being representative of the majority of boards in the timber packs to be dried.

There are benefits derived from attaching the AE transducers to end-matched boards and from attaching them to non-matched boards. When the AE Boards are not matched, the AE data provides a better representation of the possible variable drying characteristics of the timber in the stack. When the AE boards are matched, the behaviour of the same timber in different positions in the stack is recorded. Experience will reveal whether to use end-matched or non-matched AE Boards.

10.6. CKC strategy

The following section describes the strategy implemented in CKC drying trials using the research kiln described in 4.4. It is envisaged that this methodology will be particularly suitable to research kilns with capacities in the vicinity of one cubic metre of green timber. Experience will reveal whether the strategy is applicable to large industrial kilns.

A batch of green timber is obtained off the saw and the ends of the boards are painted with an impermeable coating to prevent end-drying and end-checking. It is possible that this coating procedure would be cost-effective even in standard industry length boards because significant end-checking and costly docking would be avoided. Various boards are used as sample boards to measure the bulk properties discussed in 5.7. The remaining boards are stacked in the kiln and AE transducers are clamped to three AE Boards located at stack inlet, centre and outlet at mid-stack height. An initial moisture profile is measured in an MP Board.

CKC is started and a 'safe' schedule is determined using KILNSCHED and conservative material property values. CKC implements this schedule and the user regularly measures moisture profiles, the frequency of profile measurement being rather tied to the rate of drying, since little benefit is gained by measuring successive moisture profiles with virtually the same shape. A quite accurate (within 3%) measure of the diffusion coefficient is usually obtained with MCPROFILES after approximately 48 hours. At this time, SMARTKILN is executed to develop an optimum schedule. CKC is then placed in SmartKiln mode and CKC implements the optimum schedule. The AE Controller over-rides the current optimum schedule setpoints when the AE rate exceeds ControlAE to prevent surface checking. SMARTKILN is then employed to determine a new optimum schedule.

On occasion it is envisaged that particularly refractory material may not be accurately modelled with the one-dimensional drying models. In such instances, surface checking must be prevented with the AE Controller alone and temperature changes will not be optimised. However the AE Controller applies more severe drying conditions to the kiln each time the average AE lies below LowAE in order to maintain a high surface drying rate.

10.7. CKC drying trials

Figures 10.1.1 and 10.1.2 depict measured AE and temperature behaviour respectively in a CKC drying trial in the research kiln described in 4.4. CKC was operating in 'AE mode' with InitialAE set at 40% of failure, FinalAE at 70% and LowAE at 20%.

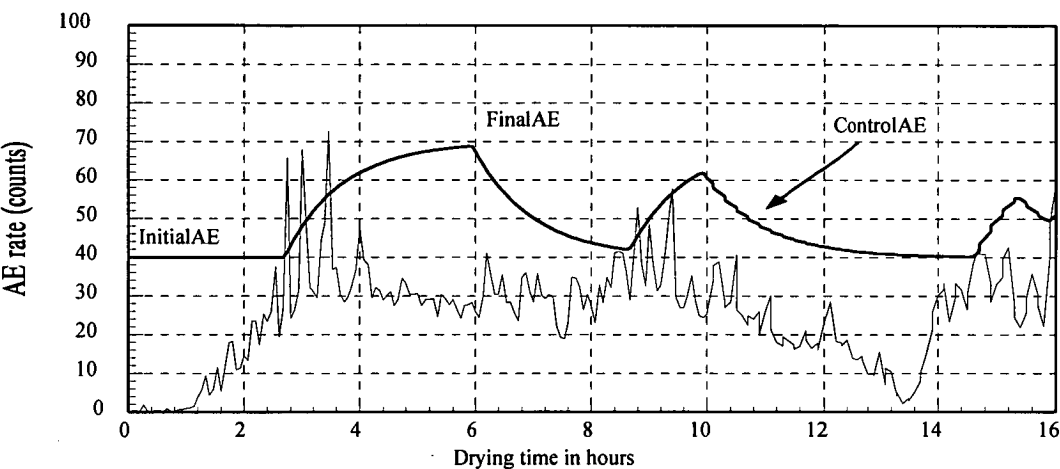


Figure 10.1.1 Measured AE and ControlAE.

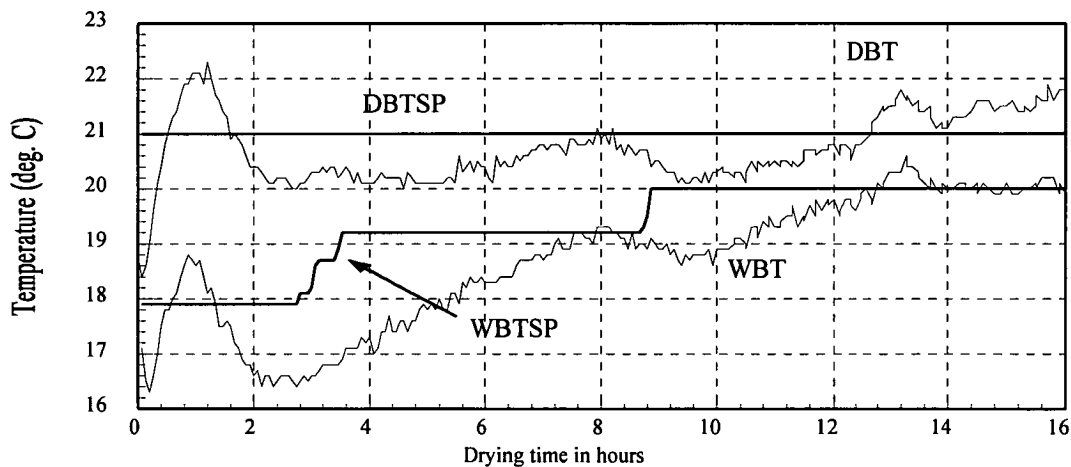


Figure 10.1.2 Setpoint temperatures and measured temperatures.

The AE rate does not resemble the intermittent nature of the AE responses in Appendix A because the peak AE level recorded during each 4-minute HKC period only is plotted. The AE rate is actually the maximum level recorded by the three transducers clamped to a single AE Board. The AE rate exceeded the 40% initial ControlAE value after 2.8 hours and the WBTSP was increased in 0.1°C increments each time the AE subsequently exceeded the increasing ControlAE. Eventually the AE levelled off and commenced to

decrease with the decreasing wet bulb depression (WBD). When the *average* AE rate decreased below the 20% LowAE level, ControlAE decreased exponentially towards InitialAE. At 8 hours drying time, the DBT and WBT decreased, causing the material surface to stiffen and thus the increasing AE. Further WBTSP changes were applied after 8.6 hours when the AE rate exceeded ControlAE. This strategy successfully ameliorated the drying conditions before the AE rate attained high levels near the AE checking threshold and thus precluded numerous setpoint changes. Despite the nearly constant 30 count AE rate recorded between 4 and 8 hours, the true AE level is near the 72 count peak AE rate recorded at 3.6 hours.

The setpoint temperatures were not altered after 9 hours, despite the AE exceeding ControlAE at 14.5 hours, because the minimum allowable WBDSP in CKC was arbitrarily set at 1.0°C.

Figures 10.2.1, 10.2.2 and 10.2.3 depict measured drying behaviour during the first 30 hours of a CKC trial at the Victorian Timber Industry Training Board facility, Creswick, Victoria. The CKC was used to control a Vanicek 20m³ industrial kiln. Heating was provided by a boiler situated beside the kiln.

Figure 10.2.1 reveals excellent (within 0.5°C) temperature control and Figure 10.2.3 presents the PID-controlled steam, vent and spray settings. The AE measured by three AE transducers clamped to three *separate* AE Boards is presented in Figure 10.2.2. The AE measured by two of the sensors in Figure 10.2.2 are closely correlated indeed, whilst the third sensor and spring-loaded clamp appear to have been knocked while stacking the timber pack (the AE sensor must be clamped hard to a board surface to minimise signal attenuation). The AE spikes at 26 hours occurred when the kiln door was opened. The close agreement between the two sensors is very encouraging and suggests three AE sensors situated throughout an entire timber stack will provide a satisfactory representation of the drying stresses in a large number of boards. This drying trial was extremely encouraging for the 20m³ kiln was the largest kiln the CKC had been used upon.

The AE rate exceeded ControlAE frequently during the first couple of hours of drying but the setpoint temperatures did not change since the initial WBD equalled the minimum 1.0°C value mentioned above.

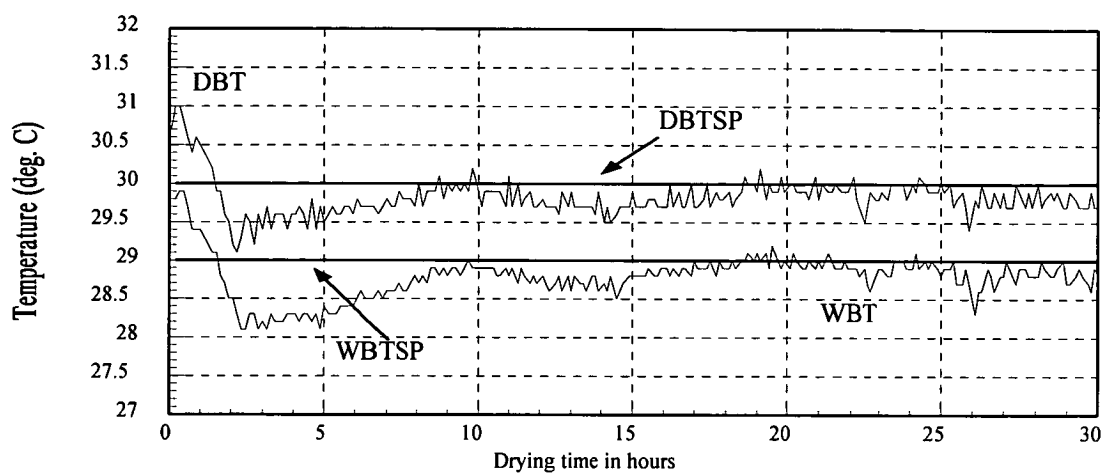


Figure 10.2.1 Setpoint temperatures and measured temperatures.

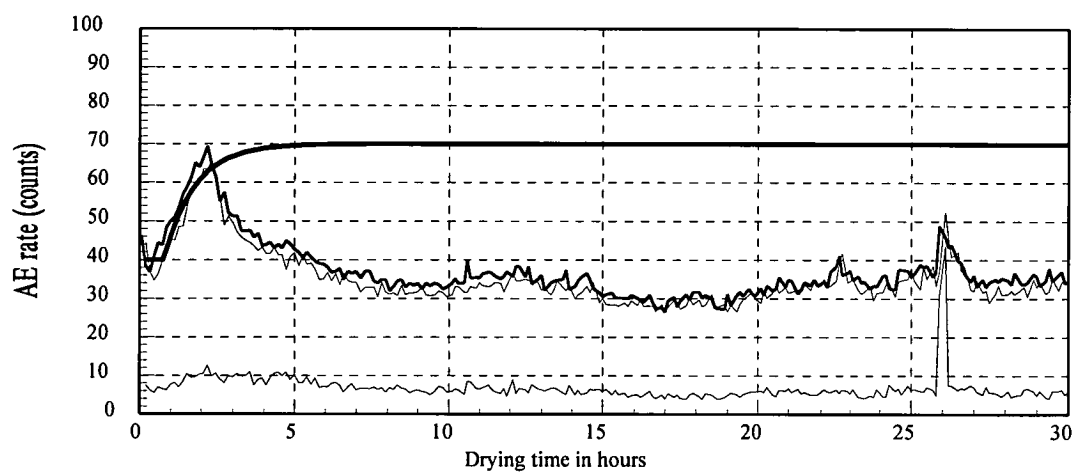


Figure 10.2.2 Measured AE and ControlAE.

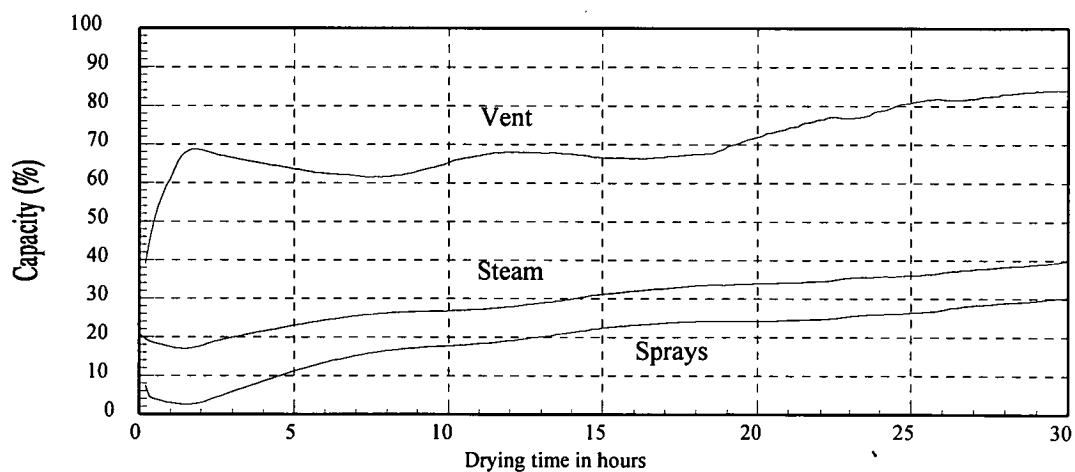


Figure 10.2.3 PID-controlled hardware settings.

Figure 10.3.1 presents a typical optimum schedule calculated by SMARTKILN with the CKC in SmartKiln mode. The schedule was calculated after 15 hours drying in the small research kiln described in 4.4, so the optimum schedule includes the corresponding period of HKC at the start of the schedule (with 22°C DBTSP and 18°C WBTSP). A Control Strain of 0.014 was used in the simulation and the corresponding surface strain behaviour is seen in Figure 10.3.2. Immediately another hour of HKC is measured, SMARTKILN resets the board state to the state calculated at 15 hours, simulates the new hour of HKC and then calculates a new optimum schedule.

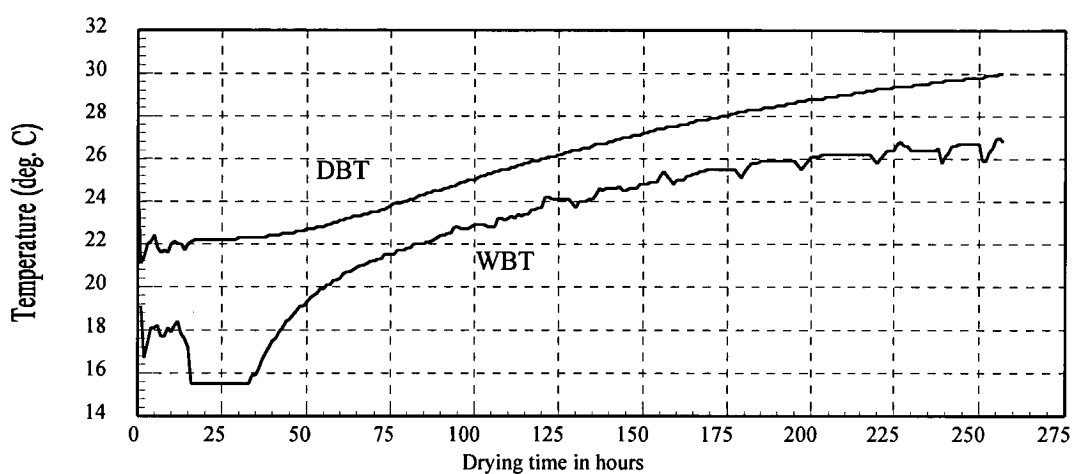


Figure 10.3.1 Calculated optimum schedule with Control Strain = 0.014

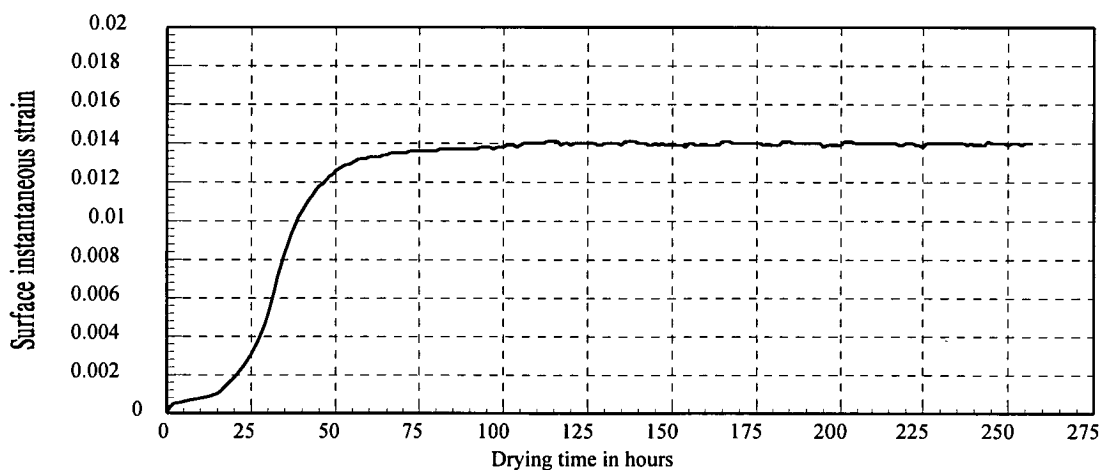


Figure 10.3.2 Calculated surface strain behaviour

10.8. Versatility of the CKC

The user modifies the PID gains by trial and error in CKC to minimise temperature deviations from their corresponding setpoints in a particular kiln. CKC may be connected to a kiln of arbitrary size with arbitrary

capacity heaters, vents and sprays as evidenced by the 20m³ trial described above. The system is not limited to the small research kiln used extensively for CKC development. Moreover, values of PID gains in pneumatic or PLC controllers known to give good control over an existing kiln can be incorporated directly into CKC.

Surface check prevention is implemented by altering setpoint temperatures. The thermal inertia of large kilns means humidification may not be as rapid as would be attained with direct spray setting changes (for example) but CKC is totally versatile and applicable to arbitrary kilns. The inertia problem is reduced by ameliorating the drying conditions 'earlier rather than later' using the varying ControlAE strategy. AE Controller promotes smooth temperature control rather than sudden, numerous temperature setpoints changes when surface checking is imminent.

CKC was progressively refined to ensure that it was a versatile 'front-end' controller for existing kilns. In the initial stages, the kiln hardware was powered directly by the 'buffer/amplification' hardware discussed in 4.4.1. This meant the wiring in existing kilns had to be disconnected to allow CKC to control the kiln. This was overcome by replacing the buffer stage on each output channel of the Analog/Digital Board with relays. Each relay is wired in series with the existing kiln hardware. The existing kiln controller (PLC for example) is used to 'power up' the kiln hardware. The relevant relays are activated by CKC only when required. This means existing kiln wiring and hardware are not removed, making CKC a fully interactive kiln control system applicable to any arbitrary kiln.

10.9. Stacking

When a log is cut into quartersawn boards, very few boards will be perfectly radial. The angle of contact between the growth rings and the wide surface will be different at each wide surface. It appears to be sensible to orientate the boards during stacking so that the surface containing the more nearly tangential growth rings is at the bottom. Then the more moderate drying conditions at the bottom of each board is applied to the more refractory surface (as discussed in 4.2).

10.10. Suggested refinements to CKC

- The R6I AE transducers are expensive (costing around \$A1400 each) and would be easily damaged when racking timber stacks in a commercial operation. In addition, the spring-loaded aluminium frame (Figure 4.2) sits approximately 70mm above the board surface. Typical sticker thicknesses lie between 17 and 25mm only, depending upon the boards being dried, and thus the board that would have lay directly above the AE Board must be cut into two lengths and carefully placed around the protruding AE sensor and clamp. It would be desirable to use smaller AE sensors that did not require the stack to be carefully constructed.
- Online moisture meters might be incorporated into CKC to provide continuous feedback on the surface moisture content of sample MP Boards. This would allow verification of drying behaviour calculated by MCPROFILES and SMARTKILN to be rather more automated than is currently the case.
- The optimum control of dry bulb temperature has not been fully addressed. Collapse imposes an upper limit on DBT in the early stages of drying but SMARTKILN contains no algorithm to *optimise* the DBT behaviour. Further work is needed in this area.
- At present, when the CKC is trialed at commercial kilns such as the Creswick 20m³ kiln, the existing temperature controller is disconnected and the CKC is wired up in its place . It would be desirable to develop serial communications functionality in CKC so that the CKC controls the kiln via existing controllers such as Programmable Logic Controllers (PLCs). This would allow the CKC to be 'closed down' whilst the PLC maintained temperature control.
- Eventually it would be desirable to introduce probabilistic effects into the drying programs. This would remove the current situation whereby an entire kiln is controlled by the state of several AE Boards and MP Boards.

References

- Adams R.D. 1969. Fracture development in wood resulting from bending stresses and detected using the acoustic emission technique. Master of Forestry thesis, University of British Columbia.
- Ansell M.P. 1982. Acoustic emission from softwoods in tension. *Wood Sci. Tech.* 16:35-58.
- Armstrong L.D., Kingston R.S.T. 1962. The effect of moisture content changes on the deformation of wood under stress. *Aus. J. Appl. Sci.* 13:257-276.
- Becker H.F. 1982. Acoustic emissions during wood drying. *Holz Roh Werkstoff.* 40(9):345-350.
- Bernatowicz G., Militzer K-E. 1992. 'Using of the acoustic emission analysis for the assessment of the material quality during the drying of wood'. Paper presented at 3rd IUFRO Drying Conference. Vienna, Austria 1992
- Booker J.D. 1990. Kiln control by acoustic emission. Honours thesis. Uni. of Tas.
- Booker J.D. 1994a. Acoustic emission related to instantaneous strain in Tasmanian eucalypt timber during seasoning. *Wood Sci. Tech.* 28(4):249-259
- Booker J.D. 1994b. Acoustic emission and surface checking in *Eucalyptus regnans* boards during drying. *Holz Roh Werkstoff.* (in press)
- Booker J.D., Doe P.E. 1995a. Acoustic emission related to strain energy during drying of *Eucalyptus regnans* boards. *Wood. Sci. Tech.* (under review)
- Booker J.D. 1995b. Optimum drying schedules for Tasmanian eucalypt material calculated with a one-dimensional non linear drying model. *Wood. Sci. Tech.* (under review)
- Bucur V. 1991. 'Acoustic emission techniques in wood science and technology'. Paper presented at Ultrasonics International 91 Conference

Campbell G.S. 1959. Can chemical seasoning help the timber industry? *CSIRO Div. For. Prod. Newsletter*. 257

Campbell G.S., Hartley J. 1978. Drying and dried wood, in *Eucalypts for wood production*. (ed. Hillis W.E. and Brown A.G.). Griffin Press.

Carslaw H.S., Jaeger J.C. 1959. *Conduction of heat in solids*. Clarendon Press.

Chafe S.C., Barnacle J.E. et al. 1992. *Collapse : an introduction*. CSIRO Div. For. Prod.

Christensen F.J., Neylon M. 1979. 'Effects of pre-freezing on the seasoning of back-sawn boards from Tasmanian-grown eucalypts'. Paper presented at 19th For. Prod. Res. Conf. Highett, Australia.

Debaise G.R., Porter A.W., Pentoney R.E. 1966. Morphology and mechanics of wood fracture. *Materials Research and Standards*. 6(10):493-499.

Dinwoodie J.M. 1966. Induction of cell wall dislocations (slip planes) during the preparation of microscope sections of wood. *Nature*. 212:525-527.

Dinwoodie J.M. 1968. Failure in Timber. Part 1. Microscopic changes in cell-wall structure associated with compression failure. *J. Inst. Wood. Sci.* 37-53.

Doe, P.E., Oliver, A.R. and Booker, J.D. 1994. 'A non-linear strain and moisture content model of variable hardwood drying schedules'. Paper presented at 4th International IUFRO wood drying conference, Rotorua, NZ, August 9-13.

Gerberich W.W., Hartbower C.E. 1967. Some observations on stress wave emission as a measure of crack growth. *Intern. J. Fract. Mech.* 3(3):185-191.

Gordon J.E. 1968. *The New Science of Strong Materials*. Penguin.

Hasan O. 1994. unpublished data.

Harris D.O., Tetelman A.S., Darwish F.A. 1972. Detection of fibre cracking by acoustic emission. *Acoustic Emission*. ASTM STP 505. 238-249.

Honeycutt R.M., Skaar C., Simpson W.T. 1985. Use of acoustic emissions to control drying rate of red oak. *For. Prod. Journ.* 35(1):48-50.

Ilic J. 1992. Personal communication.

Innes T.C. 1992. Mechanical properties of Tasmanian Oak relevant to seasoning. Honours thesis. Uni. of Tas.

Kaiser J. 1950. Untersuchungen über das Auftreten von Geräusch beim Zugversuch. Ph.D. Thesis. Technische Hochschule, Munchen.

Kauman W.G. 1964. Cell Collapse in Wood. CSIRO DFP Reprint No. 566.

Kingston RSJ., Clarke L.N. 1961. Some aspects of rheological behaviour of wood. *Aus. J. Appl. Sci.* 12:211-240.

Kitayama S., Satoyoshi K., Noguchi M. 1985a. Monitoring of wood drying process by acoustic emission. *Wood Industry.* 40:464-469.

Kitayama S., Noguchi M., Satoyoshi K. 1985b. Automatic control system of drying Zerkova wood by acoustic emission monitoring. *Acoustics Letters.* 9(4):45-48.

Kline R.A. 1983. Acoustic emission signal characterisation, in *Acoustic Emission*. (ed. James R. Matthews). Gordon and Breach Science Publishers. New York.

Kollmann F.E., Côté W.A. 1984. *Principles of Wood Science and Technology*. Springer-Verlag.

Miller D.G. 1963. Sounds generated by wood when under stress. *Research News, Canada Forestry.* 6:6-7.

Molinski W., Raczkowski J., Poliszko S. 1991. Mechanism of acoustic emission in wood soaked in water. *Holzforschung.* 45(1)13-17.

- Mudakai J., Yata S. 1986. Modelling and simulation of viscoelastic behaviour (tensile strain) of wood under moisture change. *Wood Sci. Tech.* 20:335-348.
- Nassif. N.M. 1983. Continuously varying schedule (CVS) - a new technique in wood drying. *Wood. Sci. Tech.* 17:139-144.
- Noguchi M., Kagawa Y., Katagiri J. 1980. Detection of acoustic emission during hardwoods drying. *Mokuzai Gakkaishi.* 26(9):637-638.
- Noguchi M., Kagawa Y., Katagiri J. 1983. Acoustic emission generation in the process of drying hardwoods. *Mozukai Gakkaishi.* 29(1):20-23.
- Noguchi M., Okumura S., Kawamoto S. 1985. Characteristics of acoustic emissions during wood drying. *Mozukai Gakkaishi.* 31(3):171-175.
- Noguchi M., Kitayama S., Satoyoshi K., Umetsu J. 1987. Feedback control for drying *zelkova serrata* using in-process acoustic emission monitoring. *For. Prod. Journ.* 37(1):28-34.
- Oliver A.R. 1984. 'Shrinkage and creep in drying timber'. Paper presented at 21st For. Prod. Res. Conf. Australia.
- Oliver A.R. 1991. A model of the behaviour of wood as it dries (with special reference to eucalypt materials). Research Report CM91-1. Uni of Tas.
- Panshin A.J., de Zeeuw C. 1980. *Textbook of wood technology*. McGraw-Hill.
- Parsons T.C. 1989. Development and testing of equipment for the monitoring of acoustic emissions from drying timber. B.E. thesis. Uni. of Tas.
- Porter A.W., El-Osta M.L., Kusec D.J. 1972. Prediction of failure of finger joints using acoustic emissions. *Forest Products Journal.* 22(9):74-82.
- Quarles S.L. 1988. The effect of physical and structural properties of solid wood on the attenuation of burst-type emissions. Proceedings, 9th International Acoustic Emission Symposium, 'Progress in Acoustic Emission':642-649.

Quarles S.L. 1990. Acoustic emission generated during drying. Proceedings, Western Dry Kiln Association Meeting, Reno, Nevada. May 9-11.

Quarles S.L. 1992. Acoustic emission associated with Oak during drying. *Wood and Fiber Science*. 24(1):2-12.

Ravenhall F.W. 1977. The application of stress wave emission to crack propagation in metals - a crack propagation model. *Acustica*. 37:307-316.

Rice R.W., Skaar Ch. 1990. Acoustic emission patterns from the surfaces of red oak wafers under transverse bending stress. *Wood Sci. Tech.* 24:123-129.

Rohsenow W.M., Choi H.Y. 1961. *Heat, mass and momentum transfer*. Prentice Hall.

Rotem A, Altus E. 1979. Fracture modes and acoustic emission of composite materials. *Journ. Testing and Evaluation*. 7(1):33-40.

Sato K., Fushitani M., Noguchi M. 1984. Discussion of tensile fracture of wood using acoustic emissions. *Mozukai Gakkaishi*. 30:117-123.

Schaffner R.D. 1981. Fundamental aspects of timber seasoning. MEngSci thesis, Uni of Tas.

Schaffner R.D., Doe P.E. 1981. 'An application of an orthotropic Fickian diffusion model to timber drying'. Paper presented at 20th For. Prod. Res. Conf. Melbourne, Australia. November.

Scruby C.B. 1987. An introduction to acoustic emission. *J. Phys. E. Sci. Instrum.* 20:946-953.

Siau J.F. 1984. *Transport processes in wood*. Springer Verlag. New York.

Skaar C., Simpson W.T., Honeycutt R.M. 1980. Use of acoustic emissions to indentify high levels of stress during oak lumber drying. *For. Prod. Journ.* 30(2):21-22.

Taylor G.I. 1934. The mechanism of plastic deformation of crystals. Part 1 - Theoretical. *Proc. Roy. Soc. A*. CXLV:362-387.

Tiemann H.D. 1906. Effect of moisture on the strength and stiffness of wood. *US Dept Ag, For Serv Bull* 70.

Tiemann H.D. 1915. Principles of kiln drying. *Lumber World Review*. January 15 and September 25.

Tyree M.T., Dixon M.A. 1983. Cavitation events in *Thuja occidentalis*. L. *Plant Physiology*. 72(4):1-94-1099.

Van de Vegte J. 1986. *Feedback Control Systems*. Prentice Hall Int.

Vanek M. 1991. Kontinuierliche Ermittlung von Trocknungsspannungen mittels Biegemomentmessung. *Holzforschung und Holzverwertung* 1:22-25.

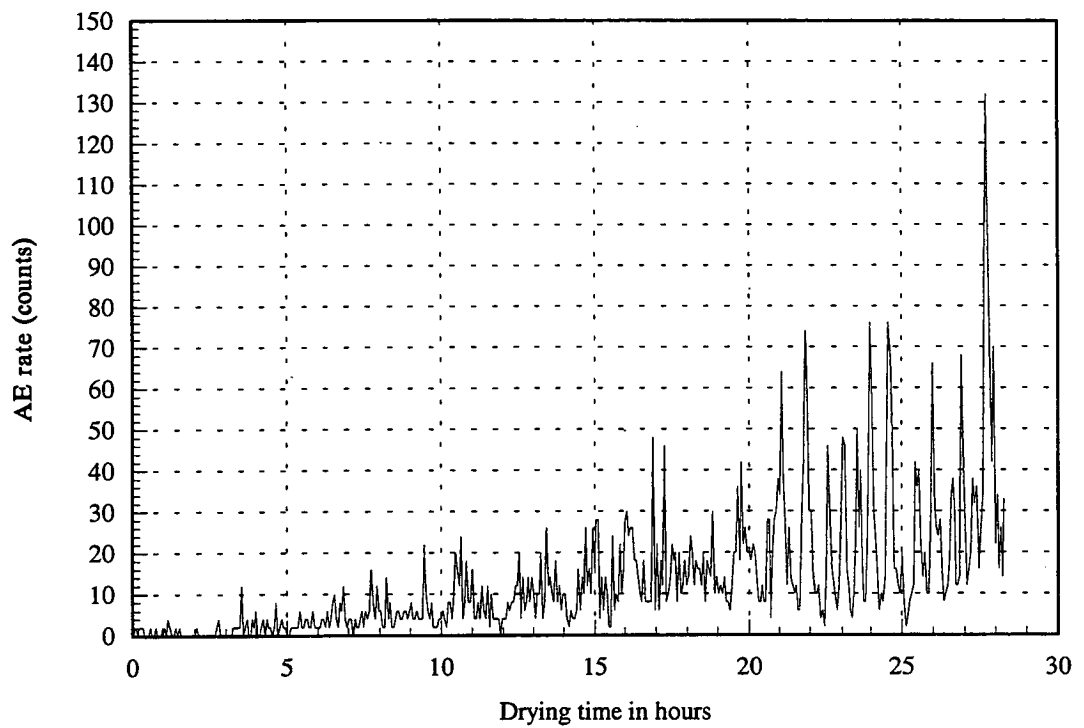
Vermaas H.F. 1992. 'Developments in wood drying theory and practice since Seattle 1989'. Paper presented at IUFRO Conference. Vienna Austria.

Vermaas H.F., Steyn W.H., Viljoen J. 1993. Optimal drying of lumber using a discrete, online mathematical model of moisture movement. *Holzforschung und Holzverwertung*. 45(1):12-15.

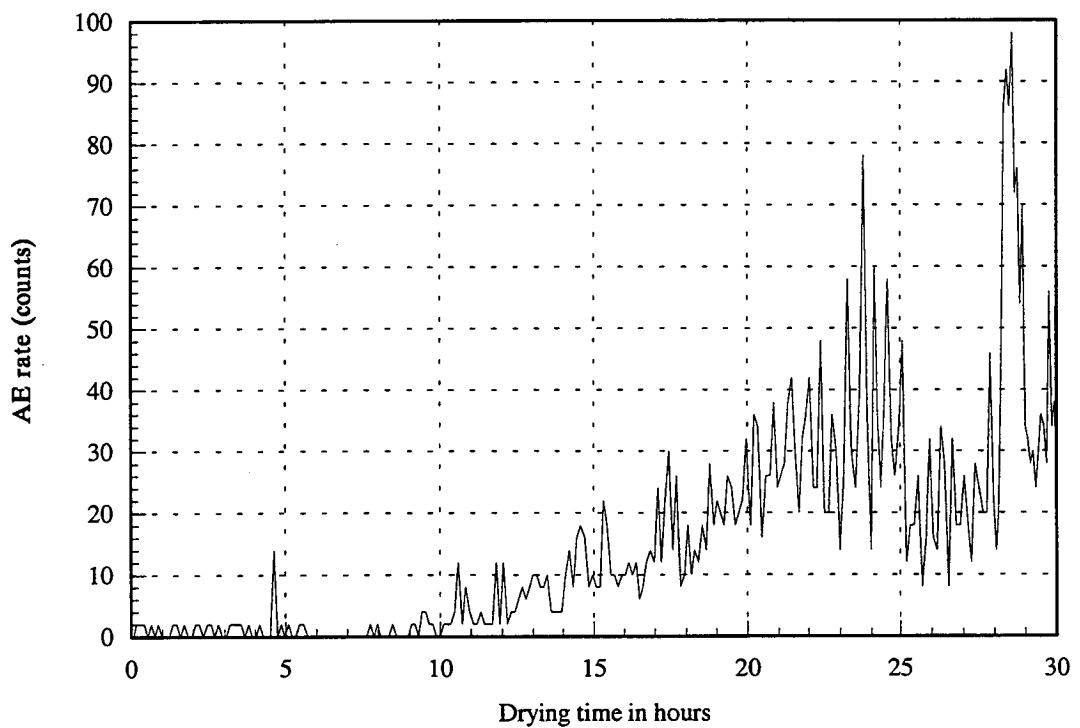
Wu Q. (1989). An investigation of some problems in drying of Tasmanian eucalypt timbers. MEngSci thesis. Uni of Tas.

Appendix A

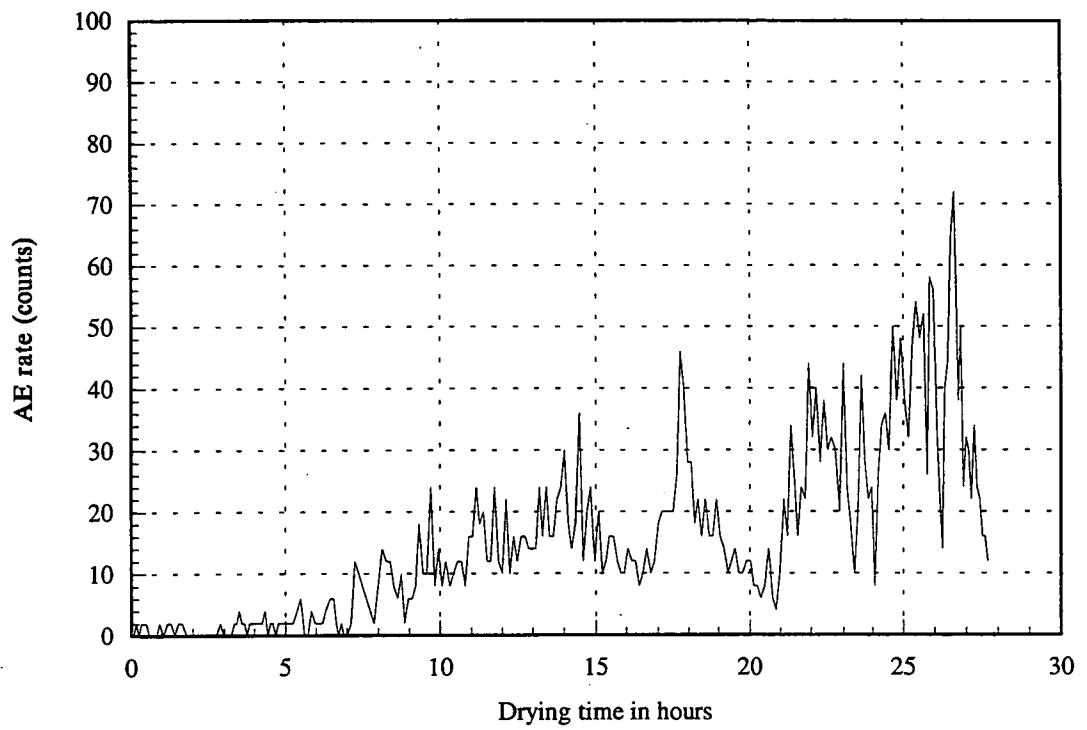
Typical AE Responses



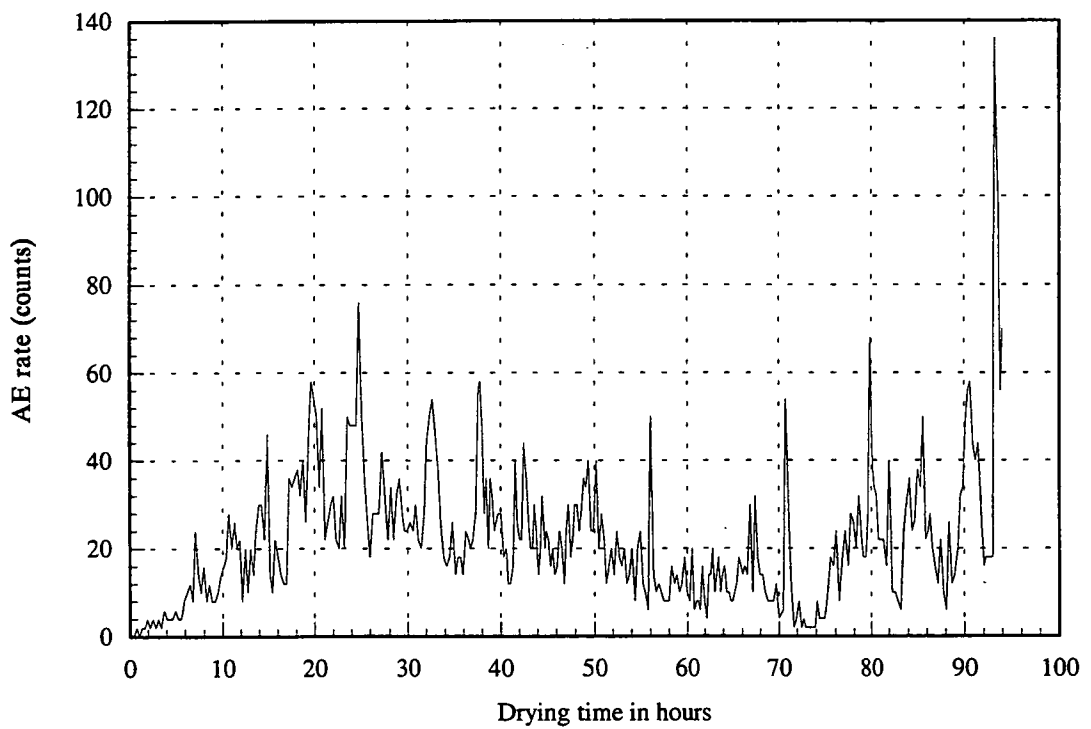
Run 8. Measured AE response in surface-checked eucalypt specimen



Run 9. Measured AE response in surface-checked eucalypt specimen



Run 11. Measured AE response in non surface-checked eucalypt specimen



Run 14. Measured AE response in surface-checked eucalypt specimen

Appendix B

Relevant Program Listings

Procedure 'SimulateDrying' in SMARTKILN

```
procedure SimulateDrying;
begin
  //set strainOk false at start of each time-step
  strainOk := false;
  TIME := Time + TimeStep;
  //copy parameters to values at end of previous time-step
  resetStatetoEndofPreviousTimeStep;

  repeat
    //iterate DBT and WBT based on error in surface strain when
    //running in 'clever' mode
    if Clever then
      Iterate_Condition;
    //copy parameters to values at start of current time-step
    resetStatetoStartofCurrentTimeStep;
    //read next drying conditions
    nextDryingConditions;
    //ensure number of grid-points promotes numerical stability
    testNumberOfGridPoints;

    //integrate error functions of moisture content and apply
    //Fourier series temperature solution (refer to 5.2)
    calculateMoisture_TemperatureProfiles;
    calculateSurfaceMoistureContent_Temperature;
    //Equ 5.9 and 5.10
    calculateStress_StrainProfiles

    //compare surface strain with bounds if in 'clever' mode
    if Clever then
      strainOk := (abs(ControlStrain - surface  $\epsilon_i$  < 1e-6)
    //retain initial constant conditions until in 'clever' mode
    else
      strainOk:=true;
    until strainOk := true;
  end

  procedure Iterate_Condition;
  begin
    //calculate rising DBT for simulating 'collapse-resistant' wood
    //based on preset collapse threshold temperature and board centre
    //moisture content.
    //Use exponential curve assuming T=20°C @ MC=100 and CollapseTemp
    //is set by user @ MC=30.
    MC := Centre_MoistureContent;
    TEMP := CollapseTemp * exp ((30-MC) * ln (CollapseTemp/20) / 70);
    if notCollapseProne then
      DBT := TEMP;

    if (surface  $\epsilon_i$  > ControlStrain) then
      TWB := TWB + 0.1
    else if (surface  $\epsilon_i$  < ControlStrain) then
      TWB:=TWB-0.1;
    end;
  end;
end;
```

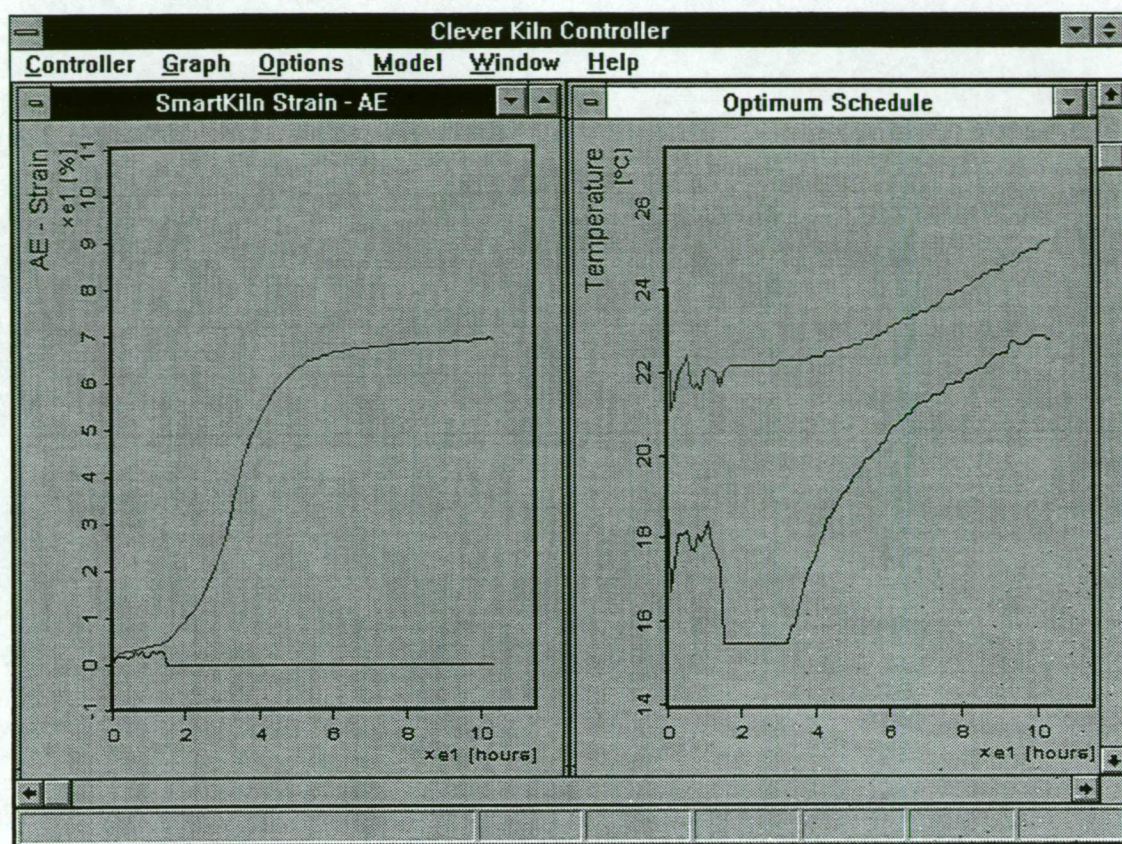
Procedure 'SimulateDrying' in KILNSCHED

```
procedure Drying_Model;
begin
  inc(TIME);
  //read next drying conditions
  nextDryingConditions;
  //ensure number of grid-points promotes numerical stability
  testNumberOfGridPoints;

  //integrate error functions of moisture content and apply
  //Fourier series temperature solution (refer to 5.2)
  calculateMoisture_TemperatureProfiles;
  calculateSurfaceMoistureContent_Temperature;
  //Equ 5.9 and 5.10
  calculateStress_StrainProfiles
end;
```

Appendix C

Clever Kiln Controller



Clever Kiln Controller user screen showing calculated surface strain behaviour and corresponding optimum schedule

Appendix D

Nomenclature

ε_i	instantaneous strain
ε_u	unconfined shrinkage strain
ε_c	creep strain
ε_m	mechano-sorptive effect
ε_n	net strain
ε_{pl}	proportional limit
ε_0	set strain
σ	stress (MPa)
σ_u	ultimate stress (MPa)
α	coefficient of heat transfer (m^2/s)
ρ	density (kg/m^3)
c_p	specific heat at constant pressure (kJ/kgK)
c_{vw}	concentration of moisture in air in contact with wood surface (kg/m^3)
c_m	concentration of moisture in mid-stream (kg/m^3)
AMC	average moisture content (kg/kg)
D	diffusion coefficient of water in wood (kg/m^2s)
D_0	value of diffusion coefficient at reference temperature (kg/m^2s)
DBT	dry bulb temperature ($^{\circ}C$)
DBTSP	setpoint dry bulb temperature ($^{\circ}C$)
E	Young's Modulus (MPa)
f	friction factor
h_m	mass flux (kg/m^2hr)
h_e	heat flux (kJ/m^2hr)
SMC	surface moisture content (kg/kg)
T_b	board thickness (m)
T_m	temperature in mid-stream ($^{\circ}C$)
T_w	temperature of air in contact with wood ($^{\circ}C$)
U	free stream air speed outside boundary layer (m/s)
u	local air velocity (m/s)
U_r	recoverable strain energy (kJ)
U_r^*	dimensionless recoverable strain energy
U_u	unrecoverable strain energy (kJ)
U_u^*	dimensionless unrecoverable strain energy
WBT	wet bulb temperature ($^{\circ}C$)
WBTSP	setpoint wet bulb temperature ($^{\circ}C$)
WBD	wet bulb depression ($^{\circ}C$)
WBDSP	setpoint wet bulb depression ($^{\circ}C$)
W_{in}	total strain energy (kJ)
W_{in}^*	dimensionless total strain energy
y	distance through board section (m)